PART II
CORROSION INHIBITION STUDIES

Shaju. K. S. “Evaluation of metal evaluation binding capacity of azomethine class of compounds, electrochemical investigations on corrosion and their biological studies ” Thesis. Department of Chemistry, St. Thomas College Thrissur, University of Calicut, 2014

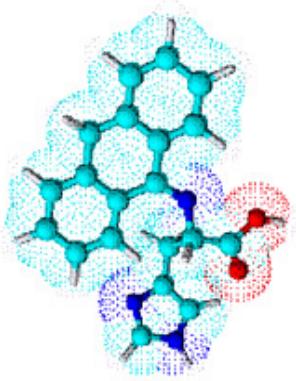

PART II

CORROSION INHIBITION STUDIES

CHAPTER 1

INTRODUCTION AND REVIEW

Corrosion is the destructive attack of a metal by chemical or electrochemical[1] reactions with its environment. Corrosion is an important factor in any chemical processing plant. It makes all the difference between a trouble free operation and a costly shut-down. The secret of effective engineering lies in controlling rather than preventing corrosion, because it is impracticable to eliminate totally the corrosion. In chemical plants the hydrogen ion environment is an important factor in corrosion reactions as well as corrosion control. Acidic media are generally more corrosive than alkaline and neutral media. Acid solutions are widely used in industry, the most important fields of application being acid pickling, industrial acid cleaning, acid descaling and oil well acidizing, because of the general aggressivity.

"The uses of chemical inhibitors have always been considered to be the first line of defence against acid corrosion"[2,3]. A great number of scientific studies have been devoted to the subject of corrosion inhibitors. However, most of what is known has grown from trial and error experiments, both in the laboratories and in the field. Rules, equations, and theories to guide inhibitor development or use are very limited.

Corrosion inhibitor

"A corrosion inhibitor is a chemical substance that, when added in small concentration to an environment, effectively decreases the corrosion rate"[4]. An efficient inhibitor is compatible with the environment, is economical for application and produces the desired effect when present in small concentrations. Inhibitor selection is based on the metal and the

environment. Inhibitors can be classified into environmental conditioners and interface inhibitors.

"Corrosion can be controlled by removing the corrosive species in the medium. Inhibitors that decrease corrosivity of the medium by scavenging the aggressive substances are called environmental conditioners or scavengers. In near-neutral and alkaline solutions, oxygen reduction is a common cathodic reaction. In such situations, corrosion can be controlled by decreasing the oxygen content using scavengers"[5].

Interface inhibitors control corrosion by forming a film at the metal/environment interface. Interface inhibitors can be classified into liquid- and vapour-phase inhibitors. Liquid-phase inhibitors are classified as anodic, cathodic, or mixed inhibitors, depending on whether they inhibit the anodic, cathodic, or both electrochemical reactions. Anodic inhibitors are usually used in near-neutral solutions where sparingly soluble corrosion products, such as oxides, hydroxides, or salts, are formed. They form, or facilitate the formation of passivating films that inhibit the anodic metal dissolution reaction. Anodic inhibitors are often called passivating inhibitors. When the concentration of an anodic inhibitor is not sufficient, corrosion may be accelerated, rather than inhibited. The critical concentration above which inhibitors are effective depends on the nature and concentration of the aggressive ions. Cathodic inhibitors control corrosion by either decreasing the reduction rate (cathodic poisons) or by precipitating selectively on the cathodic areas (cathodic precipitators). Cathodic poisons, such as sulphides and selenides, are adsorbed on the metal surface; whereas compounds of arsenic, bismuth and antimony are reduced at the cathode and form a metallic layer. In near-neutral and

alkaline solutions, inorganic anions, such as phosphates, silicates and borates, form protective films that decrease the cathodic reaction rate by limiting the diffusion of oxygen to the metal surface.

About 80% of inhibitors are organic compounds that cannot be designated specifically as anodic or cathodic and are known as mixed inhibitors. The effectiveness of organic inhibitors is related to the extent to which they adsorb and cover the metal surface. Adsorption depends on the structure of the inhibitor, on the surface charge of the metal and on the type of electrolyte.

"Mixed inhibitors protect the metal in three possible ways: physical adsorption, chemisorption and film formation. Physical (or electrostatic) adsorption is a result of electrostatic attraction between the inhibitor and the metal surface. When the metal surface is positively charged, adsorption of negatively charged (anionic) inhibitors is facilitated. Positively charged molecules acting in combination with a negatively charged intermediate can inhibit a positively charged metal. Anions, such as halide ions, in solution adsorb on the positively charged metal surface, and organic cations subsequently adsorb on the dipole. Corrosion of iron, in sulphuric acid containing chloride ions, is inhibited by quaternary ammonium cations through this synergistic effect"[6].

"Physically adsorbed inhibitors interact rapidly, but they are also easily removed from the surface. Increase in temperature generally facilitates desorption of physically adsorbed inhibitor molecules. The most effective inhibitors are those that chemically adsorb (chemisorb), a process that involves charge sharing or charge transfer between the inhibitor molecules and

the metal surface. Chemisorption takes place more slowly than physical adsorption. As temperature increases, adsorption and inhibition also increase. Chemisorption is specific and is not completely reversible"[7].

"Vapour phase inhibitors (VPI) are such organic inhibitors which readily vaporize and form a protective layer of the inhibitor on the metal surface. These are conveniently used to avoid corrosion in enclosed spaces and also during storage, packing, shipping etc. Substances having low but significant pressure of vapour with inhibiting properties are effective. The VPIs are used by impregnating wrapping paper or by placing them loosely inside a closed container"[8]. The slow vaporization of the inhibitor protects against air and moisture. In general, VPIs are more effective for ferrous than non-ferrous metals.

Amino acids as corrosion inhibitors in acid solutions – A review

"Most of the effective inhibitors contain hetero atoms in their structure and they are capable of forming coordinate covalent bond with metal owing to their free electron pairs"[9,10]. Nowadays many researchers are interested in biochemical compounds based on amino acids, which exhibit excellent properties such as good water solubility and rapid biodegradability[11,12]. These inhibitors are used for the protection against the corrosion of certain metals such as iron, steel, copper, cobalt and nickel[13,14]. "All amino acids have a central or alpha carbon, to which are bonded four groups; hydrogen, an amino, a carboxyl group and a unique side chain, also known as R-group. These molecules differ in their unique side chain, which can be used to classify the molecules into functional types". Various amino acids have been used to inhibit the corrosion of metals and alloys[15–41].

"The corrosion inhibition behaviour of nitrogen-containing amino acid, L-histidine (LHS) on mild steel in 0.1M H_2SO_4 solution in the temperature range of 30-60°C was studied by Mobin et. al[15] using weight loss measurements and potentiodynamic polarization measurements. The effect of the addition of very small amount of surfactants, sodium dodecyl sulfate (SDS) and cetyltrimethyl ammonium bromide (CTAB), on the corrosion inhibition behaviour of LHS was also studied. LHS significantly reduces the corrosion rates of mild steel, with the maximum inhibition efficiency (IE) being 71.09% at 30°C at a concentration of 500 ppm of LHS".

"A comparative study of different types of amino acids: proline, cysteine, phenyl alanine, alanine, hisitidine and glycine as inhibitors for copper corrosion in 8M phosphoric acid at different temperatures was carried out by Abdel et. al[16]. The results reveal that amino acids have strongest inhibitive effects that provide good protection to copper surface against corrosion in acid solutions".

K. F. Khaled[17] and co-workers studied "the inhibition performance of alanine on iron in 1M hydrochloric acid medium at 25 ± 1^0C adopting potentiodynamic polarization and electrochemical impedance spectroscopy (EIS) measurements. Alanine inhibits the acidic corrosion even at very low concentrations, reaching a value of inhibition efficiency 80% at a concentration of 50mM. Density functional theory (DFT) calculations have been used to investigate the minimum energy structures of alanine molecules on iron".

Using Hamiltonians, Eddy[18] predicted "the corrosion inhibition potential of nine amino acids, grouped under three skeletons. Skeleton I

consisted of cysteine (CYS), serine (SER) and amino butyric acid (ABU). Those in skeleton II are threonine (THR), alanine (ALA) and valine (VAL) while aromatic amino acids such as phenylalanine (PHE), tryptophan (TRP) and tyrosine (TYR) are included in skeleton III. The results obtained from quantum chemical parameters indicated that the trends for the variation of corrosion inhibition potentials of the studied amino acids in skeletons I, II and III are CYS > SER > ABU, THR > ALA > VAL and TRP > TYR > PHE, respectively".

The corrosion and degradation behaviour of carbon steel were investigated by Ahn et. al[19] in "CO_2 absorption process using aqueous potassium salts of glycine and taurine. The experimental parameters varied were the concentration, amino acid type, temperature, CO_2 loading and the presence of corrosion inhibitors. The corrosion characteristics of carbon steel were measured with potassium glycinate and potassium taurate solutions over a wide range of concentrations (1.5 to 5.0M) and temperatures (313.15 to 353.15 K)".

Amin et. al[20] studied the "performance of three selected amino acids, namely alanine (Ala), cysteine (Cys) and S-methyl cysteine (S-MCys) as safe corrosion inhibitors for iron in aerated stagnant 1M HCl solutions and was evaluated by Tafel polarization and impedance measurements. Results indicate that Ala acts mainly as a cathodic inhibitor, while Cys and S-MCys function as mixed-type inhibitors. Cys, which contains a mercapto group in its molecular structure, was the most effective among the inhibitors tested, while Ala was less effective than S-MCys".

"Inhibition behavior of L-tryptophan on low carbon steel in 1M HCl was investigated by Fu et. al[21] with weight loss experiment and Tafel polarization curve in the temperature range (298–328 K). The adsorption of L-tryptophan on the surface of low carbon steel obeys the Langmuir adsorption isotherm and the thermodynamic parameters were determined and discussed".

The inhibitive effect of three amino acids and their benzene sulphonyl derivatives against the corrosion of "brass in 0.6M aqueous NaCl solution have been studied by Ranjana et. al[22] using potentiodynamic polarization and EIS spectroscopy. The amino acids used are glycine, aspartic acid and glutamic acid and their corresponding benzene sulphonyl derivatives. It has been observed that introduction of C_6H_5-SO_2- group increases the inhibition efficiency of amino acids".

"The inhibiting properties of two innoxious amino acids (cysteine and phenylalanine) as bronze corrosion inhibitor in a strong acidic solution of 0.2 g/L Na_2SO_4 + 0.2 g/L $NaHCO_3$ at pH=3 was studied by Varvara and coworkers[23] using open-circuit potential measurements, electrochemical impedance spectroscopy and SEM analysis. The anticorrosive efficiencies of the investigated compounds decrease in the order: Cys (96.91 %) > PhAla (52.22 %)".

"The corrosion inhibition behaviour of four selected amino acid compounds, namely L-cysteine, L-histidine, L-tryptophan and L-serine on mild steel surface in deaerated 1M HCl solution were studied by Fu et. al[24] electrochemically by Tafel polarization, electrochemical impedance spectroscopy methods, computationally by the quantum chemical calculation and molecular dynamics simulation. Electrochemical results show that these

amino acid compounds inhibit the corrosion of mild steel in 1M HCl solution significantly".

Alagbe et. al investigated[25] "the effect of some amino acid based inhibitors on the corrosion characteristics of NST-44 carbon steel in cassava fluid. The amino acid inhibitors investigated include leucine, alanine, methionine and glutamic acid. The corroded surfaces of the specimens were characterized using the optical microscopic techniques.

The inhibition effect of four amino acids towards the corrosion of copper in 0.5M HCl solution has been studied by Zhang et. al[26] using potentiodynamic polarization and electrochemical impedance spectroscopy (EIS). The used amino acids were aspartic acid (Asp), glutamic acid (Glu), asparagine (Asn) and glutamine (Gln). The inhibition efficiency of these compounds increases in the order Gln > Asn > Glu > Asp. Addition of iodide ions into 10 mM Gln solution gave an improvement of the protection efficiency, reaching a maximum value of 93.74% for 5mM KI".

"The inhibition effect of five amino acids on the corrosion of copper in 1M HNO_3 solution was studied by Barouni et. al[27] using weight loss and electrochemical polarization measurements. Valine (Val) and glycine (Gly) accelerate the corrosion process; but arginine (Arg), lysine (Lys) and cysteine (Cys) inhibit the corrosion phenomenon. Cysteine was the best inhibitor. Correlation between the quantum chemical calculations and inhibition efficiency was discussed using semi-empirical methods (AM1 and MNDO).

L-leucine was evaluated as a potential inhibitor for mild steel in acidic medium by Singh et. al[28] using galvanostatic polarization and potentiostatic polarization techniques. Electrochemical results also showed that L-leucine

acts as a mixed type of inhibitor (blocks the cathodic and anodic sites to same extent) which was evident from insignificant shift of open circuit potential.

The electrochemical behavior of vanadium in amino acid free and amino acid containing aqueous solutions of different pH was studied by El-Rabiee et. al[29] using open circuit potential measurements, polarization techniques and electrochemical impedance spectroscopy (EIS). A group of amino acids, namely, glycine, alanine, valine, histidine, glutamic and cysteine has been investigated as environmentally safe inhibitors. The effect of Cl^- on the corrosion inhibition efficiency especially in acid solutions was investigated. In neutral and basic solutions, the presence of amino acids increased the corrosion resistance of the metal.

Kiani et. al[30] describes the inhibition effect of amino acids cysteine (Cys), methionine (Met) and alanine (Ala), towards the corrosion of lead-alloy (Pb–Ca–Sn) in H_2SO_4 solution by potentiodynamic polarization, electrochemical impedance spectroscopy (EIS), weight loss measurement and scanning electron microscopy (SEM) methods. Adsorption isotherms were fitted by Langmuir isotherm.

The corrosion inhibition of Cu–Ni alloys was investigated by Badawy et. al[31] in aqueous chloride solutions using amino acids as environmentally safe materials. The corrosion rate was calculated in the absence and presence of the corrosion inhibitor using polarization and impedance techniques. Different adsorption isotherms were tested and the corrosion inhibition process was found to depend on the adsorption of the amino acid molecules and/or the deposition of corrosion products on the alloy surface".

The study by Alagbe et. al[32] "presents the report of an investigation on the effect of some amino acid based inhibitors on the corrosion characteristics of NST-44 mild steel in lime fluid (citrus aurantifolia). The corrosion rates of the exposed mild steel were obtained using the weight loss immersion method. The amino acid inhibitors investigated include leucine, alanine, methionine and glutamic acid. The corroded surfaces of the specimens were characterized using the optical microscopic techniques.

The inhibition effect of three amino acids towards the corrosion of Pb–Sb–Se–As alloy in H_2SO_4 solution was investigated by Ghasemi and Tizpar[33] with linear polarization and weight loss measurements methods. The used amino acids were tryptophan, proline and methionine. The effect of inhibitor concentration and temperature against inhibitor action was investigated.

Corrosion inhibition of steel in hydrochloric acid by decylamides of α-amino acid derivatives was studied by Olivares et. al[34] using gravimetric and electrochemical techniques. Protection efficiencies of 90% were obtained with 100 ppm of tyrosine and glycine derivatives, while alanine and valine derivatives reached only 80%".

"The effect of two amino acid compounds, DL-alanine and DL-cysteine, on copper corrosion in an aerated 0.5M HCl solution was studied by Zhang et. al[35] by weight loss measurements, potentiodynamic polarisation curves, and electrochemical impedance spectroscopy. A conventional benzotriazole (BTA) inhibitor was also tested for comparison. DL-cysteine was shown to be the most effective inhibitor among those tested inhibitors.

The effect of cysteine, methionine, and N-acetyl cysteine on the corrosion behaviour of mild steel in 40% H_3PO_4 solution without and with

Cl^-, F^-, Fe^{3+} and their ternary mixture was studied by Morad[36] using both potentiostatic and electrochemical impedance (EIS) techniques under anodic and cathodic polarization conditions".

"The inhibition effect of some amino acids towards the corrosion of aluminum in 1M HCl + 1M H_2SO_4 solution was investigated by Ashassi-Sorkhabi et. al[37] using weight loss measurement, linear polarization and SEM techniques. The used amino acids were alanine, leucine, valine, proline, methionine and tryptophan.

The effect of some amino acids glycine, leucine, D-L aspartic acid, arginine and methionine on the corrosion behaviour of pure iron in citric acid solution at pH = 5 was investigated by Zerfaoui and coworkers[38] using weight loss, polarization and EIS measurements. Results show that methionine is the best inhibitor and its efficiency reached 96% at 2×10^{-2} M concentration. Effect of pH and temperature were also studied.

The effect of cysteine (cys) on the anodic dissolution of copper in sulfuric acid medium has been studied by Matos et. al[39] at room temperature using electrochemical methods. The anodic polarization curves showed two different regions: in the low overpotential range, the inhibitory effect of cys on the anodic dissolution was verified and in the high overpotential range this amino acid does not influence the copper anodic dissolution.

The corrosion inhibiting action of five amino acids on steel metals in 1M H_2SO_4 was measured by Gomma[40] potentiodynamically. The maximum protection efficiency was obtained with glutamic acid, while with other compounds, varying degrees of inhibition was noticed".

The effect of some α-amino acids on the inhibition of pitting corrosion of Al in 0.1M NaCl solution was studied by El-Shafei et. al[41] using potentiodynamic technique. The order of effectiveness of the inhibitors was arginine>histidine>glutamine>asparagine>alanine>glycine. The adsorption of amino acids on platinum was investigated by cyclic voltammetry using a flow cell technique.

Schiff bases as corrosion inhibitors in acid solutions – A review

"The inhibition effect of some Schiff base compounds towards the corrosion of 1018 carbon steel in hydrochloric acid solution was studied by Zaafarany[42] using weight loss, galvanostatic polarization and electrochemical impedance spectroscopy measurements. The polarization measurements indicated that the inhibitors are of mixed type and inhibit corrosion by adsorption on the steel surface".

The corrosion inhibitory effects of 1,5-dimethyl-4-((2-methylbenzylidene)amino)-2-phenyl-1*H*-pyrazol-3(2*H*)-one (DMPO) on "mild steel in 1M HCl was investigated by Sutiana et. al[43] using electrochemical impedance spectroscopy (EIS), potentiodynamic polarization, open circuit potential (OCP) and electrochemical frequency modulation (EFM). Electronic properties such as highest occupied molecular orbital energy, lowest unoccupied molecular orbital energy (E_{HOMO} and E_{LUMO}, respectively) and dipole moment (μ) were calculated and discussed".

"Sulphanilic acid and sulphanilamide schiff bases have been synthesised by Chitra et. al[44] and evaluated as inhibitors for mild steel corrosion in 1M H_2SO_4 by electrochemical and non electrochemical techniques. The adsorption of the inhibitors on the mild steel surface obeys

Langmuir and Temkin adsorption isotherms. Potentiodynamic polarization studies show that the inhibitors behave as mixed inhibitors. Addition of halide ions enhances the inhibition efficiency".

2-alkyl-N-(3-methoxy-4methylbenzylidene) hydrazinecarbothioamides of "fatty acid hydrazides from nontraditional oils (neem, rice bran and karanja) have been synthesized and evaluated by Toliwal et. al[45] as corrosion inhibitors for mild steel (MS) in hydrochloric acid solution by weight loss method. Adsorption of all Schiff bases on MS surface in acid solution obeyed Langmuir's adsorption isotherm.

The corrosion behaviour of mild steel in 1M HCl was studied using 4-(N,N-dimethylaminobenzilidine)-3-mercapto-6-methyl-1,2,4-triazin(4H)-5-one (DAMMT) as inhibitor using the conventional weight loss method, potentiodynamic polarisation studies (Tafel), linear polarisation studies (LPR), electrochemical impedance spectroscopy studies (EIS), adsorption studies and quantum chemical calculations" by Sam et. al[46].

The "inhibition effect of some phenylhydrazone derivatives, namely, [ethyl(2Z)-cyano[(4E)-5-oxo-3-phenyl-4-(phenylhydrazono)-1,3-thia-zolidin-2-ylidene] acetate (A), ethyl(2Z)-cyano[(4E)-5-oxo-3-phenyl-4-(p-methylphenylhydrazono)-1,3-thiazolidin-2-ylidene] acetate (B), ethyl(2Z)-cyano[(4E)-5-oxo-3-phenyl-4-(o-methoxyphenylhydrazono)-1,3-thiazolidin-2-ylidene] acetate (C) and ethyl(2Z)-cyano[(4E)-5-oxo-3- thiazolidin-2-ylidene] acetate (D) on the corrosion of 70Cu-30Zn brass in 2M HCl solution has been investigated by Abdallah et. al[47] using weight loss and galvanostatic polarization techniques. The addition of KI to phenylhydrazone derivatives enhanced the inhibition efficiency due to synergistic effect".

Schiff bases derived from condensation reaction of "acrolein with 2-aminophenol (SB1), cinnamaldehyde with 2-aminophenol (SB2) and cinnamaldehyde with phenylene diamine (SB3) were prepared" by Mohammed[48]. These Schiff bases were identified by UV-Vis, IR, CHN and ^{1}HNMR. The study also included the use of these Schiff bases as inhibitors for corrosion of carbon steel in acidic media (0.5M HCl).

"A comparative study of 5-amino-1,2,4-triazole (5-ATA), 5-amino-3-mercapto-1,2,4-triazole (5-AMT), 5-amino-3-methylthio-1,2,4-triazole (5-AMeTT) and 1-amino-3-methylthio-1,2,4-triazole (1-AMeTT) as inhibitors for mild steel corrosion in 0.1M HCl solution at 20^{0}C was carried out by Hamdy et. al[49]. Potentiodynamic polarization and electrochemical impedance spectroscopy (EIS) techniques were applied to study the metal corrosion behaviour in the absence and presence of different concentrations of these inhibitors under the influence of various experimental conditions.

The corrosion inhibition properties of a new class of oxadiazole derivatives, namely 3,5-bis(n-pyridyl)- 1,2,4-oxadiazoles (n-DPOX) for C38 carbon steel corrosion in 1M HCl medium were analysed by Moha et. al[50] using electrochemical impedance spectroscopy (EIS). An adequate structural model of the interface was used and the values of the corresponding parameters were calculated and discussed".

"Three new Schiff bases, viz., N,N-ethylen-bis (salicylidenimine) [S1], N,N-isopropylien-bis (salicylidenimine) [S2] and N-acetylacetone imine, N-(2-hydroxybenzophenone imine) ortho-phenylen [S3] have been investigated by Hosseini et. al[51] as corrosion inhibitors for mild steel in 0.5M H_2SO_4 using

Tafel polarization and electrochemical impedance spectroscopy (EIS). Thermodynamic calculations indicate the adsorption to be physical in nature.

QSAR study on N-containing corrosion inhibitors has been made by Zhang et. al[52] using quantum chemical approach assisted by a novel topological index. The results indicate that inhibition efficiencies relate to some parameters of corrosion inhibitors, such as E_{HOMO}, polarizability, dipole, frontier orbital charge density, the interaction mode between inhibitors and metal surface (feedback donor–acceptor coordination bonds), etc".

The "corrosion inhibitory properties on mild steel in acidic media by nitrogen containing ligands N-(4-nitrophenyl) p-anisalidine (SB1), N-(4-chlorophenyl) p-anisalidine (SB2), N-(4-phenyl) p-anisalidine (SB3), N-(4-methoxy phenyl) p-anisalidine (SB4), and N-(4-hydroxy phenyl) p-anisalidine (SB5) have been studied by Nitin and coworkers[53] using mass loss, thermometric and potentiostatic polarization techniques.

3,5-Diamino-1,2,4-triazole Schiff base derivatives and their inhibition efficiency, based on the effect of changing functional groups, were reported by Gopi et. al[54] to establish a relationship between inhibitor efficiency and molecular structure using weight loss method, electrochemical and Fourier transform infrared spectral techniques. It was found that the molecules containing more electron donating groups have higher inhibition efficiency than the corresponding compounds with low electron donating groups".

Seven Schiff bases have been examined by Desai et. al[55] as corrosion inhibitors of mild steel in 1–6M solutions of HCl. "Activation energies in the presence and absence of inhibitors have been evaluated. Galvanostatic

polarization data indicate that all these compounds are predominantly cathodic inhibitors".

The inhibitory effect "of N,N′-bis(salicylidene)-2-hydroxy-1,3-propanediamine (LOH) and N,N′-bis(2-hydroxyacetophenylidene)-2-hydroxy-1,3-propanediamine (LACOH) in 2M HCl medium on mild steel has been investigated by Kann et. al[56] at 303 K. The inhibitors appear to function through the Langmuir adsorption isotherm.

The corrosion inhibition by Schiff base compounds derived from diamines and o-hydroxy or o-methoxy aromatic aldehydes was investigated by Shokry et. al[57] using weight loss, electrochemical measurements and surface analysis of SS 400 in various aqueous solutions such as tap water (LC), concentrated tap water (HC) and HCl solutions. The maximum inhibition efficiency of N,N′-bis (salicylaldehyde)-1,12-diaminododecane (Saldn) for SS 400 in HCl solution approached 93%".

A heterocyclic Schiff base of N-(2-chlorobenzylidene)-4-acetylaniline (CBAA) was tested for its corrosion inhibition towards St3S carbon steel in acidic chloride solutions using weight loss, Tafel polarization technique, scanning electron microscopy and quantum chemical calculations by Mieczyslaw and Joanna[58] .

"Schiff base derived from the condensation reaction of analar grade 1-amino-2-naphthol 4-sulphonic acid with cinnamaldehyde was prepared by Thirugnanaselvi et. al[59] under microwave condition. The Schiff base was analysed by infrared spectroscopy. This Schiff base as a corrosion inhibitor on AZ31 magnesium alloy in 0.05 mol/l HCl solution was studied. The inhibition effect of the Schiff base compound (4Z)-4-(3-phenyl allylidene amino)-3-

hydroxy naphthalene-1-sulfonic acid (AC) on AZ31 magnesium alloy corrosion was investigated using mass loss, potentiodynamic polarization technique and electrochemical impedance spectroscopy methods. The potentiodynamic polarization curve shows that Schiff base AC inhibits both anodic and cathodic reactions at all concentration, which indicates that it is a mixed type inhibitor".

"A new class of corrosion inhibitors namely dianiline Schiff bases was synthesized and its inhibiting action on the corrosion of mild steel in 1M sulphuric acid at 30°C was investigated by Chitra et. al[60] using various corrosion monitoring techniques. Potentiodynamic polarization studies showed that the Schiff bases were mixed type inhibitors. The decrease in inhibition efficiency with increase in temperature and the less negative $\Delta G°_{ads}$ values suggest predominant physisorption of the Schiff base molecules on the steel surface.

Three Schiff's bases namely (3-phenylallylidene) amino-5-(pyridine-4-yl)-4H-1,2,4-triazole-3-thiol (SB-1), 3-mercapto-5(pyridine-4-yl)-4H-1,2,4-triazole-4-yl)imino) methyl) phenol (SB-2) and (4-nitrobenzylidene) amino)-5-(pyridine-4-yl)-4H-1,2,4-triazole-3-thiol (SB-3) were synthesized by Ansari et. al[61] and investigated as corrosion inhibitors for mild steel (MS) in 1 M HCl. SB-1 exhibited best inhibition performance (96.6 %) at 150 mg l^{-1}. The studied inhibitors follow Langmuir adsorption isotherm. Potentiodynamic polarization data suggests mixed-mode of corrosion inhibition. The effect of molecular structure on inhibition efficiency was investigated by theoretical calculations using density function theory (DFT) methods".

Suraj and coworkers[62] have been used the weight loss technique to "study the corrosion inhibition of mild steel in 0.1N HNO_3 by the Schiff base 4-chloro-2-(2-oxo-1,2-dihydro-indol-3-ylidene amino)-benzoic acid (ACBAI) and their titanium (IV), zirconium (IV), cadmium (II) and mercury (II) metal complexes".

Scope of present investigation

Carbon steel (CS) is prominently used as structural, instrumental and industrial material. Researchers and engineers are employing many experimental methods to control the corrosion of carbon steel. The use of certain organic compounds as inhibitors is the most practical method to prevent corrosion of the carbon steel in acidic media. In recent years, a number of eco-friendly corrosion inhibitors have been exploited as green alternative to toxic and hazardous compounds. The amino acids which contain carboxyl and amino functionalities, bonded to the same carbon atom are non-toxic, relatively cheap and easy to produce in high purity greater than 99%. Compounds with π-bonds generally exhibit good inhibitive properties due to interaction of π-orbital with the metal surface. Hetero atoms such as N, O, S and in some cases Se and P are capable of forming coordinate-covalent bond with metals, owing to their free electron pairs. Schiff bases with –CH=N– linkage (azomethine) have both the above features combined with their structure which make them effective potential corrosion inhibitors.

Literature survey revealed that amino acids like β-alanine (ALA), L-arginine (ARG), L-histidine (HIS), L-phenyl alanine (PHE), L-tryptophan (TRP) and L-cysteine (CYS) act as corrosion inhibitors on iron, aluminium, copper etc. No studies have been reported on the corrosion inhibition capacity

of these six amino acids on carbon steel having particular composition used for the present investigation. So it is proposed to investigate the inhibition efficiencies of amino acids using gravimetric technique. It is also planned to compare the inhibition efficiencies of these six amino acids with the inhibition efficiencies of Schiff bases which are derived from anthracene-9(10H)-one and various amino carboxylic acids. Thorough literature survey also revealed that no investigations have been reported on the corrosion inhibition capacity of Schiff bases derived from anthracene-9(10H)-one and these six amino acids. So in the present course of study an attempt was made to study the inhibition efficiency of the six Schiff bases derived from amino acids and anthracene-9(10H)-one. The corrosion inhibition efficiency of Schiff bases on carbon steel in 1M HCl and 0.5M H_2SO_4 solution is proposed to examine by weight loss measurements, Tafel polarization analysis and electrochemical impedance spectroscopic techniques. To facilitate the corrosion inhibition capacity of certain Schiff base, synergistic effect studies in H_2SO_4 medium is also proposed.

It is also aimed to carry out adsorption isotherm studies in order to get much insights into the mechanism of corrosion inhibition of the newly synthesized Schiff bases both in 1M HCl and 0.5M H_2SO_4. It is decided to study the effect of temperature on the inhibitive behaviour of Schiff bases on CS in IM HCl. Also it is planned to calculate thermodynamic parameters to confirm the nature of adsorption. To expose the surface morphology of CS, Scanning Electron Microscopy analysis will be utilized.

CHAPTER 2

MATERIALS AND METHODS

The corrosion inhibition efficiency of amino acids and Schiff bases were studied by means of conventional weight loss measurements and electrochemical methods like potentiodynamic polarization and electrochemical impedance spectroscopy techniques.

Weight loss studies

The gravimetric corrosion measurements are most widely used traditional method for *in situ* corrosion monitoring. The weight loss measurements have provided useful parameters for corrosion study.

Preparation of aggressive inhibitor solution

Anthracene-9(10H)-one (A9O), β-alanine (ALA), L-arginine (ARG), L-histidine (HIS), L-phenyl alanine (PHE), L-tryptophan (TRP), L-cysteine (CYS), 3-(anthracen-9(10H)-ylideneamino)propanoic acid [A9Y3APA], (S)-2-(Anthracen-9(10H)-ylideneamino)-5-guanidinopentanoic acid [A9Y5GPA], (S)-2-(anthracen-9(10H)-ylideneamino)-3-(1H-imidazole-4-yl)propanoic acid (A9Y3IMPA), (S)-2-(anthracen-9(10H)-ylideneamino)-3-(1H-indole-3-yl)propanoic acid (A9Y3INPA), (S)-2-(anthracen-9(10H)-ylideneamino)-3-phenylpropanoic acid [A9Y3PPA], and (R)-2-(anthracen-9(10H)-ylideneamino)-3-mercaptopropanoic acid [A9Y3MPA] were used as the inhibitors for the corrosion study. The synthesis, characterization and molecular structures of the Schiff bases were given in Part I. The aggressive solutions of 1M HCl and 0.5M H_2SO_4 were prepared by the dilution of A.R grade 37% of HCl (Merck) and A.R grade 98% of H_2SO_4 (Merck) with de-

ionized water respectively. 0.2 mM KI solution was also prepared for the synergistic study.

1.0mM of each inhibitor solution was prepared by dissolving the required amount of the each amino acid and Schiff base in 1M HCl and 0.5M H_2SO_4 and this was used as the stock solution. 0.2mM, 0.4mM, 0.6mM, 0.8mM and 1.0mM concentrations of inhibitor solutions in 50 ml of acid solution were prepared by diluting the required volume of each inhibitor stock solution. 50 ml of 1M HCl and 50 ml of 0.5M H_2SO_4 without inhibitor were considered as blank test solution. For the synergistic study, 1 ml KI solution was added along with inhibitor solution.

Preparation of metal specimens

The metal specimens used in the present investigation are Carbon Steel (CS) specimens with Composition: C,0.5%; Mn,0.07%; P,0.02%; S,0.015%; Si,0.02% and rest Fe. Metal specimens of dimension 1.5x 2x 0.1 cm were cut abraded with various grades of silicon carbide papers (200, 400, 600, 800, 1000, 1200 and 2000) in accordance with ASTM[63] (American Society for Testing and Materials G31-72, ASTM "Laboratory Immersion Corrosion Testing of Metals") standards. The exact area and thickness of each coupon were measured by using vernier callipers and screw gauge. Metal specimens were washed with soap water, and then methanol, degreased again with acetone.

Weight loss methods

In the laboratory, gravimetric corrosion measurements were carried out by exposing the metal specimens to corrosive environment like acid solution and weight loss of metal specimens were measured at regular intervals and

corrosion rates were calculated. From the corrosion rate, the inhibition capacity and surface coverage of inhibitor was calculated[64]. ASTM standard procedure for laboratory immersion corrosion testing was adopted for the determination of weight loss and corrosion rate of metal specimens in HCl and H_2SO_4.

For the present investigations of CS corrosion study, amino acid (parent amine), anthracene-9(10H)-one (parent ketone) and Schiff bases were used as inhibitor. The polished and previously weighed metal specimens were immersed in hanging position in different concentration of inhibitor and blank solutions, taken in stoppered bottles, with the help of fishing lines at room temperature (30^0C). The investigations were carried out in the open air (naturally aerated solution). After 24 hours, the metal specimens were taken outside, cleaned with acetone and water, dried and weighed. For reproducibility, duplicate experiments were carried out and the average values were taken. Corrosion rate expressed in mmy^{-1} was calculated from weight loss measurements and percentage of inhibition efficiency was calculated from the corrosion rate values. Equations 1 and 2 establish the relation between rate of corrosion and inhibition efficiency with the weight loss of metal specimens.

$$\text{Rate of corrosion } W = \frac{K \times \text{wt.loss in grams}}{\text{Area in sq.cm} \times \text{time in Hrs} \times \text{Density}} \quad (1)$$

Where 'K' =87600 (This is a factor used to convert cm/hour into mm/year), density of MS specimen= 7.88g/cc

Percentage of inhibition or the inhibition efficiency (η) is given by[65]

$$\eta = \frac{W - W'}{W} \times 100 \quad (2)$$

where W & W' are the corrosion rates of the metal specimen in the absence and presence of the inhibitor respectively.

Adsorption isotherms

In the inhibition of metallic corrosion, adsorption plays an important role on the surface of the metal by organic inhibitor molecules. In the present investigation, the adsorption isotherms were utilized to describe the mechanism of corrosion inhibition. The adsorption isotherms illustrate the molecular interactions of the inhibitor molecule with the active sites on the metal surfaces. The inhibitor molecules adsorbed on the metal surface by physically, chemically or both. The most commonly used adsorption isotherms are Langmiur, Freundlich, Temkin and Frumkin. For determining the best fit adsorption model, all the isotherms mentioned above were tried with the help of following equations[66].

Freundlich adsorption isotherm $\theta = K_{ads}C$ (3)

Temkin adsorption isotherm $e^{f\theta} = K_{ads}\,C$ (4)

Langmiur adsorption isotherm $\frac{C}{\theta} = \frac{1}{K_{ads}} + C$ (5)

Frumkin adsorption isotherm $\frac{\theta}{1-\theta}\exp(f\theta) = K_{ads}\,C$ (6)

where C is the concentration of the inhibitor, θ is the fractional surface coverage, f is the molecular interaction parameter and K_{ads} is the adsorption equilibrium constant. Among the different isotherms tried, most adequate one which have the highest value of the correlation co-efficient (R^2) was accepted for interpreting the mechanism of adsorption.

The values of θ can be calculated from the percentage inhibition efficiency using the following relation[67].

$$\theta = \frac{\text{Percentage inhibition efficiency}}{100} \quad (7)$$

The adsorption equilibrium constant K_{ads} is related to the standard free energy of adsorption ΔG^0_{ads}, by

$$\Delta G^0_{ads} = -RT\ln (55.5\ K_{ads}) \quad (8)$$

where 55.5 is the molar concentration of water, R is the universal gas constant and T is the temperature in Kelvin[68]. From different adsorption isotherms, K_{ads} and hence ΔG^0_{ads} were determined.

Effect of temperature

The activation energy of corrosion, enthalpy of activation and entropy of activation can be calculated from this study. The activation parameters give an idea about energetics and kinetics of corrosion process.

The effect of temperature on corrosion process was evaluated using weight loss measurements in the temperatures 30^0, 40^0, 50^0 and 60^0C for 24 hour in the concentration range 0.2mM to 1.0mM in 1M HCl. In the present work, Schiff bases were selected as inhibitors for this study. After immersion, the stoppered bottles are kept in a water bath which was maintained at respective temperature (40^0,50^0 and 60^0C) for 24 hour. After 24 hour, the metal specimens taken out and weights were measured. Weight loss measurements of CS specimens in the blank solution were also conducted at this temperature range.

The activation energy of corrosion with and without the inhibitor was calculated by Arrhenius equation

$$K = A \exp\left(-\frac{E_a}{RT}\right) \quad (9)$$

where K is the rate of corrosion, E_a the activation energy, A the frequency factor, T the temperature in Kelvin scale and R is the gas constant. Activation

energies can be determined from the slope of logK Vs 1000/T. Enthalpy and entropy of activation (ΔH*, ΔS*) were calculated from the transition state theory[69]

$$K = \left(\frac{RT}{Nh}\right) \exp\left(\frac{\Delta S*}{R}\right) \exp\left(\frac{-\Delta H*}{RT}\right) \quad (10)$$

where N is the Avogadros number and h is the Planks constant. A plot of log (K/T) Vs 1000/T gave straight lines with a slope of –ΔH*/R and an intercept (lnR/Nh+ΔS*/R) from which the values of ΔH* and ΔS* are calculated.

Electrochemical studies

The corrosion reaction takes place by the simultaneous occurrence of at least one anodic (metal oxidation) and one cathodic (e.g. reduction of dissolved oxygen or evolution of hydrogen) reaction. Because these partial reactions are charge-transfer processes, corrosion phenomena are essentially electrochemical in nature. Therefore electrochemical techniques have been used extensively in the study of corrosion phenomena, both to determine the corrosion rate and to define degradation mechanisms. The electrochemical method consumes short measurement time and the data provides mechanistic information which help not only in the development of corrosion protection strategies but also in the design of new inhibitors.

The measurement of corrosion rate is actually equivalent to the determination of kinetics of corrosion in electrochemical process. The common electrochemical methods used for the determination of corrosion rate and characteristics of corrosion system are electrochemical impedance spectroscopy and potentiodynamic polarization measurements.

Electrochemical impedance spectroscopy

Electrochemical Impedance Spectroscopy (EIS)[70-73] or ac impedance methods "have seen tremendous increase in popularity in recent years and used as powerful tool in corrosion and solid state laboratories. EIS measurements were carried out at different ac frequencies and, thus, the name impedance spectroscopy was later adopted. Analysis of the system response contains informations about the interface, its structure and reactions taking place there. The usefulness of impedance spectroscopy lies in the ability to distinguish the dielectric and electric properties of individual of components under investigation. The EIS experiment involves applying a small sinusoidal voltage or current perturbation around a steady-state value and measuring the resulting current or voltage along with the phase angle[74]. Using this data the real and imaginary impedances are calculated and plotted against each other for different perturbation frequencies which are called Nyquist impedance spectra. Although other types of plots-such as, the Bode plots, where the magnitude of the impedance and the phase angle are plotted against frequency, the Cole–Cole plots, where the squares of the real and imaginary impedances are plotted against each other-are also used in the literature, the Nyquist plots are the most common way of analysing impedance data. However, in Nyquist plots the frequency dependence of the impedance remains hidden. For this reason, Bode plots, which provide explicit information on the frequency dependence of the impedance, are often used.

The equivalent-circuits-based analysis involves reducing the transport processes into electrical analogues made of networks of resistors and capacitors, and sometimes, inductors. The values of the resistances and

capacitances are obtained by fitting the effective impedance of the network to experimental data. This method provides quick visualization tool to understand system behaviour and limitations".

Impedance spectroscopy is a "non-destructive technique and so can provide time dependent information about the properties but also about ongoing processes such as corrosion or the discharge of batteries and e.g. the electrochemical reactions in fuel cells, batteries or any other electrochemical process".

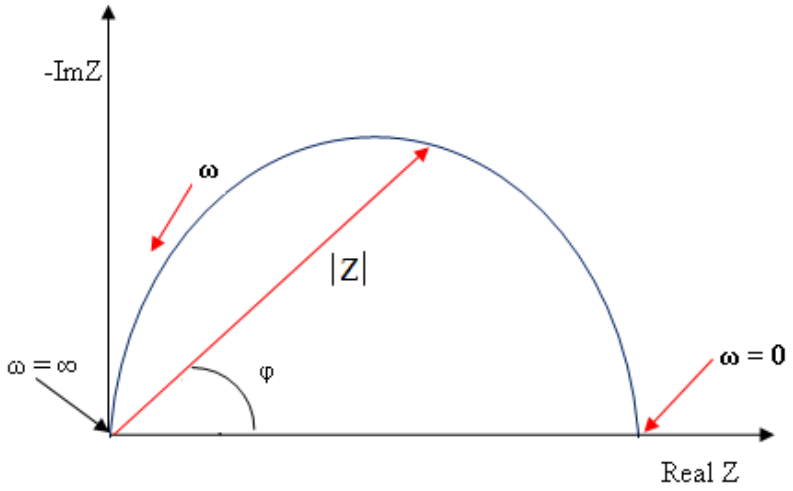

Fig. 2.1: Nyquist plot with impedance vector

An expression analogous to Ohm's Law allows us to calculate the impedance of the system as:

$$Z = \frac{E_t}{I_t} = \frac{E_0 \sin(\omega t)}{I_0 \sin(\omega t + \varphi)} = Z_0 \frac{\sin(\omega t)}{\sin(\omega t + \varphi)} \quad (11)$$

E_t is the potential at time t, E_0 is the amplitude of the signal, and ω is the radial frequency. I_t is the response signal, φ is the phase, I_0 is the amplitude.

The impedance is then represented as a complex number,

$$Z(\omega) = \frac{E}{I} = Z_0 exp(j\varphi) = Z_0(cos\ \varphi + jsin\ \varphi) \quad (12)$$

The expression for Z(ω) is composed of a real and an imaginary part. If the real part is plotted on the Z axis and the imaginary part on the Y axis of a chart, we get a "Nyquist plot" (Figure 2.1). "In this plot the y-axis is negative and that each point on the Nyquist plot is the impedance at one frequency. Figure 2.1 has been annotated to show that low frequency data are on the right side of the plot and higher frequencies are on the left. This is true for EIS data where impedance usually falls as frequency rises (this is not true of all circuits). On the Nyquist plot the impedance can be represented as a vector of length |Z|. The angle between this vector and the x-axis is φ.

The Nyquist plot in Figure 2.1 results from the electrical circuit of Figure 2.2. The semicircle is characteristic of a single "time constant". Electrochemical Impedance plots often contain several time constants. Often only a portion of one or more of their semicircles is seen.

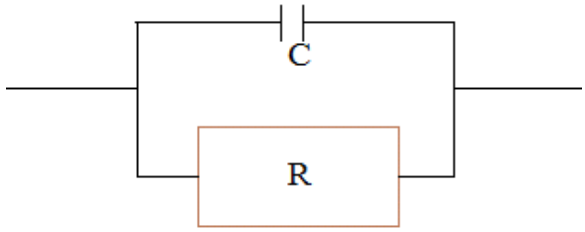

Fig. 2.2: Simple equivalent circuit with one time constant

Extracting parameters from data

EIS data is generally analyzed in terms of an equivalent circuit model. The analyst tries to find a model whose impedance matches the measured data. The type of electrical components in the model and their interconnections controls the shape of the model's impedance spectrum. The model's parameters (i.e. the resistance value of a resistor) control the size of each feature in the spectrum. Both these factors affect the degree to which the model's impedance spectrum matches a measured EIS spectrum.

Electrolyte resistance

Solution resistance is often a significant factor in the impedance of an electrochemical cell. A modern 3 electrode potentiostat compensates for the solution resistance between the counter and reference electrodes. However, any solution resistance between the reference electrode and the working electrode must be considered. The resistance of an ionic solution depends on the ionic concentration, type of ions, temperature and the geometry of the area in which current is carried.

Charge transfer resistance

A resistance is formed by a single kinetically controlled electrochemical reaction. Consider a metal substrate in contact with an electrolyte.

$$Red \Leftrightarrow Ox + ne^- \quad (13)$$

In the forward reaction in the equation (13), electrons enter the metal and metal ions diffuse into the electrolyte. Charge is being transferred. This charge transfer reaction has a certain speed which depends on the kind of reaction, the temperature, the concentration of the reaction products and the potential.

The general relation between the potential and the current is:

$$i = i_0\left(\frac{C_0}{C^{*0}}\exp\left(\frac{\alpha nF\eta}{RT}\right) - \left(\frac{C_R}{C^{*R}}\exp\left(\frac{-(1-\alpha)nF\eta}{RT}\right)\right)\right) \quad (14)$$

i_0 = exchange current density

C_0 = concentration of oxidant at the electrode surface

C^{*0} = concentration of oxidant in the bulk

C_R = concentration of reductant at the electrode surface

C^{*R} = concentration of reductant in the bulk

η = overpotential ($E_{app} - E_0$)

F = Faradays constant

T = temperature

R = gas constant

α = reaction order

n = number of electrons involved

When the concentration in the bulk is the same as at the electrode surface, C_0=C^{*0} and C_R=C^{R*}. This simplifies equation (14) into:

$$i = i_0(\exp\left(\alpha\frac{nF}{RT}\eta\right) - \exp\left(-(1-\alpha)\frac{nF}{RT}\eta\right) \quad (15)$$

This equation is called the Butler-Volmer[74,75] equation. It is applicable when the polarization depends only on the charge transfer kinetics. When the overpotential is very small and the electrochemical system is at equilibrium, the expression for the charge transfer resistance changes into:

$$R_{ct} = \frac{RT}{nFi_0} \quad (16)$$

From this equation the exchange current density can be calculated when Rct is known".

Constant phase element

Capacitors in EIS experiments often do not behave ideally. Instead, "they act like a constant phase element (CPE). The impedance of a capacitor has the form:

$$Z = A(j\omega)^{-\alpha} \quad (17)$$

When this equation describes a capacitor, the constant A = 1/C (the inverse of the capacitance) and the exponent α = 1. For a constant phase element, the exponent is less than one. The "double layer capacitor" on real cells often behaves like a CPE instead of like a capacitor. Several theories have been

proposed to account for the non-ideal behavior of the double layer but none has been universally accepted.

Randles Cell

The Randles cell is one of the simplest and most common cell models. It includes a solution resistance, a double layer capacitor and a charge transfer or polarization resistance. In addition to being a useful model in its own right, the Randles cell model is often the starting point for other more complex models. The equivalent circuit for the Randles cell is shown in figure 2.3. The double layer capacity is in parallel with the impedance due to the charge transfer reaction".

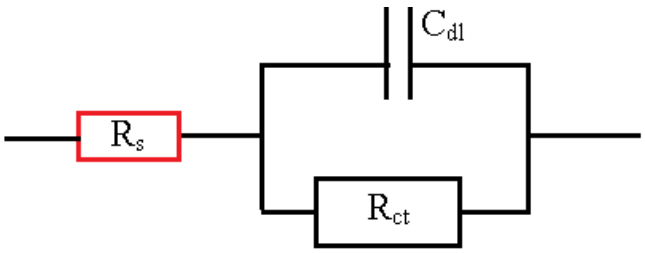

Fig. 2.3: Randles cell schematic Diagram

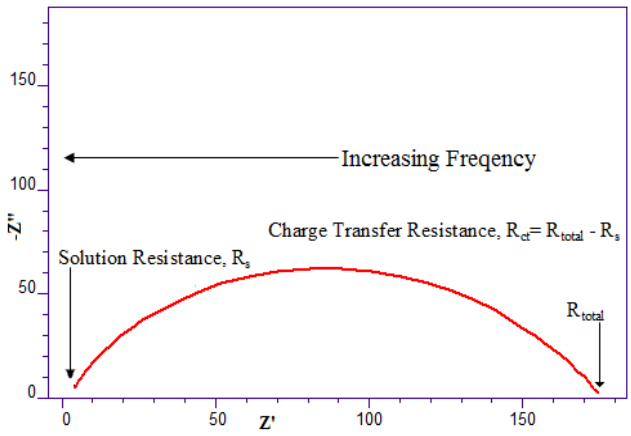

Fig. 2.4: Nyquist plot for a Randles cell

The Nyquist plot for a Randles cell is always a semicircle and shown in the figure 2.4. "The solution resistance (R_s) can found by reading the real axis value at the high frequency intercept. This is the intercept near the origin

of the plot. The real axis value at the other (low frequency) intercept is the sum of the polarization resistance (R_{ct} or R_p) and the solution resistance (R_s). The diameter of the semicircle is therefore equal to the polarization resistance (R_{ct} or R_p).

Knowledge of R_{ct} permits the calculation of inhibition efficiency of a molecule on the metal surface.

$$\eta_{EIS}\,\% = \frac{R_{ct} - R'_{ct}}{R_{ct}}\ X100 \qquad (18)$$

where R_{ct} and R'_{ct} are the charge transfer resistances of working electrode with and without inhibitor, respectively[77].

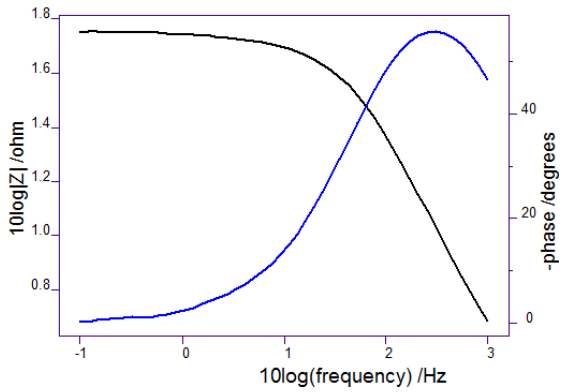

Fig. 2.5: Bode plot for a Randles cell

Another presentation method is the "Bode plot". The impedance is plotted with log frequency on the x-axis and both the absolute value of the impedance ($|Z| = Z_0$) and phase-shift on the y-axis. Figure 2.5 shows the Bode plot for the randles cell. The solution resistance and the sum of the solution resistance and the polarization resistance can be read from the magnitude plot. The phase angle does not reach 90° as it would for pure capacitive impedance. If the values for R_s and R_{ct} were more widely separated the phase would approach 90°".

Potentiodynamic polarization measurements

Whenever the potential of an electrode is forced away from its value at open circuit is referred to as "polarizing" the electrode. "The change of electrode potential is referred to as polarization and the deviation from the reversible electrode potential is called the over potential, η. Generally, polarization can be categorized as activation polarization and concentration polarization. Activation polarization is also called as charge transfer polarization, which is caused by the resistance generated when electrical charges transfer through double layer. Concentration polarization results from the concentration gradient produced between the interface of the electrode and the bulk solution. That is, the rate of electrochemical reaction is much faster than the diffusion of reactants from the bulk solution to the electrode interface, which makes the concentration of reactant, at electrode interface, less than that in the bulk solution. If only activation and concentration polarization are considered in an electrochemical system, the activation polarization is predominant within small polarization current/potential range. In comparison, concentration polarization is the dominant mechanism when the electrochemical system is polarized far from equilibrium. When the polarization current/potential is in the range of activation polarization, two areas, the linear polarization area and the Tafel area, are interesting for most corrosion researchers. The first one is located approximately ±10 mV from the equilibrium potential and the second one is around ±50 Mv".

Tafel equation and Tafel plots

The Tafel equation was first found empirically by Tafel in 1905[78]. This can be deduced from the equation (15) for sufficiently high values of applied

potential. "As over potentials, either positive or negative, become larger than about $5x10^{-2}$ V, the second or the first term of Butler-Volmer equation becomes negligible, respectively. In corrosion studies, the exchange current density, i_o in the equation (15) is referred to as the corrosion current. That is, $i_o = i_{corr}$ α k, where k is the corrosion rate. Hence determination of i_{corr} is fundamental importance.

For anodic polarization, when η >>RT/ (1-α) nF, the following equations are obtained.

$$i = i_{corr}[\exp\left(\alpha \frac{nF}{RT}\eta\right)] \quad (19)$$

$$\text{ie, } \eta = -\frac{2.303\,RT}{\alpha F}\log i_{corr} + \frac{2.303\,RT}{\alpha F}\log i \quad (20)$$

For cathodic polarization, when -η>> RT/αnF

$$i = i_{corr}[\exp\left(-(1-\alpha)\frac{nF}{RT}\eta\right)] \quad (21)$$

$$\text{i.e, } -\eta = -\frac{2.303\,RT}{(1-\alpha)F}\log i_{corr} + \frac{2.303\,RT}{(1-\alpha)F}\log i \quad (22)$$

The equations (20) and (22) have the form of Tafel equation as shown in the equation (23)

$$|\eta| = a + b\log i \quad (23)$$

where 'a' and 'b' are constants, $a = -\frac{2.303\,RT}{\alpha F}\log i_{corr}$ and $b = \frac{2.303\,RT}{\alpha F}$ for anodic polarization or $a = -\frac{2.303\,RT}{(1-\alpha)F}\log i_{corr}$ and $b = \frac{2.303\,RT}{(1-\alpha)F}$ for cathodic polarization.

Hence, simple exponential relationships between current i.e. rate and over potential are obtained, or the over potential can be considered as logarithmically dependent" on the current density [79,80].

Tafel slope analysis

A plot of electrode potential versus the logarithm of current density is called the "Tafel plot" and the resulting straight line, the "Tafel line". Tafel analysis is "performed by extrapolating the linear portions of a log current versus potential plot back to their intersection. The value of either the anodic or the cathodic current at the intersection" is I_{corr}. The slope of a Tafel plot, "b", provides information about the mechanism of the reaction. The intercept "a" at $\eta = 0$ gives the exchange current density i_0 and provides information about the rate constant of the reaction. This type of analysis is referred to as Tafel slope analysis. The percentage of inhibition efficiency ($\eta_{pol\%}$) was evaluated from the measured I_{corr} values using the following relation[81]

$$\eta_{pol}\,\% = \frac{I_{corr} - I'_{corr}}{I_{corr}} X100 \qquad (24)$$

where I_{corr} and I'_{corr} are the corrosion current densities of the exposed area of the working electrode in the absence and presence of inhibitor respectively. The figure 2.6 illustrate taffel slope analysis

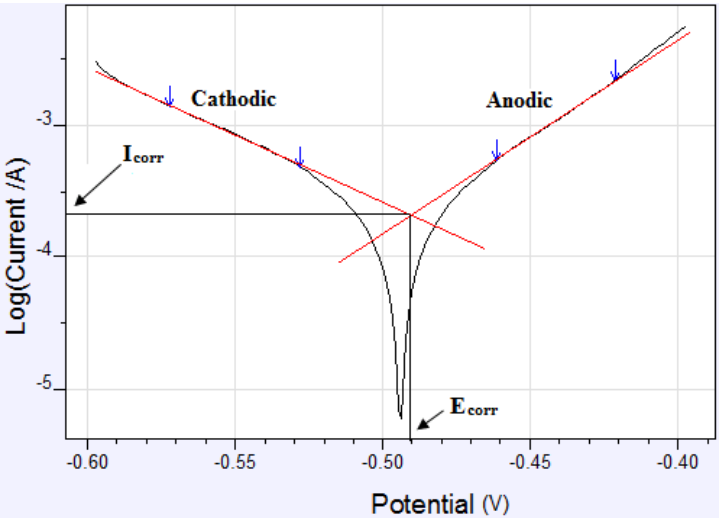

Fig. 2.6: Tafel plot

Linear polarization

A corroding metal in a solution takes up a potential, the corrosion potential, such that the rate of the anodic reaction of metal dissolution is equal to the rate of the cathodic reactions of hydrogen and/or oxygen reduction. If the "potential of the corroding metal is displaced slightly from the corrosion potential, E_{corr}, either by galvanostatic or potentiostatic polarisation, then the potential E is initially a linear function of the current density i (the current per unit area). This linear relationship holds for a potential displacement of up to 10 mV. The slope of the linear polarisation curve dE/di is termed the polarisation resistance R_p[82]. Slope can be determined by drawing a line that is tangential to the curve at E_{corr} and at zero current. The linear polarisation plot is shown in the figure 2.7.

In the corrosion inhibition studies, the rate of charge transfer process will be decreased as the inhibitor molecules adsorb on the surface of the corroding metal. This will cause to minimize the rate of corrosion or to increase the polarization resistance. From the slope analysis of the linear polarization curves in the vicinity of corrosion potential of blank and different concentrations of the inhibitor, the values of polarization resistance in the corrodent were obtained".

From the evaluated polarization resistance, the inhibition efficiency was calculated using the relationship

$$\eta_{R_p}\,\% = \frac{R'_p - R_p}{R'_p}\,X100 \qquad (25)$$

where R'_p and R_p are the polarization resistance in the presence and absence of inhibitor respectively[83] .

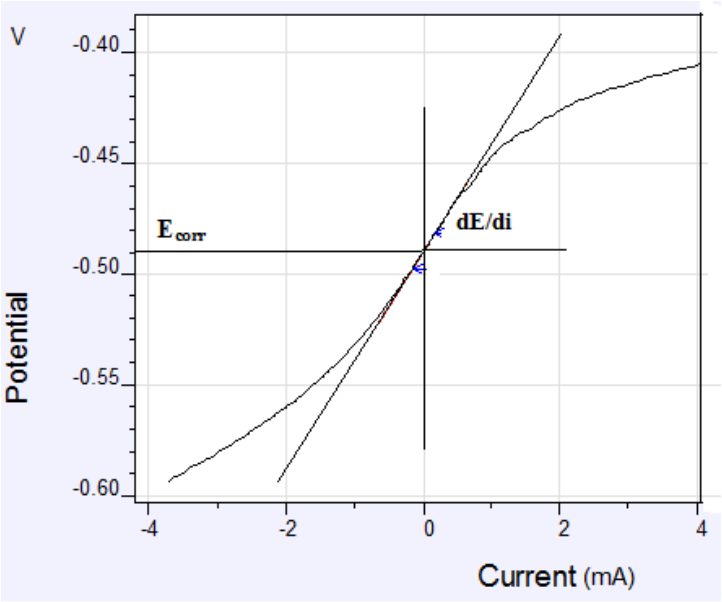

Fig. 2.7: Linear polarization plot

Instrumental setup and methods for electrochemical studies

The EIS measurements were performed in a three electrode assembly (figure 2.9). Saturated calomel electrode (SCE) was used as the reference electrode (RE). Platinum electrode having $1cm^2$ area was taken as counter electrode (CE).Metal specimens with an exposed area of $1cm^2$ were used as the working electrode (WE).

The EIS experiments were carried out on an Ivium compactstat-e electrochemical system connected to software "Ivium soft". 100 ml of 1M HCl and 100 ml of 0.5M H_2SO_4 (no deaereation, no stirring) were taken as the electrolyte and the working area of the metal specimens were exposed to the electrolyte for 1 h prior to the measurement. In the synergistic study, 2 ml of 0.2 mM KI solution was also added along with H_2SO_4. EIS measurements were performed at constant potential (OCP) in the frequency range from 1 KHz to 100 mHz with amplitude of 10 mV as excitation signal. The percentage of inhibitions from impedance measurements were calculated using

charge transfer resistance values by the expression (18). For the analysis of nyquist plot, open the corresponding plot in ivium programme, select the most fitted equivalent circuit and find out the EIS parameters.

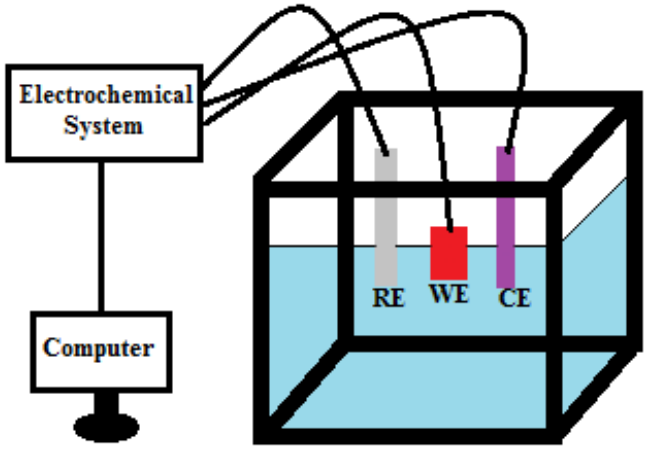

Fig. 2.8: Representation of instrumental set up for electrochemical studies

Potentiodynamic polarization studies on metal specimens in 1M HCl or 0.5M H_2SO_4 with and without inhibitor were performed by recording anodic and cathodic potentiodynamic polarization curves. Polarization plots were obtained in the electrode potential range from -100 to +100 mV versus equilibrium potential (E_{corr}) at a scan rate of 1mV/sec. Tafel polarization analysis were done by extrapolating anodic and cathodic curves to obtain corrosion current densities (I_{corr}). The percentage of inhibition efficiency ($\eta_{pol\%}$) was evaluated from the measured I_{corr} values using the relation (24).

From the slope analysis of the linear polarization curves in the vicinity of corrosion potential of blank and different concentrations of the inhibitor, the values of polarization resistance (R_p) in 1M HCl or 0.5M H_2SO_4 solution were obtained. From the evaluated polarization resistance, the inhibition efficiency was calculated using the relationship (25).

Scanning electron microscopy

Surface analyses were performed using scanning electron microscope (model Hitachi SU6600). SEM images were obtained from CS surface after the immersion in 1M HCl and 0.5M H_2SO_4 solutions in the absence and presence of the inhibitors (1mM) for 24 h at 30 ^{0}C. Also the SEM images of metal specimens in the presence of 0.5M H_2SO_4 with 1ml KI solutions were taken. The SEM images were utilized to study the surface morphology of the corroding metal which provides an insight to the mechanism of inhibition.

CHAPTER 3

CORROSION INHIBITION STUDIES ON AMINO ACIDS IN 1M HCl AND 0.5M H_2SO_4 ON CARBON STEEL

The inhibition effect of six amino acids on the corrosion of carbon steel in 1M HCl and 0.5M H_2SO_4 were studied by gravimetric measurements. The results obtained from the experimental studies are described in this chapter. These results are used for comparing the inhibition efficiencies of amino acids and their Schiff bases. The mechanism of inhibition was studied by adsorption isotherm analysis. The structural role of these inhibitors in preventing the corrosion of CS in acidic media was clearly established by this investigation. The results obtained from different analytical methods are tabulated and discussed below.

Weight loss studies

Weight loss of CS specimens in 1M HCl and 0.5M H_2SO_4 at 30^0C was determined at 24 h in the presence of various concentrations of amino acids β-Alanine (ALA), L-Arginine (ARG), L- Histidine (HIS), L- Phenyl Alanine (PHE), L- Tryptophan (TRP) and L- Cysteine (CYS). The corrosion rates, inhibition efficiencies (η_w%) and surface coverage (θ) were determined from weight loss measurements.

Corrosion rates studies in HCl medium

Table 2.1 shows the corrosion rates determined by weight loss studies for CS specimens immersed in 1M HCl medium for 24 h in the presence and absence of different concentrations of amino acids. The comparison of corrosion rate of CS in the presence of varying concentration of amino acids in HCl medium for 24 h is shown in figure 2.9. The figure clearly establishes that

the corrosion rates markedly decreased with inhibitor concentration from 0 to 0.2mM. Beyond this concentration, corrosion rate showed a gradual decrease. A corrosion rate of 6.5 mm/year was observed for blank and all the CS specimens showed corrosion rates below 6.5 mm/year in the presence of amino acids.

Table. 2.1. Corrosion rates of CS at different concentrations of amino acids for 24 h in 1M HCl medium at 30^0C.

C (mM)	Corrosion Rate (mm/year)					
	ALA	**ARG**	**HIS**	**TRP**	**PHE**	**CYS**
Blank	6.5					
0.2	3.69	4.32	3.58	3.59	4.13	3.46
0.4	3.55	4.13	3.40	3.41	3.95	3.04
0.6	3.42	3.94	3.16	3.27	3.67	2.75
0.8	3.27	3.84	3.02	3.05	3.46	2.51
1.0	3.14	3.66	2.72	2.79	3.25	2.28

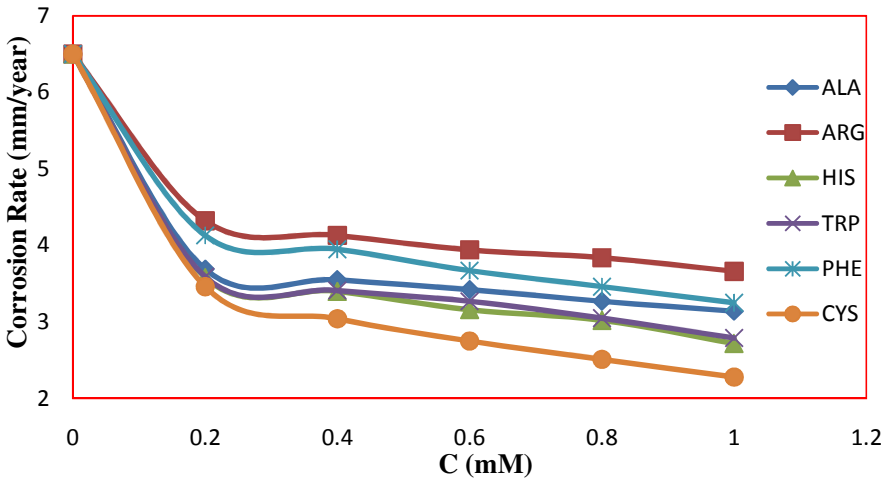

Fig. 2.9: Corrosion rates of CS in 1M HCl with and without the amino acids

From table 2.1 it is evident that the corrosion rates of CS showed less than 4 mm/ year in the presence of all amino acids except ARG. A maximum corrosion rate of 3.66 mm/year was observed for CS in the presence of ARG at 1.0mM concentration. At a concentration of 1.0mM of PHE, corrosion rate of CS was 3.25 mm/year and the corrosion rates shown by CS in the presence

of ALA, HIS, TRP and CYS were 3.14, 2.72, 2.79, and 2.28 mm/year respectively. Comparing the corrosion rates of CS in the presence of amino acid at a concentration of 1.0mM, the amino acid ARG showed higher corrosion rate and CYS the least value.

Corrosion inhibition efficiency of amino acids on CS in HCl medium

To calculate the percentage of inhibition efficiency, corrosion rates of CS in the presence and absence of amino acids were taken. Table 2.2 shows the percentage inhibition values obtained for amino acids on CS immersed in 1M HCl medium for 24 h. From the table it is clear that the all amino acids except ARG showed the inhibition values (η_w%) above 50% for 1.0mM concentration but ARG showed 43.78% of inhibition efficiency at the same concentration. Comparison of percentage inhibition efficiencies of amino acids is represented in the figure 2.10. It is apparent from the figure that inhibition efficiency increases with increasing concentration. Comparing the inhibition capacities of amino acids studied for the maximum concentration of 1.0mM, the amino acid ARG showed lower inhibition capacity and CYS exhibited higher inhibition capacity. The inhibition capacity of amino acids increases in the order ARG < PHE ≤ ALA < TRP ≤HIS < CYS for the maximum concentration of 1.0mM.

Table. 2.2. Corrosion inhibition efficiencies at different concentrations of amino acids on CS for 24 h in 1M HCl medium at 30^0C.

C (mM)	Inhibition Efficiency (η_w%))					
	ALA	ARG	HIS	TRP	PHE	CYS
0.2	43.22	33.65	44.94	44.84	36.47	46.73
0.4	45.47	36.53	47.76	47.60	39.25	53.19
0.6	47.38	39.38	51.40	49.73	43.52	57.68
0.8	49.75	41.03	53.53	53.04	46.86	61.39
1.0	51.79	43.78	58.21	57.16	50.05	64.90

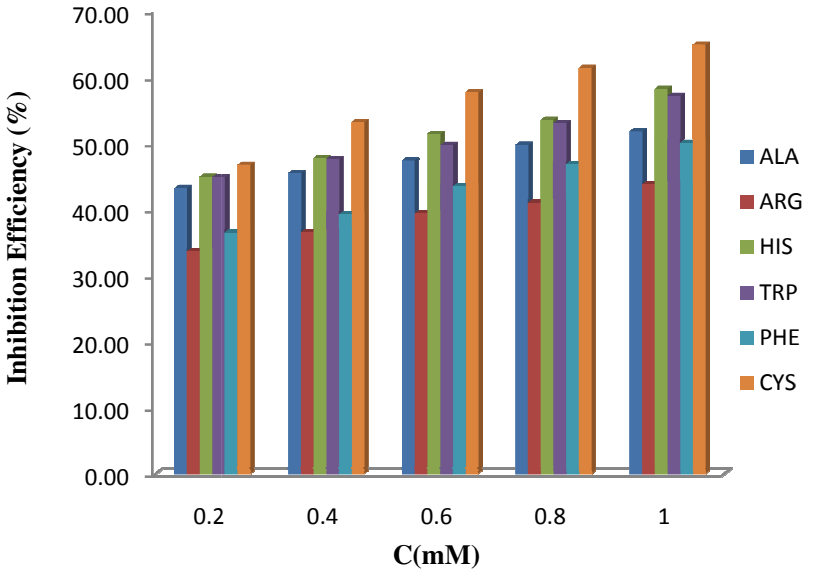

Fig. 2.10: Percentage inhibition efficiencies of amino acids in 1M HCl medium

Adsorption isotherm studies in HCl medium

The adsorption behaviour of amino acids on the metal surface was studied in order to understand the mechanism of corrosion. Surface coverage (θ) can be calculated from the percentage inhibition values using the equation (7). Table 2.3 describes the surface coverage obtained for different concentration of amino acids for 24 h in 1M HCl at 30^0C. The values of surface coverage (θ) represented graphically by fitting into various adsorption isotherms like Freundlich, Langmuir, Temkin and Frumkin.

Table. 2.3. Surface coverage at different concentrations of amino acids on CS for 24 h in 1M HCl medium at 30^0C.

C (mM)	Surface Coverage (θ)					
	ALA	**ARG**	**HIS**	**TRP**	**PHE**	**CYS**
0.2	0.44	0.34	0.45	0.45	0.36	0.47
0.4	0.45	0.37	0.48	0.48	0.39	0.53
0.6	0.47	0.39	0.51	0.50	0.44	0.58
0.8	0.50	0.41	0.54	0.53	0.47	0.61
1.0	0.52	0.44	0.58	0.57	0.50	0.65

Among the isotherms considered, Langmuir isotherm found to provide best description of the adsorption behaviour of the studied amino acids in HCl medium. The different adsorption isotherms are shown in the figures 2.11 to 2.16.

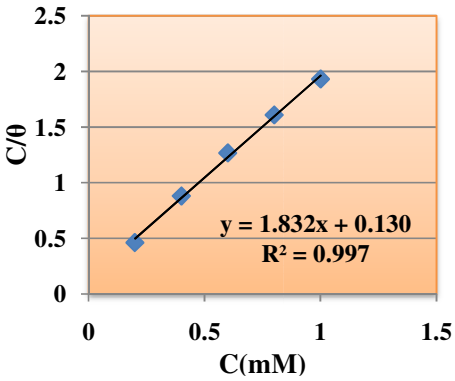

Fig. 2.11: Langmuir adsorption isotherm for adsorption of ALA on CS surface in 1M HCl

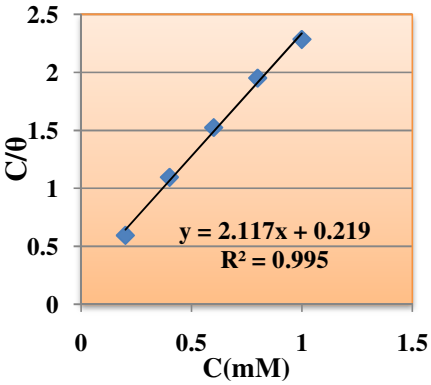

Fig. 2.12: Langmuir adsorption isotherm for adsorption of ARG on CS surface in 1M HCl

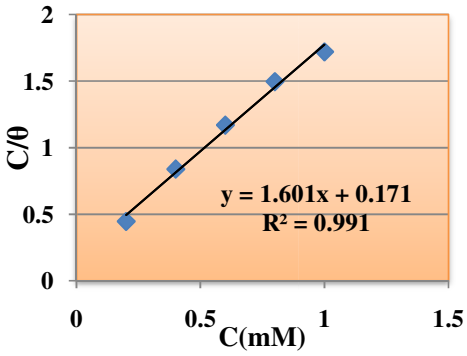

Fig. 2.13: Langmuir adsorption isotherm for adsorption of HIS on CS surface in 1M HCl

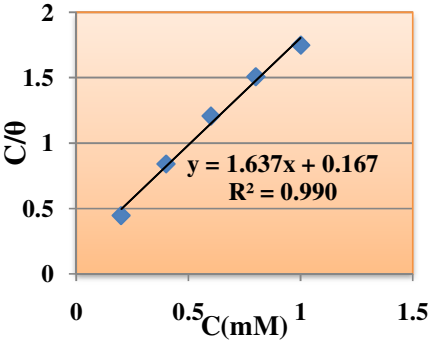

Fig. 2.14: Langmuir adsorption isotherm for adsorption of TRP on CS surface in 1M HCl

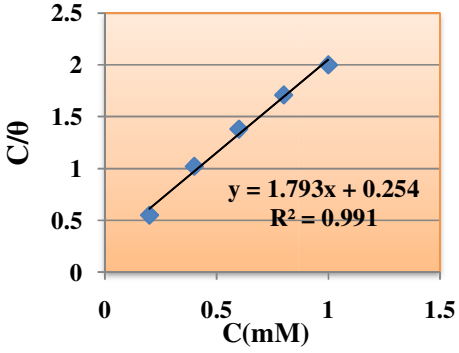

Fig. 2.15: Langmuir adsorption isotherm for adsorption of PHE on CS surface in 1M HCl

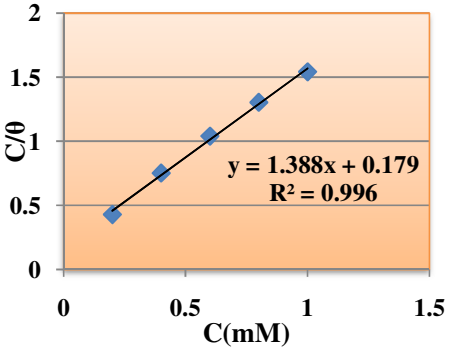

Fig. 2.16: Langmuir adsorption isotherm for adsorption of CYS on CS surface in 1M HCl

Table. 2.4. Thermodynamic parameters for the adsorption of amino acids on CS in 1M HCl

Amino acid	Isotherm	K_{ads}	ΔG^0_{ads}(kJ/mol)
ALA	Langmuir	7680	-32.61
ARG	Langmuir	4566	-31.30
HIS	Langmuir	5848	-31.92
TRP	Langmuir	5988	-31.98
PHE	Langmuir	3937	-30.93
CYS	Langmuir	5562	-31.79

The values of free energy of adsorption ($\Delta G^0_{ads)}$ from the adsorption isotherms in 1M HCl is shown in the table 2.4. The large negative values of ΔG^0_{ads} indicate that adsorptions of amino acids were spontaneous in HCl medium[84]. The ΔG^0_{ads} values calculated were fall in the range of -30 to -33 kJ mol^{-1}. Generally, values of ΔG^0_{ads} around -20 kJ mol^{-1} or lower are consistent with the electrostatic interaction between the charged molecules and the charged metal (physisorption); those around -40 kJ mol^{-1} or higher involve charge sharing or charge transfer from organic molecules to the metal surface so as to form a coordinate type of bond (chemisorption)[85]. The calculated ΔG^0_{ads} value showed, therefore, that the adsorption mechanism of amino acids on carbon steel involves both two types of interaction. Indeed, due to the strong adsorption of water molecules on the surface of carbon steel, one can assume that adsorption occurs first due to the physical force. The removal of water molecules from the surface is accompanied by strong interaction between the metal surface and adsorbate and that may turns to chemisorptions[86].

Corrosion rates in H_2SO_4 medium

The table 2.5 shows the corrosion rates determined by weight loss studies for CS specimens immersed in 0.5M H_2SO_4 medium for 24 h in the presence and absence of different concentration of amino acids. The variation

of corrosion rate with the concentration of amino acids in H_2SO_4 medium for 24 h is shown in figure 2.17. From the figure it is clear that the corrosion rates noticeably decreased with inhibitor concentration from 0 to 0.2mM. After this concentration, corrosion rate showed a gradual decrease. The blank solution showed a corrosion rate of 24.0 mm/year. It is evident from the table 2.5 that, the corrosion rates of CS in the presence of six amino acids were not so much differences among themselves. The corrosion rate of CS in the presence of all amino acids except CYS falls in the range of 15-20 mm/year for the concentration range 0.2mM-1.0mM. The amino acid CYS shows the corrosion rate in the range of 17-10 mm/year for the concentration range 0.2mM-1.0mM. The corrosion rate of CS observed for ALA, ARG, HIS, TRP, PHE and CYS are 15.29, 15.01, 15.49, 16.08, 17.13 and 10.88 mm/year respectively at a concentration of 1.0mM. For the concentration of 0.8mM and 1.0mM, the corrosion rate of CS in the presence of ARG, HIS, TRP, and PHE are almost same. Among the studied amino acids, it is noticed that CS shows highest corrosion rate in the presence of PHE while the lowest value in the presence of CYS, at a concentration of 1.0 mM.

Table. 2.5. Corrosion rates of CS at different concentrations of amino acids for 24 h in 0.5M H_2SO_4 medium at 30^0C.

C	Corrosion Rate (mm/year)					
(mM)	ALA	ARG	HIS	TRP	PHE	CYS
Blank	24.00					
0.2	19.50	17.23	17.82	18.32	19.72	16.90
0.4	18.59	16.46	17.15	17.69	19.24	14.97
0.6	17.60	15.70	16.51	17.16	18.61	12.70
0.8	16.59	15.39	16.08	16.34	17.99	11.80
1.0	15.29	15.01	15.49	16.08	17.13	10.88

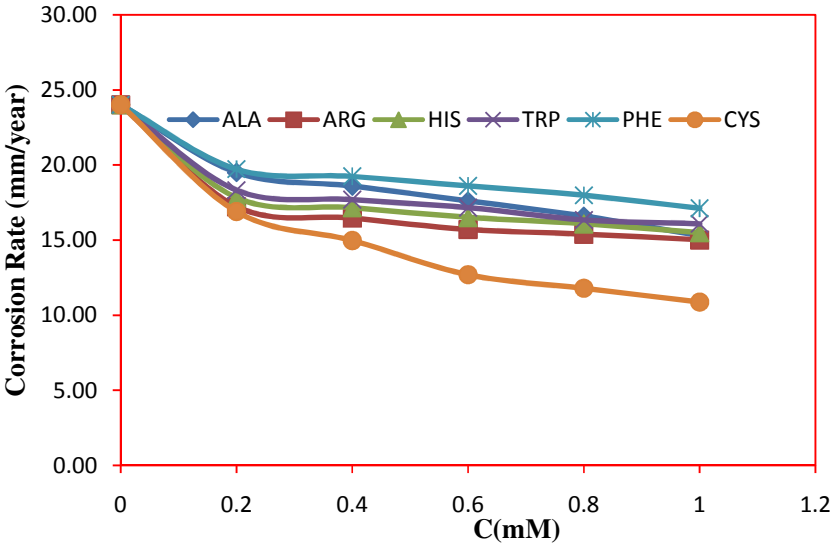

Fig. 2.17: Corrosion rates of CS in 0.5M H_2SO_4 with and without the amino acids

Corrosion inhibition studies of amino acids on CS in H_2SO_4 medium

Table 2.6 shows the percentage inhibition values obtained for CS specimens immersed in 0.5M H_2SO_4 medium for 24 h in the presence of different concentrations of amino acids. The percentage inhibition values of ALA, ARG, HIS, TRP, PHE and CYS are 36.30, 37.49, 35.49, 33.00, 28.65, and 54.67 respectively for the maximum concentration of 1.0mM. The figure 2.18 shows the comparison of percentage inhibition efficiencies of amino acids.

Table. 2.6. Corrosion inhibition efficiencies at different concentrations of amino acids on CS for 24 h in 0.5M H_2SO_4 medium at 30^0C.

C	Inhibition Efficiency (mm/year)					
(mM)	ALA	ARG	HIS	TRP	PHE	CYS
0.2	18.79	28.21	25.76	23.70	17.87	29.62
0.4	22.54	31.43	28.55	26.30	19.87	37.65
0.6	26.68	34.61	31.23	28.52	22.46	47.11
0.8	30.89	35.88	33.02	31.91	25.06	50.83
1.0	36.30	37.49	35.49	33.00	28.65	54.67

It is apparent from the figure that inhibition efficiency increases with increase in concentration. Comparing the inhibition capacities of amino acid at a concentration of 1.0 mM, PHE showed lower inhibition capacity and CYS displayed higher inhibition capacity on CS surface. The inhibition capacity of amino acids increases in the order PHE < TRP < HIS ≤ ALA≤ ARG < CYS for the maximum concentration 1.0mM.

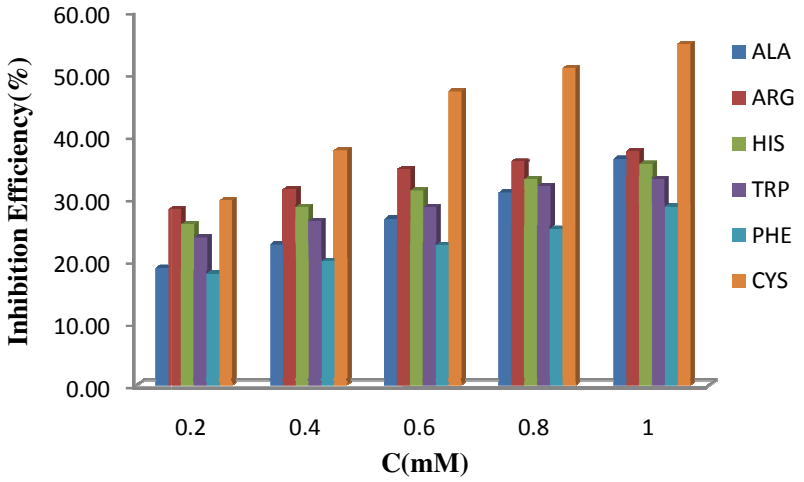

Fig. 2.18: Percentage inhibition efficiencies of amino acids in 0.5M H_2SO_4 medium

Adsorption isotherm studies in H_2SO_4 medium

The amino acids compounds inhibit the corrosion of the carbon steel by adsorbing on the metal surface in acid solution. A useful method that assists in the understanding the mechanism of corrosion inhibition is to study the adsorption isotherm. The values of surface coverage (θ) corresponding to different concentrations of the inhibitor have been used to determine the adsorption isotherm (table 2.5). Among the isotherm considered, ALA and PHE followed Freundlich adsorption isotherm and other amino acids obeyed Langmuir adsorption isotherm. The different adsorption isotherms are exhibited in the figures 2.19 to 2.24.

Table. 2.7. Surface coverage obtained at different concentrations of amino acids on CS for 24 h in 0.5M H_2SO_4 medium at 30^0C.

C (mM)	Surface Coverage (θ)					
	ALA	ARG	HIS	TRP	PHE	CYS
0.2	0.19	0.28	0.26	0.24	0.18	0.30
0.4	0.23	0.31	0.29	0.26	0.20	0.38
0.6	0.27	0.35	0.31	0.29	0.22	0.47
0.8	0.31	0.36	0.33	0.32	0.25	0.51
1.0	0.36	0.37	0.35	0.33	0.29	0.55

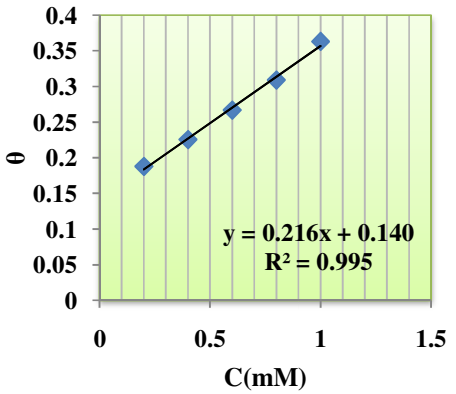

Fig. 2.19: Freundlich adsorption isotherm for adsorption of ALA on CS surface in 0.5M H_2SO_4

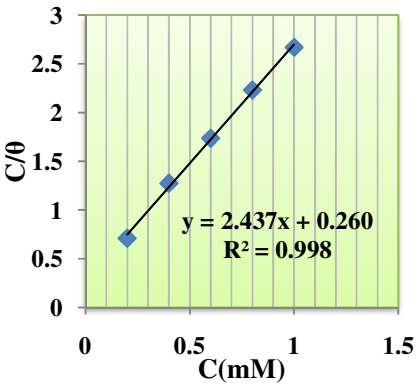

Fig. 2.20: Langmuir adsorption isotherm for adsorption of ARG on CS surface in 0.5M H_2SO_4

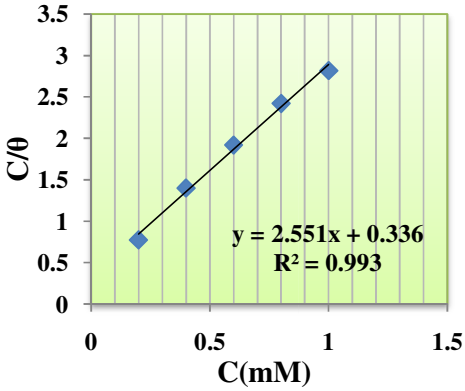

Fig. 2.21: Langmuir adsorption isotherm for adsorption of HIS on CS surface in 0.5M H_2SO_4

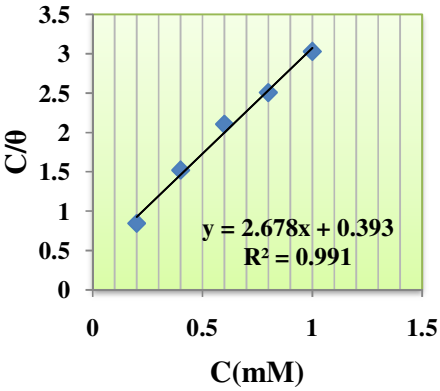

Fig. 2.22: Langmuir adsorption isotherm for adsorption of TRP on CS surface in 0.5M H_2SO_4

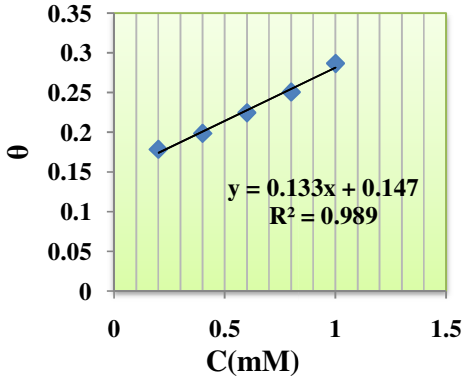

Fig. 2.23: Freundlich adsorption isotherm for adsorption of PHE on CS surface in 0.5M H_2SO_4

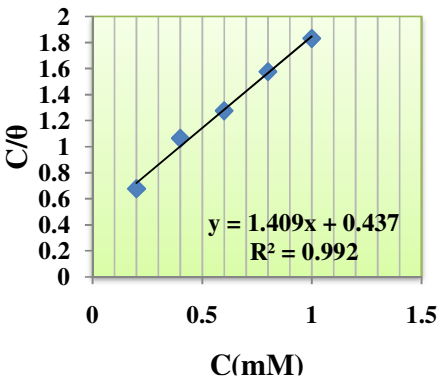

Fig. 2.24: Langmuir adsorption isotherm for adsorption of CYS on CS surface in 0.5M H_2SO_4

Table. 2.8. Thermodynamic parameters for the adsorption of amino acids on CS in 0.5M H_2SO_4

Amino acid	Isotherm	K_{ads}	ΔG^0_{ads}(kJ/mol)
ALA	Freundlich	216.9	-23.63
ARG	Langmuir	3841.72	-30.87
HIS	Langmuir	2976.19	-30.23
TRP	Langmuir	2540.00	-29.83
PHE	Freundlich	133.8	-22.42
CYS	Langmuir	5561.73	-29.57

The free energy change for the adsorption process (ΔG^0_{ads}) for the different inhibitors at 30^0C were calculated and are given in table 2.8. It is clear from table, that the adsorption free energies have negative values between -40 kJ mol^{-1} and -20 KJ mol^{-1}, meaning that the adsorption of the inhibitor molecules on CS surface in sulphuric acid is spontaneous and there exists the electrostatic and chemical interactions between the charged inhibitor molecules and the charged metal surface.

Mechanism of inhibition

Organic inhibitors protect the metal by forming a hydrophobic film on the metal surface. The effectiveness of an inhibitor depends on the chemical composition, its molecular structure and affinity for the metal

surface. The protective films of adsorbed molecules on the surface provide a barrier to the dissolution of the metal in the electrolyte.

The mechanism anodic dissolution of iron can be represented as follows.

i) In aqueous solutions

$$Fe + H_2O \leftrightarrow [FeOH]_{ads} + H^+ + e^- \quad (26)$$

$$[FeOH]_{ads} \leftrightarrow [FeOH]^+_{ads} + e^- \quad (27)$$

$$[FeOH]^+_{ads} + H^+ \leftrightarrow Fe^{2+} + H_2O \quad (28)$$

ii) In aqueous solution containing A^- ions (A= Cl^-, or SO_4^{2-}) ions

$$Fe + H_2O + A^- \leftrightarrow [FeAOH]^-_{ads} + H^+ + e^- \quad (29)$$

$$[FeAOH]^-_{ads} \leftrightarrow [FeAOH]_{ads} + e^- \quad (30)$$

$$[FeAOH]_{ads} + H^+ \leftrightarrow Fe^{2+} + A^- + H_2O \quad (31)$$

where $[FeOH]_{ads}$ and $[FeAOH]^-_{ads}$ are the adsorbed intermediates which are involved in the rate determining step (Equations 27 and 30, respectively) of carbon steel dissolution according to mechanism (i) and (ii), respectively.

The cathodic hydrogen evolution mechanism can be illustrated by the following equations

$$Fe + H^+ \leftrightarrow (FeH^+)_{ads} \quad (32)$$

$$(FeH^+)_{ads} + e^- \leftrightarrow (FeH)_{ads} \quad (33)$$

$$(FeH)_{ads} + H^+ + e^- \leftrightarrow Fe + H_2 \quad (34)$$

The protonated inhibitor molecules adsorb at cathodic sites in competition with hydrogen ions and hence reduce the H_2 gas evolution.

From the results obtained from weight loss measurements, it was concluded that the amino acids inhibit the corrosion of carbon steel in 1M HCl and 0.5M H_2SO_4 by adsorption at metal solution interface. As the concentration increases, the number of inhibitor molecule on the metal surface increases through adsorption and thus surface coverage also increases. As a result, the inhibitor molecule blocks the corrosion reaction and rate of corrosion decreases with the inhibitor concentration from 0mM to 1.0mM. The amino acid molecules may adsorb on the metal surface in four different ways such as

i. Electrostatic interaction between the charged molecules and the charged metal,
ii. Interaction of unshared electron pairs in the molecule with the metal,
iii. Interaction of pi-electrons with the metal and
iv. A combination of types (i-iii).

The adsorption process of inhibitor molecules mainly depends on the number of adsorption sites on the metal surface, charge density on molecules, molecular size and interaction mode with the metallic surface[87]. In acidic solutions, the amino acid molecules exists in the protonated form ($–NH_2$ group of amino acid in acid medium is readily protonated) and could adsorb on the metal surface through the nitrogen, the oxygen or sulphur atoms, which form a barrier on the metallic surface and decreasing the corrosion rate appreciably. The maximum inhibition efficiency of CYS on CS corrosion in HCl and H_2SO_4 is probably as the consequence of its adsorption on the metal surface as a bidentate ligand in which surface coordination is taking place through both the amino group and the –S– moiety[88]. TRP may be adsorbed via donor-

acceptor interactions between the π electrons of the indole rings and the unshared electron pairs of the heteroatom, to form a bond with vacant d-orbital of the metal surface[89]. Similarly in HIS, π electrons of the imidazole group and the unshared electron pair interact with the empty d- orbital of the metal atom. In the case of phenylalanine, the phenyl- ring could impart a steric hindrance, which adversely affects the adsorption of the organic molecule on CS surface and thus shows lower inhibition efficiency. ALA and ARG may interact with the metal surface by its cationic form. The molecular structure of the amino acids and schematic presentation of the mode of adsorption of amino acids on the metal surface are shown in the figure 2.25 and figure 2.26 respectively.

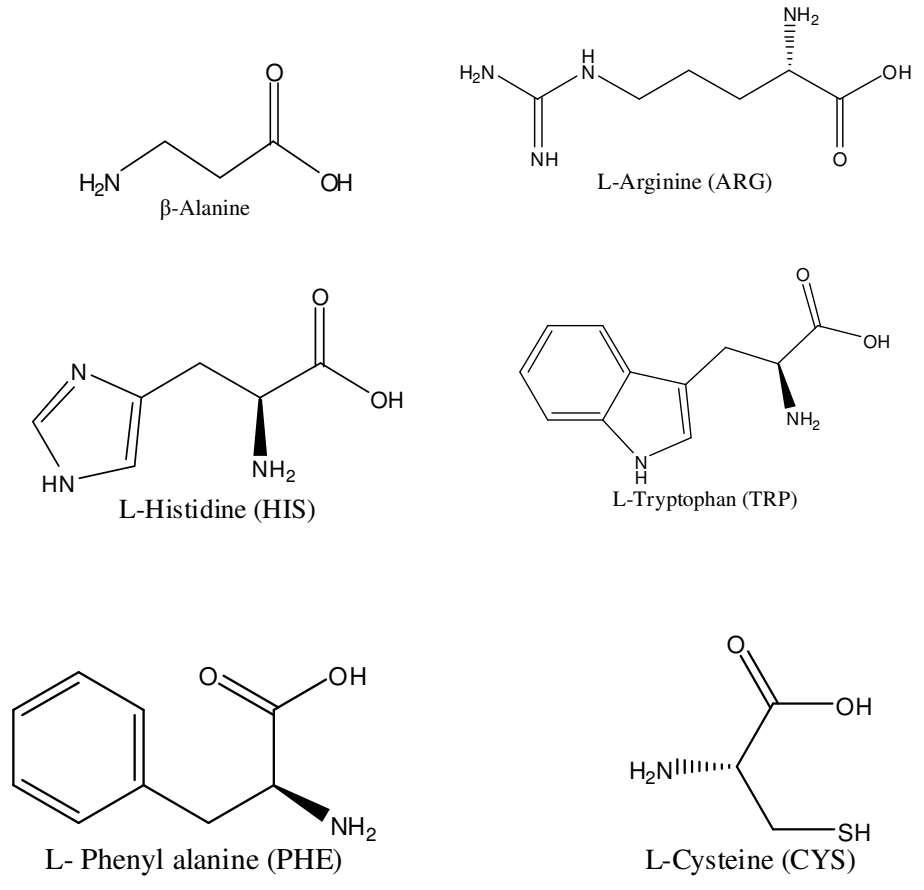

Fig. 2.25: Molecular structures of amino acids

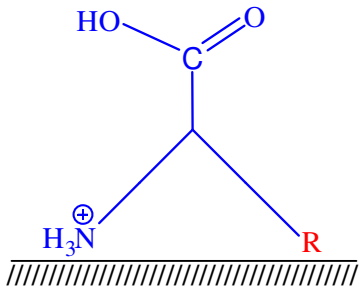

Where 'R' group represents:

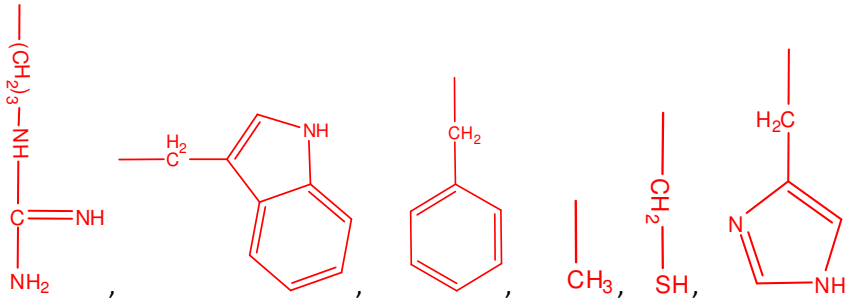

Fig. 2.26: Schematic representation of the mode of adsorption of amino acids over the metal surface

Corrosion inhibition efficiency of amino acids in 1M HCl and 0.5M H_2SO_4 – A comparative study

The figure 2.27 illustrate the comparative study on corrosion inhibition efficiency at 1.0mM concentrations of amino acids in 1M HCl and 0.5M H_2SO_4.

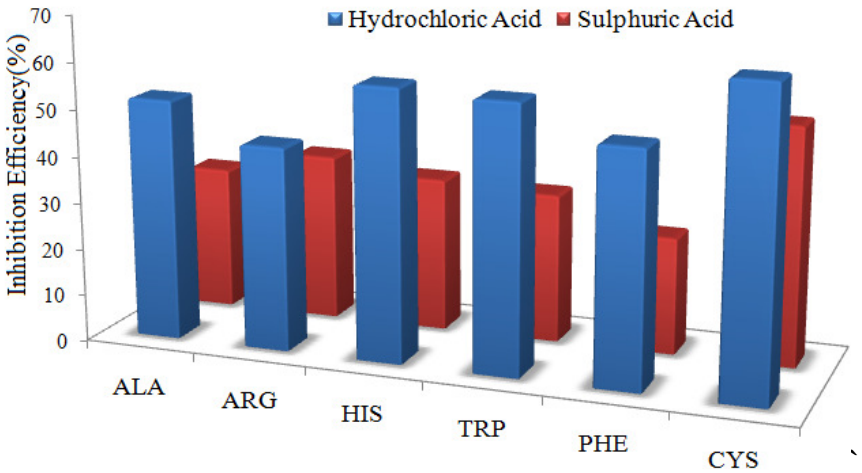

Fig. 2.27: Comparative study on corrosion inhibition efficiency of amino acids in 1M HCl and 0.5M H_2SO_4

When comparing the inhibition efficiencies of amino acids in HCl and H_2SO_4, it is clear that all the amino acids exhibit higher inhibition efficiency in HCl medium than in H_2SO_4. It is believed that the Cl^- ions can more strongly adsorb than SO_4^{2-} on the metal surface and creates an excess of negative charge on metal surface. This will favor the adsorption of protonated amino acids, more on the Cl^- adsorbed metal surface and hence reduce the dissolution of Fe to Fe^{2+}.

Moreover the aggressive nature of H_2SO_4 is higher than that of HCl (due to two H^+ ions) which leads to the increased corrosion rate of carbon steel. This may be the second factor which cause to lowering of corrosion inhibition efficiency of amino acids in H_2SO_4 medium.

Therefore in short, corrosion inhibition efficiency of the amino acid in 1M HCl medium is quite higher (≈ 60 %) than that in 0.5M H_2SO_4 medium (≈ 40 %).

CHAPTER 4

CORROSION INHIBITION STUDIES ON SCHIFF BASES IN 1M HCl ON CARBON STEEL

Corrosion inhibitors are of considerable practical importance, as they are extensively employed in reducing metallic waste during production and in minimizing the risk of material failure, both of which can result in the sudden shut-down of industrial processes, which in turn leads to added costs. Like most chemical reactions, the rate of corrosion of iron and steel increases with temperature especially in media in which evolution of hydrogen accompanies corrosion. Acid pickling of steel is usually carried out at elevated temperature up to 60°C in hydrochloric acid solutions. Accordingly, pickling inhibitors are expected to be chemically stable to provide high protective efficiency under the conditions mentioned above. Schiff bases have been reported to be effective inhibitors for the corrosion of steel in acid media by several authors. The corrosion inhibition efficiency of synthesized Schiff bases is monitored using different analytical methods and the results are well documented in this chapter.

The results of inhibition efficiency and temperature effects on carbon steel corrosion in 1M HCl solutions in the absence and presence of various concentrations of synthesized Schiff bases using gravimetric method, EIS and potentiodynamic polarization method are determined and discussed. Various thermodynamic parameters for inhibitor adsorption on carbon steel surface were estimated and explained. Kinetic parameters for carbon steel corrosion in the absence and presence of the inhibitors were evaluated and interpreted in this chapter.

Weight loss studies

Weight loss measurements grant the most consistent results regarding the efficiency of given inhibitor compound. So the synthesized six Schiff bases A9Y3APA, A9Y5GPA, A9Y3IMPA, A9Y3INPA, A9Y3PPA and A9Y3MPA were subjected to weight loss studies before performing electrochemical analysis. The loss in the weight of CS specimens in 1M HCl at 30^0C was determined at 24 h in the presence of various concentrations of Schiff bases. From this data, the corrosion rates, inhibition efficiencies and surface coverage (θ) were calculated.

Corrosion rates studies in HCl medium

The corrosion rates determined by the weight loss studies of CS specimens immersed in 1M HCl medium for 24 h in the presence and absence of different concentrations of Schiff bases are presented in the table 2.9. Figure 2.28 depicts the variation of corrosion rate with the concentration of Schiff bases in HCl medium for 24 h.

Table. 2.9. Corrosion rates of CS at different concentrations of Schiff bases for for 24 h in 1M HCl medium at 30^0C.

C	Corrosion Rate (mm/year)					
(mM)	A9Y3APA	A9Y5GPA	A9Y3IMPA	A9Y3INPA	A9Y3PPA	A9Y3MPA
Blank	6.50					
0.2	3.48	3.44	1.60	0.95	2.80	0.77
0.4	3.10	2.91	1.28	0.67	2.33	0.47
0.6	2.50	2.38	0.92	0.46	1.74	0.42
0.8	1.59	1.97	0.79	0.40	1.11	0.35
1.0	1.04	1.72	0.47	0.38	0.50	0.28

From the analysis of figure it is clear that the corrosion rate markedly decreased with inhibitor concentration from 0 to 0.2mM. Corrosion rate

showed a gradual decrease after the concentration 0.2mM, i.e., the corrosion rates of CS decreased with the Schiff bases concentration. Corrosion rate of CS in the absence of Schiff base was 6.5 mm/year and it was considerably lowered in the presence of all Schiff bases.

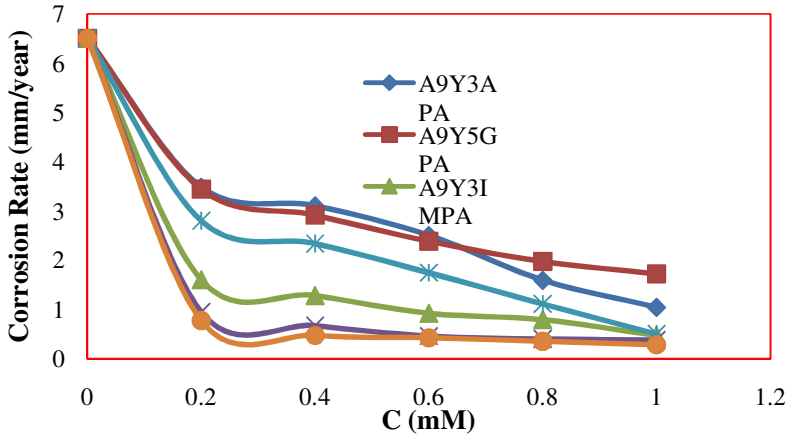

Fig. 2.28: Corrosion rate of CS in 1M HCl with and without Schiff base at 30^0C for 24 h.

From table 2.9, comparing the corrosion rates of CS in the presence of various concentrations of Schiff bases, it is quite evident that, corrosion rates are below 3.50 mm/year in the presence of Schiff bases. The corrosion rate of CS in the presence of A9Y5GPA is slightly lower than the values of A9Y3APA for the concentration 0.2mM, 0.4mM and 0.6mM. For the concentrations 0.8mM and 1.0mM the corrosion rates of CS in the presence of A9Y5GPA are higher than the values of A9Y3APA. The maximum corrosion rate of 1.72 mm/year was observed in the presence of A9Y5GPA at 1.0mM concentration. In the case of A9Y3APA inhibitor at a concentration of 1.0mM, the value of corrosion rate of CS was 1.04 mm/year and the corrosion rate of CS in the presence of A9Y3MPA, A9Y3INPA, A9Y3PPA and A9Y3MPA are 0.47, 0.38, 0.50, 0.28 mm/year respectively at a concentration of 1.0mM. The corrosion rate of CS in the presence of A9Y5GPA showed higher value and

showed lower value in the presence of A9Y3MPA at the concentration of 1.0mM.

Corrosion inhibition efficiency of Schiff bases on CS in HCl medium

The corrosion inhibition efficiency (η_w%) can be calculated from the corrosion rates as described in the chapter 2. Table 2.10 shows the percentage inhibition values for Schiff bases on CS specimens immersed in 1M HCl medium for 24 h. From the table it is clear that the inhibition efficiency increases with increase in concentration of Schiff bases. The three Schiff bases A9Y3IMPA, A9Y3INPA and A9Y3MPA showed the inhibition efficiency above 75% for the concentration ranges 0.2mM to 1.0mM. All the Schiff bases except A9Y3APA and A9Y5GPA showed inhibition efficiency values above 90% for the maximum concentration 1.0mM. The inhibition efficiency of A9Y3APA and A9Y5GPA were 83.98% and 73.50% respectively for the concentration of 1.0mM.

Comparison of percentage inhibition efficiencies of Schiff bases showed in the figure 2.29. At a concentration of 1.0mM, the corrosion inhibition efficiency of Schiff bases on CS increases in the following order A9Y5GPA < A9Y3APA <A9Y3PPA ≤ A9Y3IMPA < A9Y3INPA < A9Y3MPA.

Table. 2.10. Corrosion inhibition efficiencies at different concentrations of Schiff bases on CS for 24 h in 1M HCl medium at 30^0C.

C	Inhibition Efficiency (η_W %)					
(mM)	A9Y3APA	A9Y5GPA	A9Y3IMPA	A9Y3INPA	A9Y3PPA	A9Y3MPA
0.2	46.54	47.09	75.46	85.39	56.91	88.23
0.4	52.35	55.31	80.31	89.69	64.11	92.81
0.6	61.53	63.37	85.91	92.95	73.26	93.52
0.8	75.62	69.72	87.80	93.82	82.96	94.58
1.0	83.98	73.50	92.75	94.23	92.36	95.71

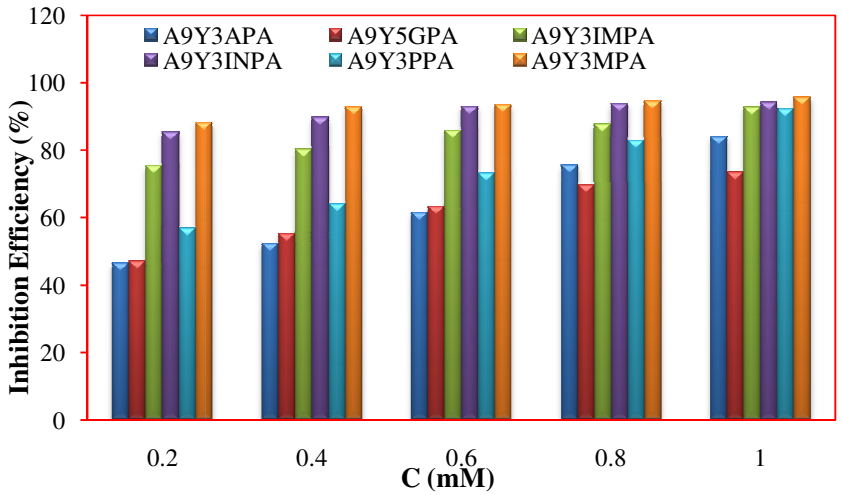

Fig. 2.29: Comparison of corrosion inhibition efficiency of Schiff bases in 1M HCl medium

The weight loss data clearly established that the corrosion rates markedly decreased with inhibitor concentration. This response is due to the fact that the surface coverage (θ) of the inhibitor molecules on the metal through adsorption increases with increasing concentration and the surface is efficiently separated from the medium. The results of the corrosion inhibition studies of six Schiff bases on CS in 1M HCl solution at 30^0C by weight loss studies concluded that all Schiff bases act as efficient corrosion inhibitors in 1M HCl medium. The inhibition efficiency of the Schiff bases increases with the concentration suggest that inhibition was a result of adsorption of Schiff bases on the metal surface and these compounds act as adsorption inhibitors.

Electrochemical impedance spectroscopy studies

The corrosion response of CS in 1M HCl in the presence of various concentrations of inhibitor has been investigated using electrochemical impedance spectroscopy at 30^0C. Figure 2.30 to 2.41 represents the Nyquist plots and corresponding Bode plots for CS specimens in 1M HCl in the presence of various concentrations of inhibitor. It is evident from the plots that the impedance response of metal specimens has marked difference in the

presence and absence of the inhibitors. The EIS parameters such as R_{ct}, C_{dl} and the values of percentage of inhibition (η_{EIS} %) are listed in table 2.11.

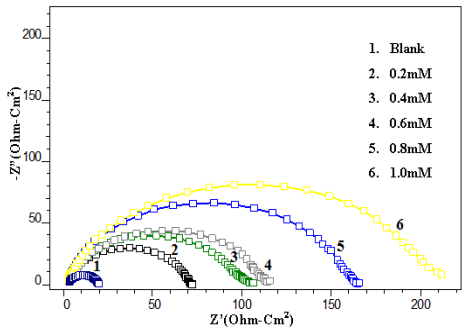

Fig. 2.30: Nyquist plots for CS in A9Y3APA-1M HCl solutions

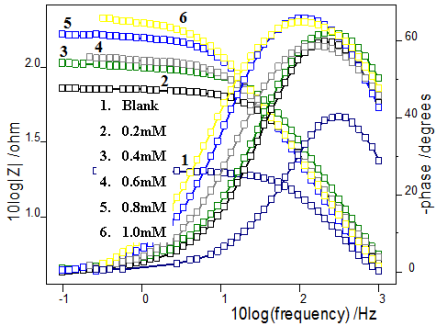

Fig. 2.31: Bode plots for CS in A9Y3APA-1M HCl solutions

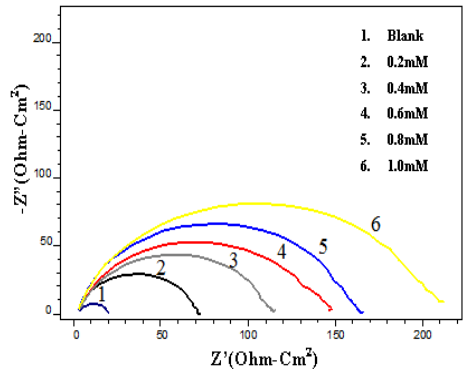

Fig. 2.32: Nyquist plots for CS in A9Y5GPA-1M HCl solutions

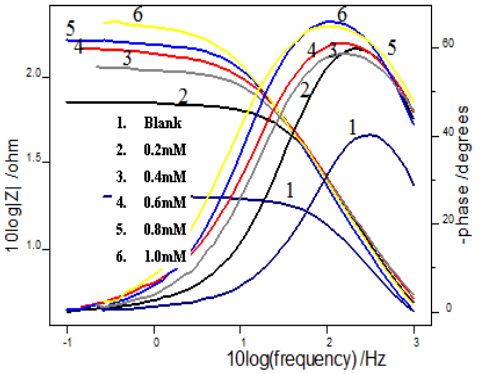

Fig. 2.33: Bode plots for CS in A9Y5GPA-1M HCl solutions

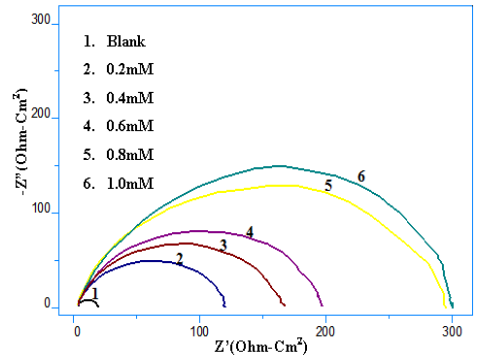

Fig. 2.34: Nyquist plots for CS in A9Y3IMPA-1M HCl solutions

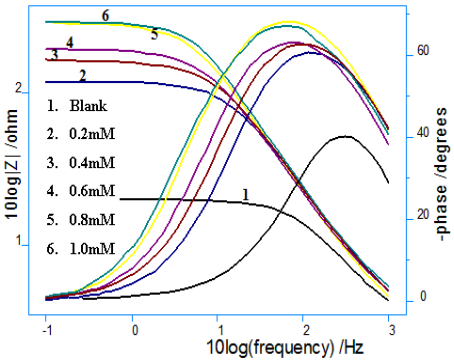

Fig. 2.35: Bode plots for CS in A9Y3IMPA-1M HCl solutions

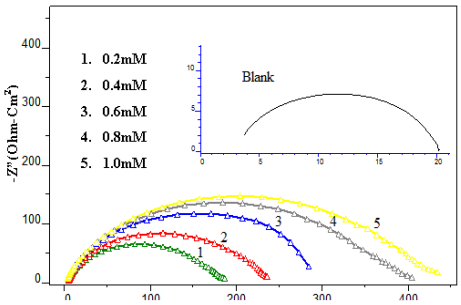

Fig. 2.36: Nyquist plots for CS in A9Y3INPA-1M HCl solutions

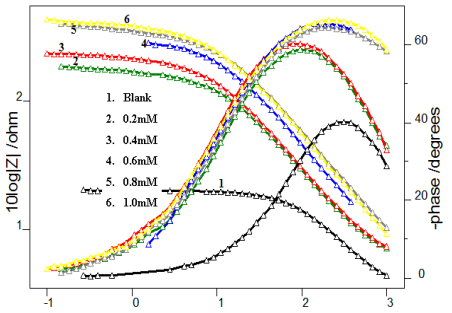

Fig. 2.37: Bode plots for CS in A9Y3INPA-1M HCl solutions

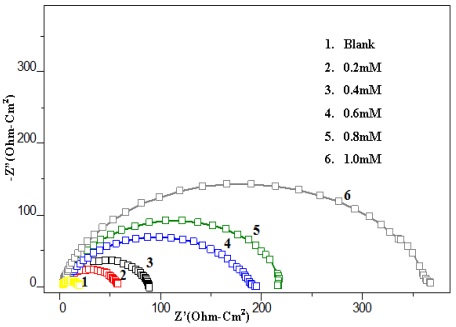

Fig. 2.38: Nyquist plots for CS in A9Y3PPA-1M HCl solutions

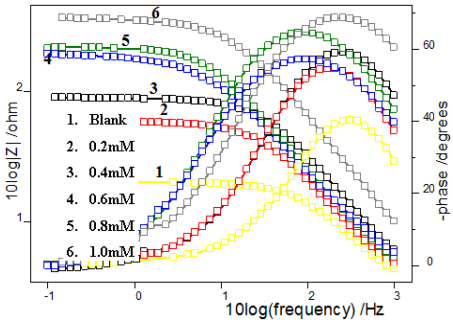

Fig. 2.39: Bode plots for CS in A9Y3PPA-1M HCl solutions

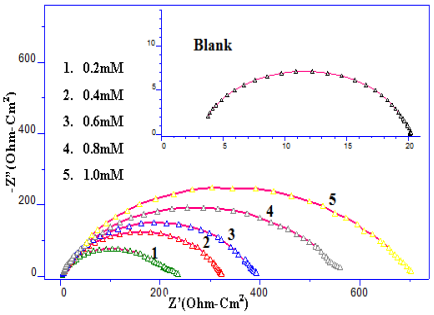

Fig. 2.40: Nyquist plots for CS in A9Y3MPA-1M HCl solutions

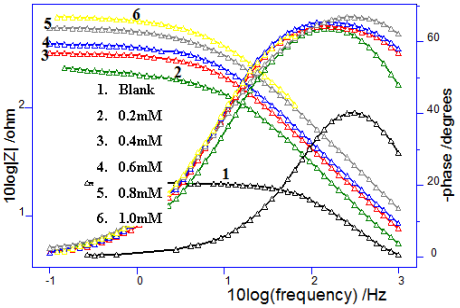

Fig. 2.41: Bode plots for CS in A9Y3MPA-1M HCl solutions

From the Nyquist plots, it is clear that all the curves are semicircle in nature and display a single capacitive loop. The diameter of the semicircle increased with increase in Schiff base concentration.

The table 2.11 shows that R_{ct} values of CS specimens increases with the inhibitor concentration. The C_{dl} values were decreased with increase in

inhibitor concentration. The inhibition efficiencies calculated from R_{ct} values were also increased with the inhibitor concentration. The maximum inhibition efficiency was obtained for the Schiff base inhibitor A9Y3MPA at 1.0mM concentration and the value is 97.28%. At a maximum concentration of 1.0mM Schiff bases, A9Y5GPA and A9Y3APA showed η_{EIS}% 91.65% and 91.82% respectively on CS in 1M HCl. The other three Schiff base inhibitors A9Y3IMPA, A9Y3INPA and A9Y3PPA display an inhibition efficiency value of 94.39%, 95.72% and 95.24% respectively at 1.0mM concentration. These values are in good agreement with the inhibition efficiencies obtained from weight loss studies.

The Nyquist plots and Bode plots reveal that the corrosion of the CS in aggressive solution mainly controlled by charge transfer process. The difference in real impedance at lower and higher frequencies is commonly considered as a charge transfer resistance in Nyquist plot. Impedance behaviour can be well explained by pure electric models that could verify and enable to calculate numerical values corresponding to the physical and chemical properties of electrochemical system under examination[92]. The simple equivalent circuit that fit to many electrochemical systems composed of a double layer capacitance, R_s and R_{ct}[93,94]. To reduce the effects due to surface irregularities of metal, constant phase element (CPE) is introduced into the circuit instead of a pure double layer capacitance which gives more accurate fit[95] as shown in the figure 2.3(chapter 2).

The impedance of CPE can be expressed as $Z_{CPE} = \frac{1}{Y_0 \ (j\omega)^n}$ (35)

where Y_0 is the magnitude of CPE, n is the exponent (phase shift), ω is the angular frequency and j is the imaginary unit.

Table. 2.11. Electrochemical impedance parameters of CS specimens in 1M HCl at 30^0C in the absence and presence of Schiff bases

Schiff Base	C (mM)	R_{ct} (Ωcm^2)	C_{dl} ($\mu F\ cm^{-2}$)	$\eta_{EIS\%}$
Blank	0	15.7	104	-
A9Y3APA	0.2	59.8	102	73.75
	0.4	92.9	84.2	83.10
	0.6	98.9	80.8	84.13
	0.8	145.0	74.6	89.17
	1.0	192.0	60.9	91.82
A9Y5GPA	0.2	64.2	93.3	75.55
	0.4	91.1	92.6	82.77
	0.6	128.0	69.9	87.73
	0.8	149.0	60.8	89.46
	1.0	188.0	59.8	91.65
A9Y3IMPA	0.2	109.2	101.2	85.62
	0.4	151.2	97.2	89.62
	0.6	181.0	90.3	91.33
	0.8	275.8	86.8	94.31
	1.0	280.0	81.4	94.39
A9Y3INPA	0.2	157	90.8	90.00
	0.4	204	89.4	92.30
	0.6	257	52.3	93.89
	0.8	337	49.6	95.34
	1.0	367	47	95.72
A9Y3PPA	0.2	50.9	92.4	69.16
	0.4	79.8	90.9	80.33
	0.6	167	83.8	90.60
	0.8	203	57.1	92.27
	1.0	330	33.8	95.24
A9Y3MPA	0.2	195	85.1	91.95
	0.4	288	62.3	94.55
	0.6	350	53.4	95.51
	0.8	481	41.9	96.74
	1.0	577	41.2	97.28

CPE may be resistance, capacitance and inductance depending upon the values of n[96]. In all experiments the observed value of n ranges between 0.75 and 1.0, suggesting the capacitive response of CPE.

The capacitance value C_{dl} decreases with inhibitor concentration and may be explained on the basis that the double layer between the charged metal surface and the solution may acts as an electrical capacitor. The increase in the thickness of the electrical double layer[97] cause a decrease in C_{dl} and these results suggest that the inhibitor molecules function by adsorption at the metal/solution interface.

The addition of Schiff base inhibitors to the corrosive medium provides lower C_{dl} values, probably due to the replacement of water molecules by Schiff bases at the electrode surface. Also the inhibitor molecules may reduce the capacitance by increasing the double layer thickness according to the Helmholtz model

$$C_{dl} = \frac{\varepsilon\varepsilon_0 A}{\delta} \qquad (36)$$

Where ε is the dielectric constant of the medium, ε_0 is the vacuum permittivity, A is the electrode surface area and δ is the thickness of the protective layer. The value of C_{dl} is always smaller in the presence of the inhibitor than its absence, as a result of the effective adsorption of the Schiff bases.

Potentiodynamic polarization studies

Figure 2.42 to 2.53 represents potentiodynamic and linear polarization curves for CS specimens in 1M HCl at 30^0C in the absence and presence of various concentrations of Schiff bases inhibitor studied. Polarization parameters like corrosion current densities (I_{corr}), corrosion potential (E_{corr}),

cathodic Tafel slope (b_c), anodic Tafel slope (b_a), inhibition efficiency (η_{pol} %) and linear polarization parameters like polarization resistance (R_p) and inhibition efficiency (η_{Rp} %) for CS specimens are listed in table 2.12.

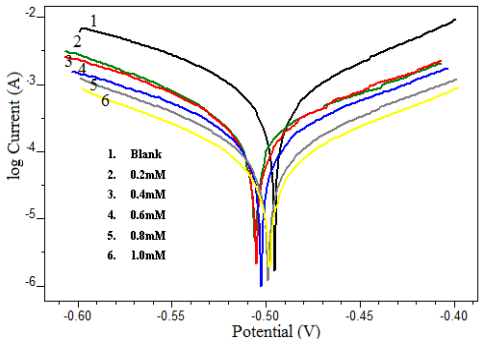

Fig. 2.42: Tafel plots for CS in A9Y3APA-1M HCl solutions

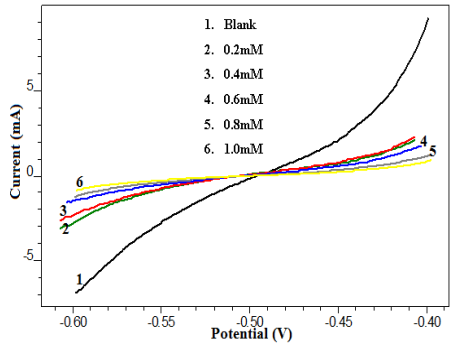

Fig. 2.43: Linear polarization plots for CS in A9Y3APA-1M HCl solutions

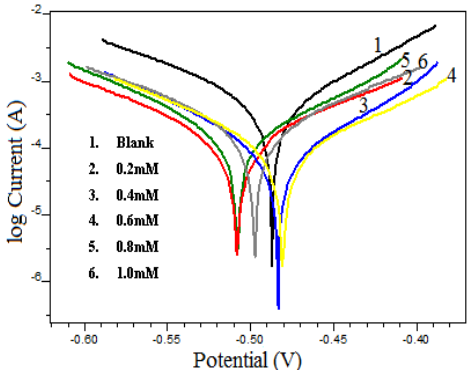

Fig. 2.44: Tafel plots for CS in A9Y5GPA-1M HCl solutions

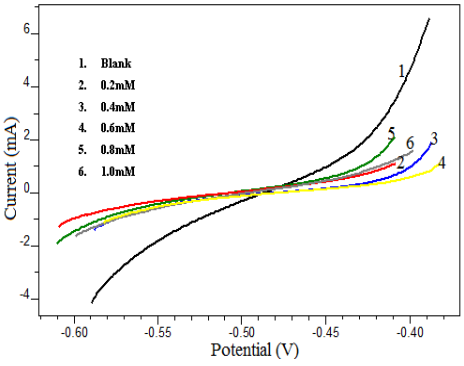

Fig. 2.45: Linear polarization plots for CS in A9Y5GPA-1M HCl solutions

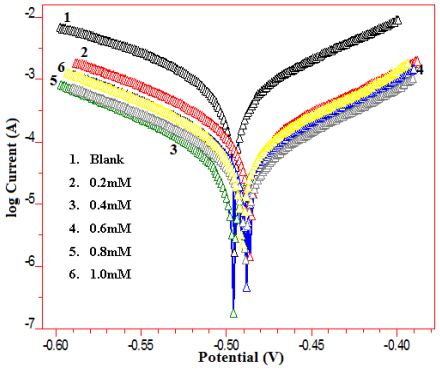

Fig. 2.46: Tafel plots for CS in A9Y3IMPA-1M HCl solutions

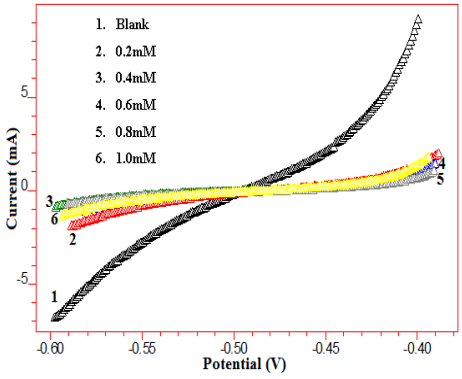

Fig. 2.47: Linear polarization plots for CS in A9Y3IMPA- 1M HCl solutions

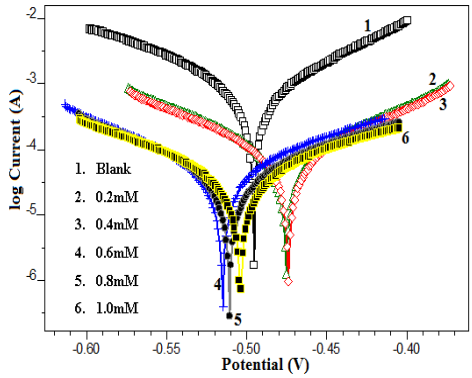

Fig. 2.48: Tafel plots for CS in A9Y3INPA-1M HCl solutions

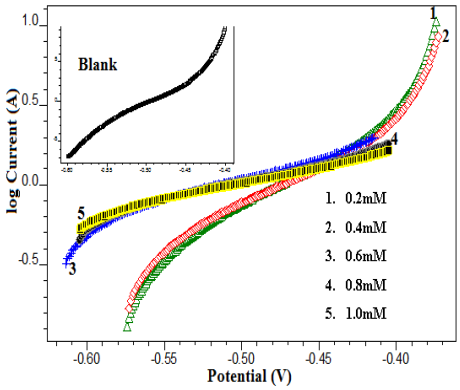

Fig. 2.49: Linear polarization plots for CS in A9Y3INPA-1M HCl solutions

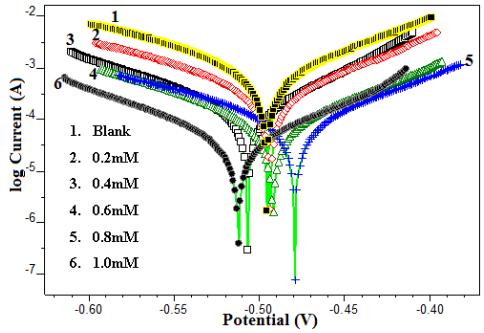

Fig. 2.50: Tafel plots for CS in A9Y3PPA-1M HCl solutions

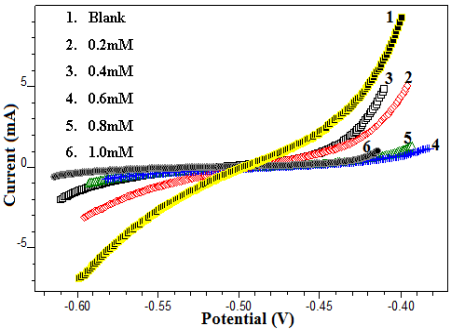

Fig. 2.51: Linear polarization plots for CS in A9Y3PPA-1M HCl solutions

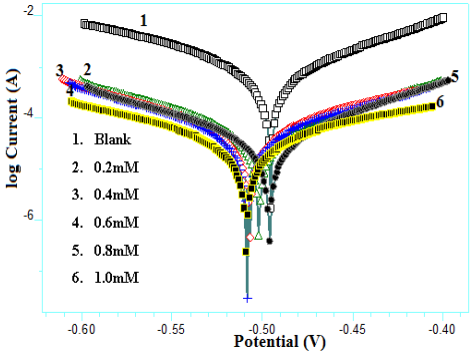

Fig. 2.52: Tafel plots for CS in A9Y3MPA-1M HCl solutions

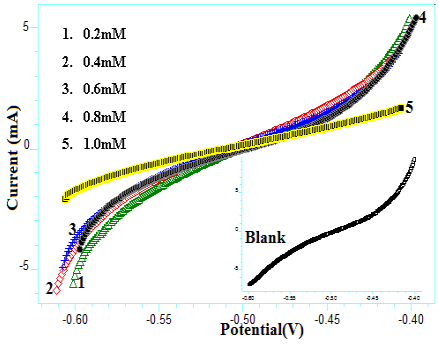

Fig. 2.53: Linear polarization plots for CS in A9Y3MPA-1M HCl solutions

Table. 2.12. Potentiodynamic and linear polarization parameters of CS specimens in 1M HCl at 30^0C in the absence and presence of Schiff bases

Schiff Base	C (mM)	Tafel Data					Linear Polarisation Data	
		E_{corr} (mV/SCE)	I_{corr} (mA/cm^2)	b_a (V/dec)	$-b_c$ (V/dec)	η_{pol}%	R_p (ohm)	η_{Rp}%
	Blank	-489	0.6282	0.076	0.096	-	29	-
A9Y3APA	0.2	-502	0.2186	0.1	0.085	65.2	91	67.81
	0.4	-500	0.2003	0.085	0.088	68.12	94	68.63
	0.6	-500	0.1603	0.093	0.098	74.48	129	77.28
	0.8	-495	0.0921	0.083	0.089	85.34	202	85.48
	1.0	-498	0.0654	0.088	0.087	89.59	291	89.91
A9Y5GPA	0.2	-495	0.1441	0.076	0.096	77.06	138	78.74
	0.4	-505	0.1225	0.090	0.094	80.50	151	80.50
	0.6	-510	0.106	0.084	0.086	83.13	193	84.76
	0.8	-478	0.0793	0.098	0.090	87.38	225	86.95
	1.0	-479	0.0686	0.090	0.088	89.08	244	87.98
A9Y3IMPA	0.2	-486	0.1160	0.078	0.082	81.53	150	80.43
	0.4	-490	0.0817	0.076	0.084	86.99	212	86.15
	0.6	-488	0.0706	0.074	0.081	88.76	238	87.66
	0.8	-489	0.0479	0.073	0.085	92.38	356	91.75
	1.0	-492	0.0432	0.076	0.079	93.12	388	92.43
A9Y3INPA	0.2	-474	0.0733	0.091	0.093	88.33	272	89.21
	0.4	-473	0.0666	0.091	0.095	89.40	303	90.32
	0.6	-516	0.0381	0.107	0.09	93.94	557	94.73
	0.8	-511	0.0327	0.112	0.091	94.79	665	95.59
	1.0	-504	0.0314	0.11	0.102	95.00	733	96.00
A9Y3PPA	0.2	-489	0.2627	0.076	0.094	58.18	69	57.75
	0.4	-502	0.1209	0.061	0.087	80.75	129	77.20
	0.6	-479	0.0729	0.077	0.101	88.40	261	88.76
	0.8	-489	0.0678	0.076	0.086	89.21	258	88.64
	1.0	-509	0.0323	0.075	0.083	94.86	531	94.47
APY3MPA	0.2	-501	0.0472	0.094	0.095	92.49	435	93.25
	0.4	-508	0.045	0.099	0.094	92.84	465	93.68
	0.6	-508	0.039	0.099	0.092	93.79	531	94.47
	0.8	-495	0.0314	0.078	0.094	95.00	588	95.00
	1.0	-510	0.0264	0.119	0.103	95.80	907	96.76

A marked decrease in the corrosion current density (I_{corr}) was observed in the presence of Schiff bases. A highest value of I_{corr} (0.0686 mA/cm^2) was noticed for CS in the presence of A9Y5GPA at a concentration of 1.0mM and the same was exhibited a maximum inhibition efficiency of 89.08%. The I_{corr} value of CS in the presence of A9Y3APA (1.0mM) was 0.0654mA/cm^2 and the corresponding inhibition efficiency value was 89.59%. An I_{corr} value of

0.0432mA/cm^2 was shown by the inhibitor A9Y3IMPA and the inhibition efficiency (η_{pol} %) value was 93.12% for the concentration of 1mM. The corrosion current densities of CS specimens in the presence of the Schiff base (at a concentration of 1.0mM) A9Y3INPA, A9Y3PPA and A9Y3MPA were 0.0314, 0.0323, and 0.0264 respectively and the corresponding η_{pol} % were 95%, 94.86% and 95.80% respectively. From the table it is clear that the maximum polarization resistance is shown by the inhibitor A9Y3MPA and hence maximum inhibition efficiency. The values of inhibition efficiency are in good agreement with the impedance studies.

The polarization data showed that, addition of the Schiff base to acid media affectes both the cathodic and anodic parts of the Tafel curves and it may be assumed that the inhibitor molecules were adsorbed on anodic and cathodic sites uniformly. Thus both anodic metal dissolution and cathodic hydrogen evolution were inhibited by the addition of Schiff base inhibitors to 1M HCl solution. From Tafel and LPR plots it was clear that both the anodic and cathodic current values of CS were considerably increased in 1M HCl solution compared with those obtained for CS in 1M HCl solution containing inhibitor. This result can be explained with an increase in surface area of the CS because of the excess dissolution of iron. It was also evident that corrosion current density of the CS was smaller when Schiff bases were added to 1M HCl solution and the corrosion potential E_{corr} changes. A change in the slope of both anodic and cathodic Tafel line was observed in the inhibited solution when compared to uninhibited solution. This indicates the modification of anodic and cathodic reaction mechanisms in inhibited solutions. Generally if the shift of E_{corr} is >85 with respect to E_{corr} of uninhibited solution, the

inhibitor can be viewed as either cathodic or anodic type[98, 99]. In the present study the maximum shift of E_{corr} is 27mV, suggesting that all the studied inhibitors act as a mixed type inhibitor for CS specimens in 1M HCl.

The inhibitor molecules are first adsorbed onto the CS surface and, therefore, resist by merely blocking the reaction sites of the CS surface. The surface available for H^+ ions is decreased by the adsorption of inhibitor molecules. With higher inhibitor concentrations, higher coverage of the inhibitor on the surface was obtained. The formation of surface inhibitor film on the carbon steel provides considerable protection to carbon steel against corrosion. This film reduces the active surface area exposed to the corrosive environment and delays the hydrogen evolution and iron dissolution.

Effect of temperature

The effect of temperature on corrosion was also evaluated using weight loss measurement in the temperature range of 40-60^{0}C. The corrosion rate and percentage inhibition efficiency are exhibited in the table 2.13 and 2.14 respectively.

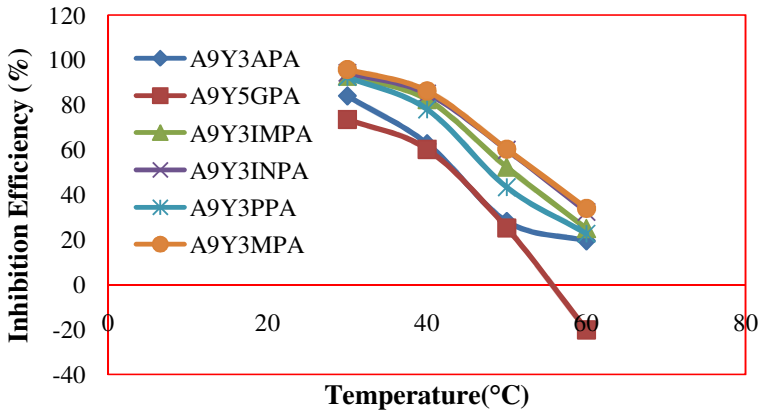

Fig. 2.54: Comparison of inhibition efficiency of Schiff bases (1mM) in 1M HCl medium at different temperatures for 24 h

Table. 2.13. Corrosion rates of CS in 1M HCl at different temperatures in the presence and absence of Schiff bases for 24 h.

Temp.	C (mM)	Corrosion Rate (mm/year)					
		A9Y3APA	**A9Y5GPA**	**A9Y3IMPA**	**A9Y3INPA**	**A9Y3PPA**	**A9Y3MPA**
40^0C	Blank	12.60					
	0.2	8.04	8.32	6.33	3.53	6.55	3.26
	0.4	7.14	7.76	5.17	3.21	6.18	2.80
	0.6	6.03	6.29	3.99	2.57	5.51	2.35
	0.8	5.07	5.50	3.09	2.17	4.81	2.02
	1.0	4.69	5.01	2.23	1.90	2.77	1.74
50^0C	Blank	22.67					
	0.2	21.59	21.98	17.33	13.57	18.74	12.84
	0.4	20.62	21.02	14.91	12.23	17.51	11.30
	0.6	18.49	18.84	13.70	10.39	15.90	10.97
	0.8	17.03	17.83	12.83	9.87	14.25	9.96
	1.0	16.27	16.96	10.83	9.07	12.84	9.01
60^0C	Blank	35.50					
	0.2	39.02	39.81	33.40	32.77	35.41	26.60
	0.4	35.99	47.84	31.16	26.33	32.65	25.02
	0.6	31.91	41.70	29.03	25.09	30.43	24.22
	0.8	29.87	42.65	27.87	24.22	28.39	23.53
	1.0	28.56	42.65	26.64	24.00	27.44	23.44

Table. 2.14. Corrosion inhibition efficiencies of Schiff bases on CS in 1M HCl at various concentrations in the temperature range 40-60^{0}C for 24 h.

Temp.	C (mM)	Inhibition Efficiency (η_W %)					
		A9Y3APA	A9Y5GPA	A9Y3IMPA	A9Y3INPA	A9Y3PPA	A9Y3MPA
40^{0}C	0.2	36.14	33.97	49.71	71.95	47.96	74.15
	0.4	43.32	38.37	58.94	74.51	50.92	77.73
	0.6	52.12	50.04	68.29	79.63	56.28	81.38
	0.8	59.77	56.32	75.50	82.81	61.84	83.98
	1.0	62.75	60.21	82.33	84.94	78.00	86.16
50^{0}C	0.2	4.74	3.03	23.57	40.13	17.33	43.37
	0.4	9.04	7.28	34.22	46.04	22.77	50.13
	0.6	18.42	16.91	39.59	54.15	29.86	51.59
	0.8	24.90	21.33	43.42	56.45	37.13	56.06
	1.0	28.22	25.17	52.24	59.97	43.34	60.26
60^{0}C	0.2	-9.92	-12.15	5.92	7.70	0.26	25.07
	0.4	-1.38	-34.77	12.22	25.82	8.02	29.53
	0.6	10.11	-17.47	18.23	29.31	14.29	31.78
	0.8	15.85	-20.13	21.49	31.77	20.02	33.73
	1.0	19.53	-20.16	24.95	32.39	22.69	33.97

The percentage inhibition efficiencies of six Schiff bases at different temperatures for the concentration of 1.0mM are also plotted and shown in the figure 2.54. It has been found that the inhibition efficiency depends on temperature and decreases with increasing temperature, indicating that at higher temperature, dissolution of Schiff bases from carbon steel predominates. The increase in temperature has an adverse effect on the adsorption process where it weakens the adsorption process and encourages desorption process.

The activation energy of corrosion can be calculated by Arrhenius equation,

$$K = A \exp\left(-\frac{E_a}{RT}\right) \quad (9)$$

Linear plots between log K and 1000/T (Fig. 2.55 to 2.60) having regression coefficients close to unity indicate that the corrosion of CS in HCl could be explained by the simple kinetic model. Enthalpy and entropy of activation (ΔH*, ΔS*) were calculated from the transition state theory,

$$K = \left(\frac{RT}{Nh}\right) \exp\left(\frac{\Delta S^*}{R}\right) \exp\left(\frac{-\Delta H^*}{RT}\right) \quad (10)$$

where N is the Avogadro number and h is the Planks constant. A plot of log (K/T) Vs 1000/T gave straight lines for the corrosion of CS in 1M HCl in the presence and absence of the inhibitor (figures 2.61 to 2.66). Table 2.15 shows the activation energy and thermodynamic parameters of corrosion of CS in 1M HCl with and without the inhibitor. The thermodynamic parameters indicate that the values of activation energy, E_a and pre-exponential factor or frequency factor, A in the presence of inhibitors are higher than that in the absence of inhibitor.

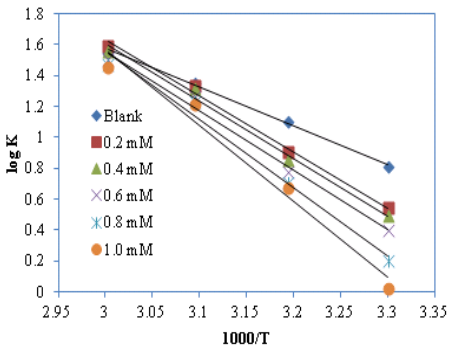

Fig. 2.55: Arrhenius plots for A9Y3APA

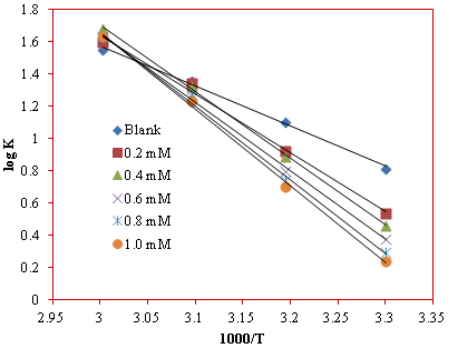

Fig. 2.56: Arrhenius plots for A9Y5GPA

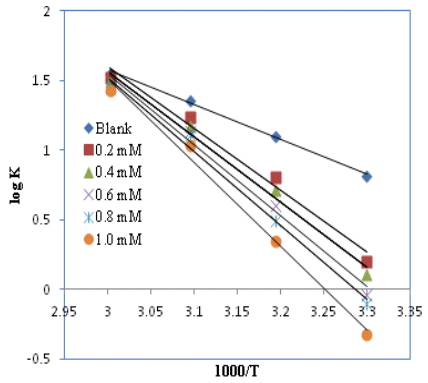

Fig. 2.57: Arrhenius plots for A9Y3IMPA

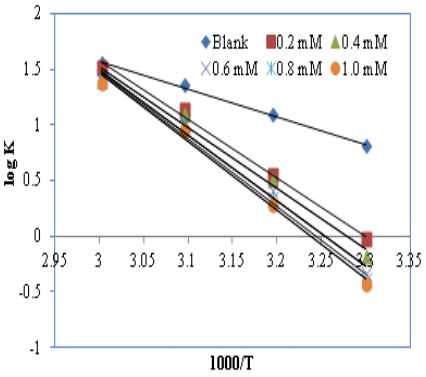

Fig. 2.58: Arrhenius plots for A9Y3INPA

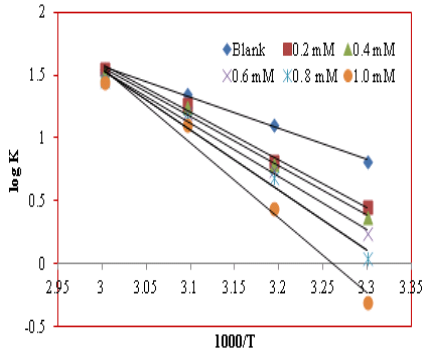

Fig. 2.59: Arrhenius plots for A9Y3PPA

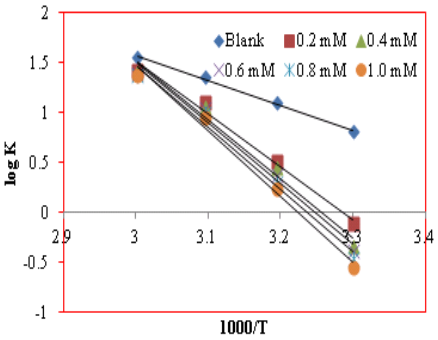

Fig. 2.60: Arrhenius plots for A9Y3MPA

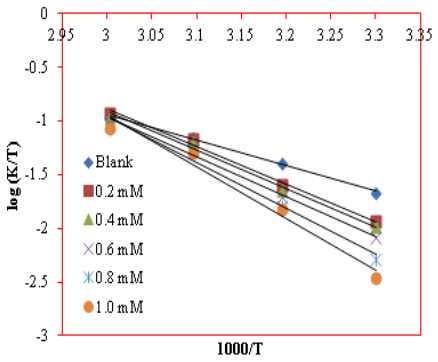

Fig.2.61: Plots of log (K/T) Vs 1000/T for A9Y3APA

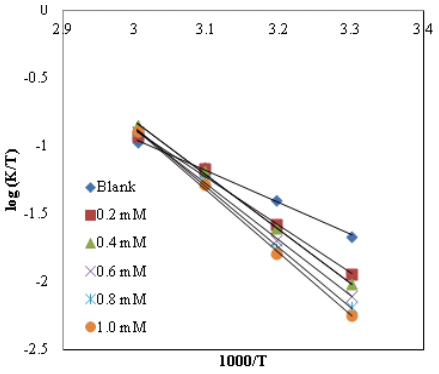

Fig. 2.62: Plots of log (K/T) Vs 1000/T for A9Y5GPA

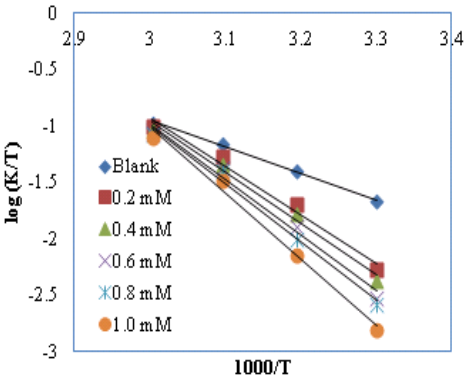

Fig. 2.63: Plots of log (K/T) Vs 1000/T for A9Y3IMPA

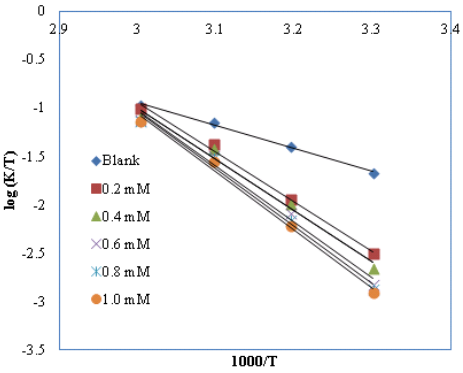

Fig. 2.64: Plots of log (K/T) Vs 1000/T for A9Y3INPA

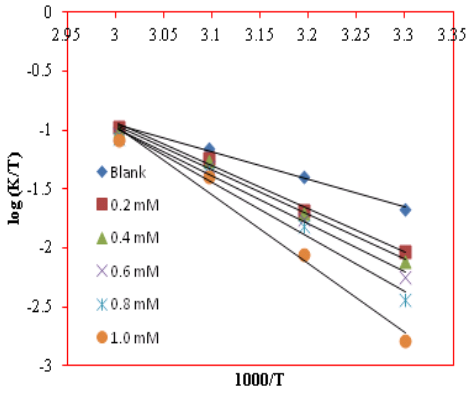

Fig. 2.65: Plots of log (K/T) Vs 1000/T for A9Y3PPA

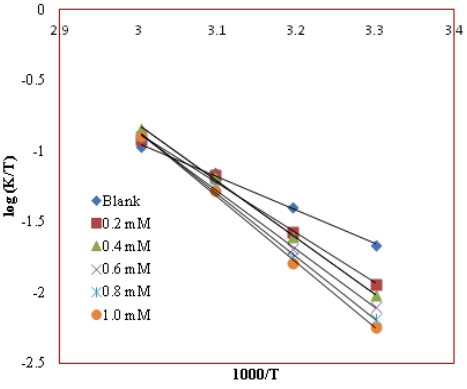

Fig. 2.66: Plots of log (K/T) Vs 1000/T for A9Y3MPA

Table. 2.15. Thermodynamic parameters of corrosion of CS in 1M HCl

Schiff Base	C (mM)	E_a (kJ mol^{-1})	A	ΔH* (kJ mol^{-1})	ΔS* (J mol^{-1} K^{-1})
	Blank	47.73	1.1×10^{9}	45.09	-80.44
A9Y5GPA	0.2	69.89	3.9×10^{12}	67.24	-12.68
	0.4	78.90	1.2×10^{14}	76.24	15.47
	0.6	81.29	2.4×10^{14}	78.63	21.64
	0.8	87.31	2.2×10^{15}	84.64	39.83
	1.0	91.02	8.2×10^{15}	88.36	50.95
A9Y3APA	0.2	69.24	$3.0X10^{12}$	66.60	-14.87
	0.4	70.73	$4.8X10^{12}$	68.08	-10.93
	0.6	73.61	$1.2X10^{13}$	70.97	-3.12
	0.8	84.32	$5.9X10^{14}$	81.70	29.01
	1.0	94.21	$2.1X10^{16}$	91.60	58.90
A9Y3PPA	0.2	72.78	$9.5X10^{12}$	70.13	-5.15
	0.4	75.3	$2.3X10^{13}$	72.66	1.94
	0.6	81.13	$1.8X10^{14}$	78.48	19.17
	0.8	91.15	$6.6X10^{15}$	88.49	49.04
	1.0	114.26	$2.9X10^{19}$	111.6	118.73
A9Y3IMPA	0.2	85.32	$9.3X10^{14}$	82.68	32.76
	0.4	89.52	$3.9X10^{15}$	86.87	44.63
	0.6	97.63	$6.9X10^{16}$	94.99	68.76
	0.8	101.78	$3.0X10^{17}$	99.12	80.63
	1.0	115.08	$3.5X10^{19}$	112.43	120.27
A9Y3INPA	0.2	100.57	$2.1X10^{17}$	97.92	77.95
	0.4	103.96	$6.3X10^{17}$	101.31	87.14
	0.6	112.87	$1.5X10^{19}$	110.23	113.37
	0.8	116.26	$4.9X10^{19}$	113.62	123.33
	1.0	118.05	$9.1X10^{19}$	115.4	128.31
A9Y3MPA	0.2	101.13	$2.3X10^{17}$	98.45	78.52
	0.4	112.33	$1.3X10^{19}$	109.69	112.03
	0.6	115.33	$3.7X10^{19}$	112.68	120.84
	0.8	119.51	$1.6X10^{20}$	116.87	133.09
	1.0	125.67	$1.5X10^{21}$	123.02	151.48

Also the result establishes that activation energy of dissolution of the metal increased with the inhibitor concentration. This implies that the reluctance of dissolution of metal was increased with the inhibitor concentration. A higher value of E_a in the presence of inhibitors is a good sign of inhibitive action of inhibitor by increasing the energy barrier for the corrosion process. This higher value of E_a can also be correlated with the

increase in thickness of the double layer that enhances the E_a of the corrosion process[90]. The pre-exponential factor and activation energy varies in the same way. Positive signs of enthalpies with a regular rise reflect the endothermic nature of dissolution and the increasing difficulty for corrosion with the inhibitor. It is evident from the table 2.15 that the entropy of activation increases with the inhibitor concentration. For the blank and lower concentration of the inhibitors, A9Y3APA, A9Y5GPA and A9Y3PPA the entropy of activation was negative. This implies that in the rate determining step there is more association rather than dissociation, indicating that a decrease in disordering takes place on going from reactants to the activated complex and the activated molecules were in higher order state than that at the initial state. But as the concentration of inhibitor rises, the disordering of activated complex rises and the entropy of activation acquires positive values. In the case of A9Y3IMPA, A9Y3INPA and A9Y3MPA, even at lower concentrations, positive entropy values show that in all concentrations there was dissociation and hence disorderness of activated complex rises as the concentration increases. The shift of ΔS to more positive values on increasing the concentration of the inhibitor was the driving force that can overcome the barriers for the adsorption of inhibitor onto the carbon steel surface[91].

Adsorption isotherm studies in HCl medium

The mechanism of adsorption and the surface behaviour of organic molecules can be easily viewed through adsorption isotherms. Different models of adsorption isotherms considered are Langmuir, Temkin, Frumkin and Freundlich isotherms. For the evaluation of thermodynamic parameters it is necessary to determine the best fit isotherm with the aid of correlation

coefficient (R^2). Among the isotherms mentioned above, the best description of the adsorption behaviour of inhibitors on CS specimens in 1M HCl was Freundlich adsorption isotherm and Langmuir adsorption isotherms.

Figure 2.67 to 2.72 represents the adsorption plot of inhibitors obtained by the weight loss measurements of CS steel specimens in 1M HCl at 30^0C for 24 h. The value of adsorption equilibrium constant K_{ads} is related to the standard free energy of adsorption ΔG^0_{ads}. The thermodynamic parameters obtained from weight loss studies are represented in the table 2.16.

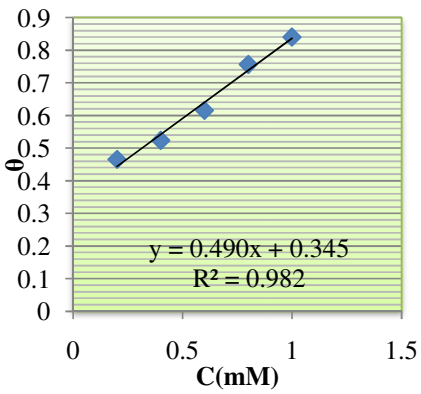

Fig.2.67: Freundlich adsorption isotherm for A9Y3APA in 1M HCl

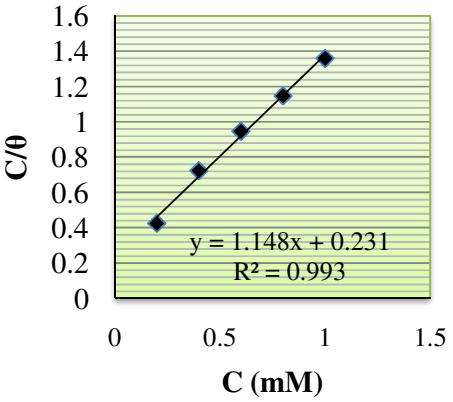

Fig.2.68: Langmuir adsorption isotherm for A9Y5GPA in 1M HCl

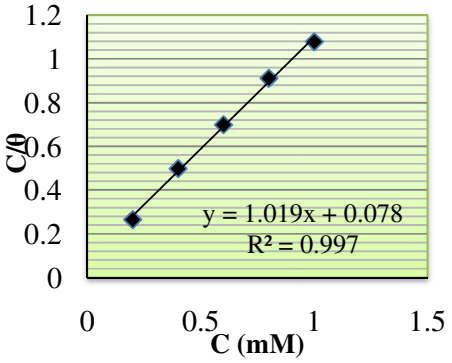

Fig. 2.69: Langmuir adsorption isotherm for A9Y3IMPA in 1M HCl

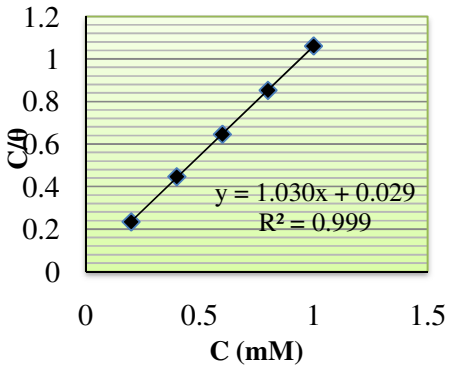

Fig. 2.70: Langmuir adsorption isotherm for A9Y3INPA in 1M HCl

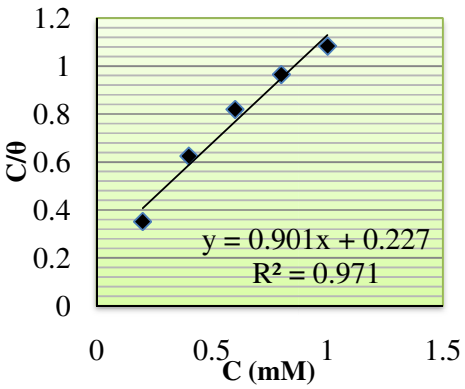

Fig. 2.71: Langmuir adsorption isotherm for A9Y3PPA in 1M HCl

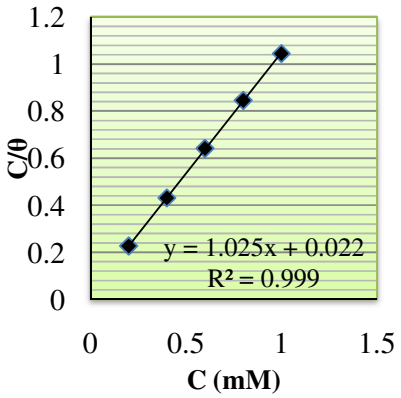

Fig. 2.72: Langmuir adsorption isotherm for A9Y3MPA in 1M HCl

Table. 2.16. Thermodynamic parameters for the adsorption of Schiff bases on CS in 1M HCl

Schiff base	Isotherm	K_{ads}	ΔG^0_{ads}(kJ/mol)
A9Y3APA	Freundlich	490.7	-25.69
A9Y5GPA	Langmuir	4316	-31.16
A9Y3IMPA	Langmuir	12771	-33.89
A9Y3INPA	Langmuir	33670	-36.33
A9Y3PPA	Langmuir	4397	-31.21
A9Y3MPA	Langmuir	45455	-37.09

The values of surface coverage (θ) have been used to explain best isotherm to determine the adsorption process. The Schiff base inhibitor A9Y3APA obeys Freundlich adsorption isotherm and other Schiff base inhibitors obey Langmuir adsorption isotherms. The organic molecules, significantly larger than water, can interact with the metal surface. The adsorption of organic corrosion inhibitor at the metal-solution interface is a substitutional adsorption process between molecules and the metallic surface.

ΔG^0_{ads} for Schiff bases on CS showed negative values indicating the spontaneity of the process. The value of ΔG^0_{ads} less than -20kJ mol^{-1} was an indication of the electrostatic interaction of the charged molecule and the

charged surface of the metal (physisorption) while ΔG^0_{ads} data more negative than -40 kJ/mol implies that inhibitor molecules are adsorbed strongly on the metal surface through co-ordinate type bond (chemisorptions)[100,101]. In the present investigation, the inhibitor molecules showed ΔG^0_{ads} in between -25.69 and -37.09 kJ/mol for CS specimens suggesting that the adsorption of inhibitor involves both electrostatic and chemical interactions. Higher values of the adsorption constant and negative free energy of adsorption can be reasoned for better adsorption and higher inhibition efficiency. These findings were consistent with data obtained from electrochemical investigations.

Scanning electron microscopy studies

The surface morphology of carbon steel surface was evaluated by scanning electron microscopy (SEM). Only three SEM images are presented for the discussion purpose.

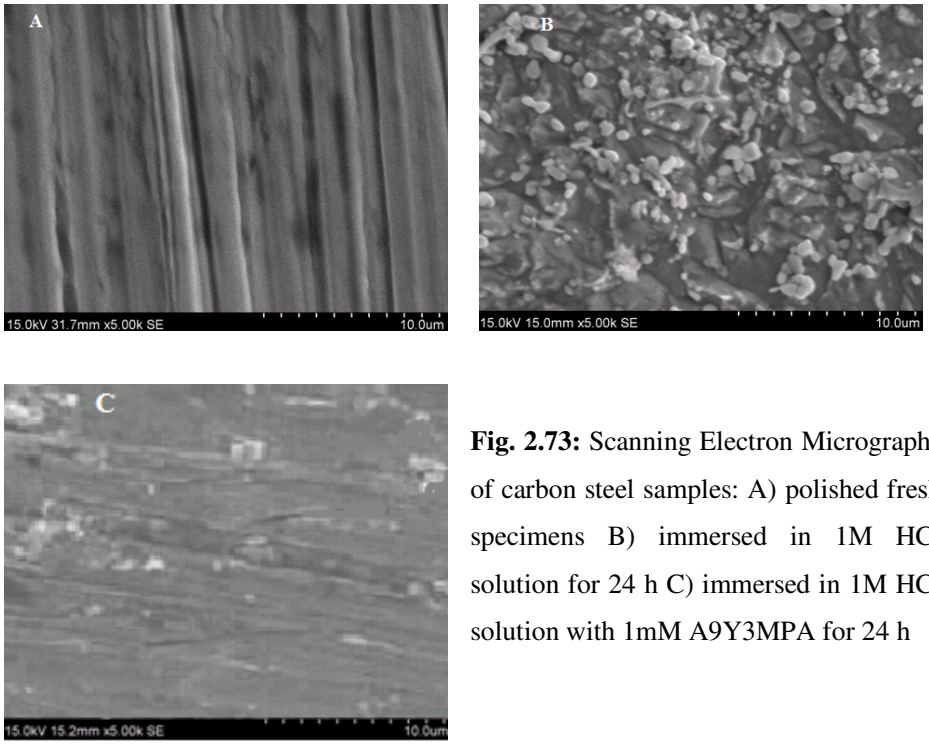

Fig. 2.73: Scanning Electron Micrographs of carbon steel samples: A) polished fresh specimens B) immersed in 1M HCl solution for 24 h C) immersed in 1M HCl solution with 1mM A9Y3MPA for 24 h

Figures 2.73 A, B and C shows the scanning electron micrographs of the bare carbon steel surface, CS in HCl and CS in HCl with presence of A9Y3MPA respectively. The morphology revealed that in the absence of A9Y3MPA, the surface was highly corroded. However in the presence of inhibitor the rate of corrosion was suppressed. These observations suggest that the inhibitor forms a protective layer on the surface that prevents the attack of acid on the corroding metal CS.

Comparison of inhibition efficiency of Schiff base with its parent compounds

To compare the inhibition efficiencies of Schiff base, parent ketone anthracene-9 (10H)-one, and parent amines, weight loss measurements of CS specimens were performed in 1M HCl at 30^0C.

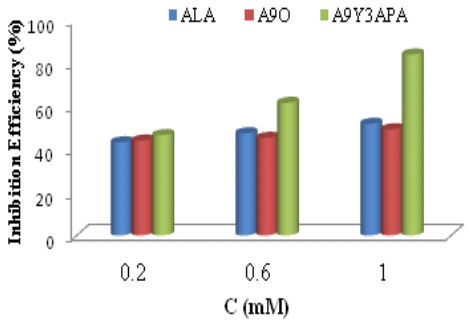

Fig. 2.74: Comparison of inhibition efficiency of ALA, A9O and A9Y3APA in 1M HCl

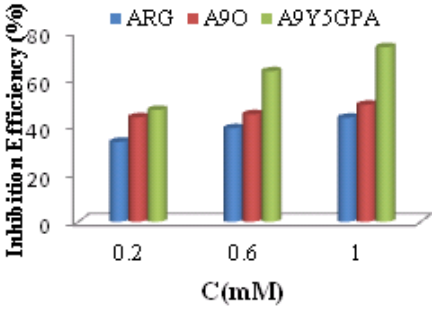

Fig. 2.75: Comparison of inhibition efficiency of ARG, A9O and A9Y5GPA in 1M HCl

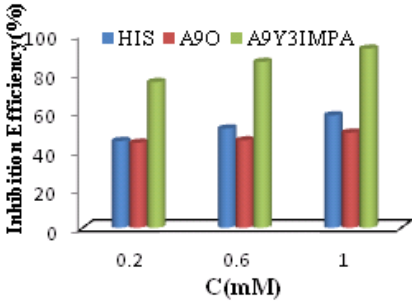

Fig. 2.76: Comparison of inhibition efficiency of HIS, A9O and A9Y3IMPA in 1M HCl

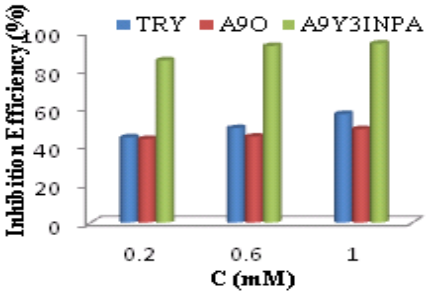

Fig. 2.77: Comparison of inhibition efficiency of TRY, A9O and A9Y3INPA in 1M HCl

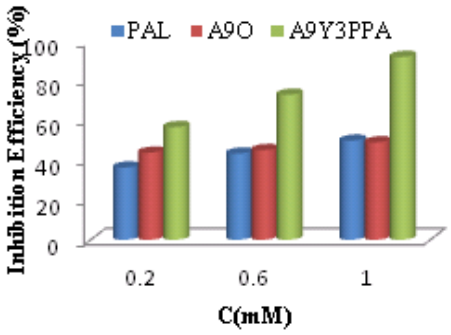

Fig. 2.78: Comparison of inhibition efficiency of PAL, A9O and A9Y3PPA in 1M HCl

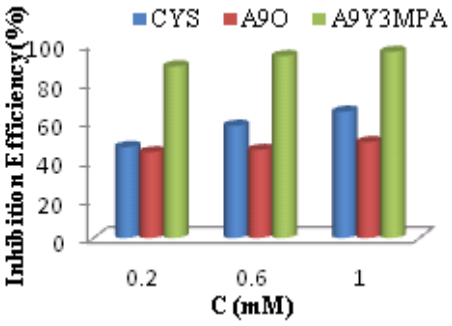

Fig. 2.79: Comparison of inhibition efficiency of CYS, A9O and A9Y3MPA in 1M HCl

The percentage of corrosion inhibition efficiencies obtained for Schiff base, parent ketone and parent amine on CS are represented in the figures 2.74 to 2.79. The inhibition efficiency of the six Schiff base inhibitors was markedly higher than that of parent ketone and parent amine for the studied concentrations. This investigation clearly establishes the role of azomethine linkage (>C=N) present in the Schiff base which actively participate in the corrosion inhibition mechanism.

Mechanism of inhibition

The electrochemical reaction of iron corrosion involves transfer of two electrons, and then there are two steps each one represents transfer of one electron and one of them may be considered as rate determining step. The detailed mechanism and equations are discussed in the chapter 3.

According to the detailed mechanism, "displacement of some adsorbed water molecules on the metal surface by inhibitor species takes place and reduces the amount of $[FeClOH]^-_{ads}$ available for the rate determining step and consequently retard anodic dissolution[102] of Fe. The protonated inhibitor molecules were adsorbed at cathodic sites in competition with hydrogen ions and hence reduced the H_2 gas evolution".

Another explanation based on the above described mechanism is that "the adsorption of Cl^- ions on the metal surface and creates an excess of negative charge on the surface. This will favour the adsorption of protonated Schiff base on the surface[103], thus interfere the anodic and cathodic reactions and hence reduce the dissolution of Fe to Fe^{2+} (Figure 2.80). Besides this electrostatic interaction between the protonated Schiff base and the metal surface, other possible interactions are i) interaction of unshared electron pairs in the molecule with the metal ii) interaction of π-electrons with the metal and iii) a combination of types (i–ii)[104,105]. The π-electron cloud of the aromatic rings and the azomethine linkage also participate in the inhibition mechanism. Furthermore, the double bonds in the inhibitor molecule permit the back donation of metal d electrons to the π* orbital and this type of interaction cannot occur with" the amines[106]. This can be justified by the lower inhibition efficiency of the parent amine than that of Schiff base.

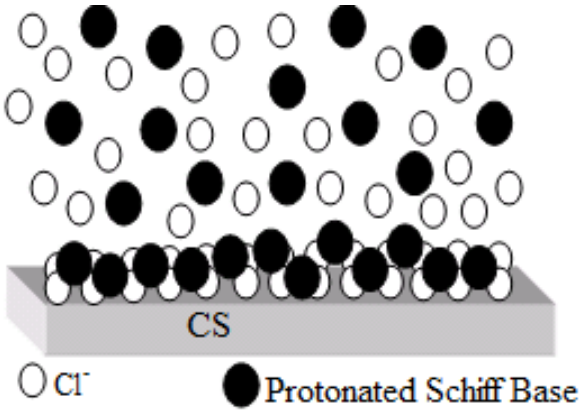

Fig. 2.80: Schematic representation of mechanism of inhibition

CHAPTER 5

CORROSION INHIBITION STUDIES ON SCHIFF BASES IN 0.5M H_2SO_4 ON CARBON STEEL

Corrosion of metals has continued to receive attention in the technological world. Corrosion scientists are relentless in seeking better and more efficient ways of combating the corrosion of metals. Addition of inhibitors to the corrosive medium has been employed as an efficient method to control corrosion. The efficiency of these inhibitors is sometimes improved by the addition of certain other compounds which play effective role in synergism mechanism. In this chapter, the inhibition efficiency of the synthesized Schiff base and synergistic role of halide ion in enhancing the corrosion inhibition efficiency in 0.5M H_2SO_4 are described.

The details of the inhibitive action of synthesized Schiff base towards the corrosion of CS in 0.5M H_2SO_4 solution using gravimetric, polarization and impedance studies are well documented and discussed. A detailed discussion about the synergistic inhibition of Schiff base in the presence of I^- ions on the corrosion inhibition of CS in sulphuric acid solutions is also presented in this chapter. Attempts were made in this chapter to explain the adsorption isotherms and mechanism of inhibition.

Weight loss studies

Weight loss of CS specimens in 0.5M H_2SO_4 at 30^0C was determined at 24 h in the presence of various concentrations of Schiff bases A9Y3APA, A9Y5GPA, A9Y3IMPA, A9Y3PPA, A9Y3INPA, and A9Y3MPA. From the weight loss data of CS specimens in the presence of various concentrations of

Schiff bases, the corrosion rates, inhibition efficiencies and surface coverage (θ) were determined.

Corrosion rates studies in H_2SO_4 medium

The corrosion rates of CS calculated for various concentrations of Schiff bases in 0.5M H_2SO_4 medium for a period of 24 h are represented in the table 2.17. The comparison of corrosion rate of CS in the presence of various concentration of Schiff bases are illustrated in the figure 2.81. From the results represented, the corrosion rate was observed to decrease progressively with the concentration of added inhibitor. The corrosion rate of CS in the presence of A9Y5GPA was found to be 15.21 mm/year which is the highest corrosion rate value among the corrosion rate of CS in the presence of Schiff bases at the concentration of 1.0mM. The lowest corrosion rate value 2.07 mm/year was showed by CS in the presence of A9Y3MPA at the concentration of 1.0mM. The corrosion rate of CS in the presence of A9Y3APA, A9Y3IMPA, A9Y3INPA and A9Y3PPA are 13.50, 4.26, 7.73, and 10.65 mm/year respectively at the concentration of 1.0mM. In short it is noticed that all the studied inhibitors reduce the corrosion rate of CS at 30^0C.

Table. 2.17. Corrosion rates of CS at different concentrationsof Schiff bases for 24 h in 0.5M H_2SO_4 medium at 30^0C.

C	Corrosion Rate (mm/year)					
(mM)	A9Y3APA	A9Y5GPA	A9Y3IMPA	A9Y3INPA	A9Y3PPA	A9Y3MPA
Blank	24.01					
0.2	18.06	20.37	6.96	11.98	16.22	6.32
0.4	17.19	19.36	6.68	10.99	14.75	5.46
0.6	15.96	18.13	5.61	9.63	12.91	3.60
0.8	14.58	16.93	4.85	8.59	11.71	2.67
1.0	13.50	15.21	4.26	7.73	10.65	2.07

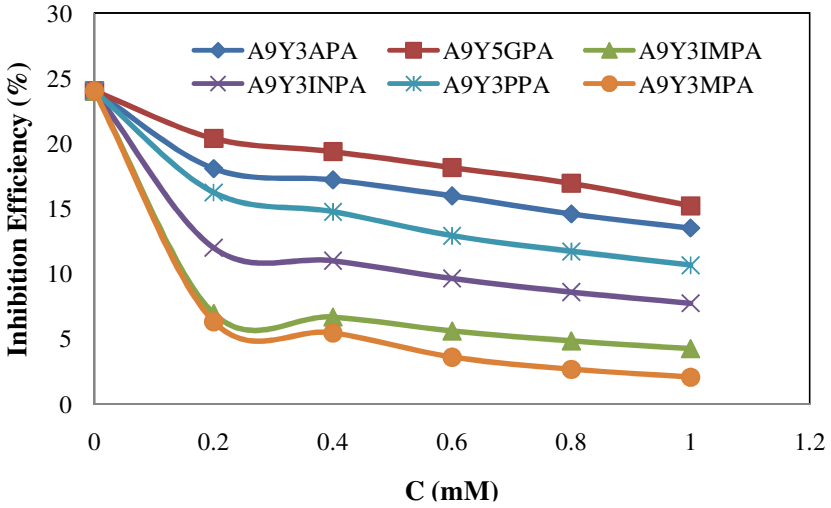

Fig. 2.81: Corrosion rate of CS in 0.5M H_2SO_4 with and without Schiff bases at 30^0C for 24 h.

Corrosion inhibition efficiency of Schiff bases on CS in H_2SO_4 medium

The inhibition efficiency determined by corrosion rate analysis is presented in the table 2.18. The table establishes that all studied Schiff bases except A9Y3MPA show the inhibition efficiency values below 90% for the concentration 1.0mM. The Schiff base A9Y3APA and A9Y5GPA showed inhibition values below 50% and the other three Schiff bases A9Y3IMPA, A9Y3INPA and A9Y3PPA exhibited the values of 82.25%, 67.81% and 55.65% respectively for the concentration of 1.0mM. Figure 2.82 represents the comparison of percentage inhibition efficiencies with the concentration of Schiff bases in 0.5M H_2SO_4 medium at 30^0C. The corrosion inhibition efficiency of the studied Schiff bases increases in the order A9Y5GPA<A9Y3APA<A9Y3PPA<A9Y3INPA<A9Y3IMPA<A9Y3MPA at all concentrations.

From table 2.18, it is also evident that the inhibition efficiency increased with increasing concentration. At the inhibitor concentration of 1.0mM, the maximum η_W% was found to be low for the inhibitors A9Y3APA,

A9Y5GPA, A9Y3INPA, and A9Y3PPA which shows that individual inhibitor molecules cannot protect much effectively the corrosion of CS in 0.5M H_2SO_4.

Table. 2.18. Corrosion inhibition efficiencies at different concentrations of Schiff bases on CS for 24 h in 0.5M H_2SO_4 medium at 30^0C.

C	Inhibition efficiency (η_W %)					
(mM)	A9Y3APA	A9Y5GPA	A9Y3IMPA	A9Y3INPA	A9Y3PPA	A9Y3MPA
0.2	24.77	15.14	71.00	50.10	32.43	73.68
0.4	28.38	19.36	72.19	54.21	38.57	77.26
0.6	33.54	24.48	76.62	59.90	46.22	84.99
0.8	39.25	29.50	79.80	64.20	51.24	88.88
1.0	43.75	36.65	82.25	67.81	55.65	91.37

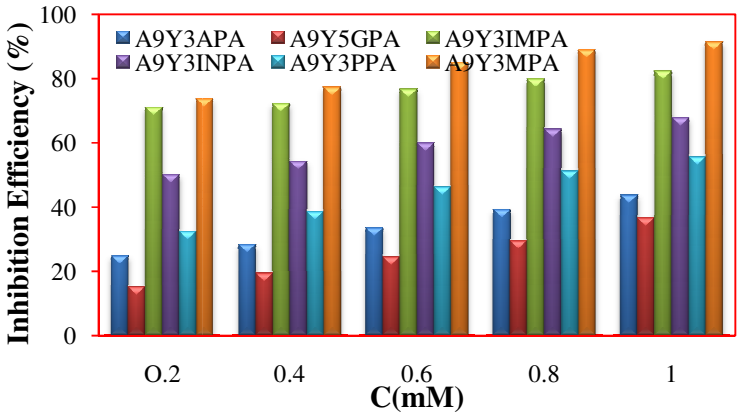

Fig. 2.82: Comparison of inhibition efficiency of Schiff bases in 0.5M H_2SO_4 medium

Synergistic studies

Gravimetric corrosion analysis of CS in the presence Schiff bases in 0.5M H_2SO_4 medium at 30^0C showed that the inhibition efficiency of A9Y3APA, A9Y5GPA, A9Y3INPA and A9Y3PPA was significantly low and to enhance the inhibition efficiency, synergistic effect studies with iodide ion was carried out. Table 2.19 and 2.20 show the corrosion rates of CS and corrosion inhibition efficiency values for different concentrations of Schiff bases.

Table. 2.19. Corrosion rates of CS at different concentrations of Schiff bases with 0.2mM KI for 24 h in 0.5M H_2SO_4 medium at 30^0C.

C (mM)	Corrosion Rate (mm/year)			
	A9Y3APA	A9Y5GPA	A9Y3INPA	A9Y3PPA
Blank + 0.2mM KI	19.40			
0.2+ 0.2mM KI	10.88	7.70	4.83	7.19
0.4+ 0.2mM KI	10.22	6.61	4.15	5.89
0.6+ 0.2mM KI	9.08	4.87	2.69	4.43
0.8+ 0.2mM KI	6.84	4.16	1.96	3.59
1.0+ 0.2mM KI	5.58	3.52	1.72	2.54

Table. 2.20. Corrosion inhibition efficiency at different concentrations of Schiff bases with 0.2mM KI on CS for 24 h in 0.5M H_2SO_4 medium at 30^0C.

C (mM)	Inhibition Efficiency (mm/year)			
	A9Y3APA	A9Y5GPA	A9Y3INPA	A9Y3PPA
Blank + 0.2mM KI	19.16			
0.2+ 0.2mM KI	54.67	67.94	79.86	70.04
0.4+ 0.2mM KI	57.41	72.45	82.72	75.46
0.6+ 0.2mM KI	62.16	79.71	88.78	81.53
0.8+ 0.2mM KI	71.49	82.65	91.85	85.04
1.0+ 0.2mM KI	76.75	85.34	92.84	89.43

Data from the tables 2.19 and 2.20 establish that the addition of KI drastically decreases the corrosion rate and hence increases the η_W % values. Inhibition efficiency values also explain the synergism played in the medium for the enhancement of corrosion inhibition. In order to illustrate the synergistic effect in detail, the corrosion rate values and inhibition efficiency values at 1.0mM concentrations of the inhibitor molecule were considered. The values corresponding to 1.0mM concentration are represented as bar diagram and exhibited in figures 2.83 and 2.84. From the figures it is clear that the corrosion rate values are decreased by the addition of KI and the inhibition efficiencies are increased by the addition of KI. The inhibition efficiency value (η_W %) of blank solution with 0.2mM KI was found to be 19.16%.

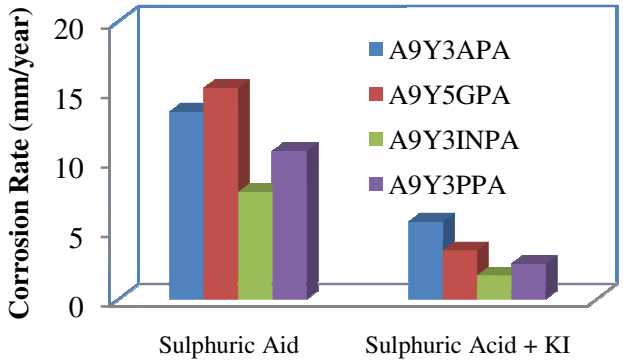

Fig. 2.83: Comparison of corrosion rate of CS in the presence of Schiff base (1.0mM) in 0.5M H_2SO_4 and 0.5M H_2SO_4+KI

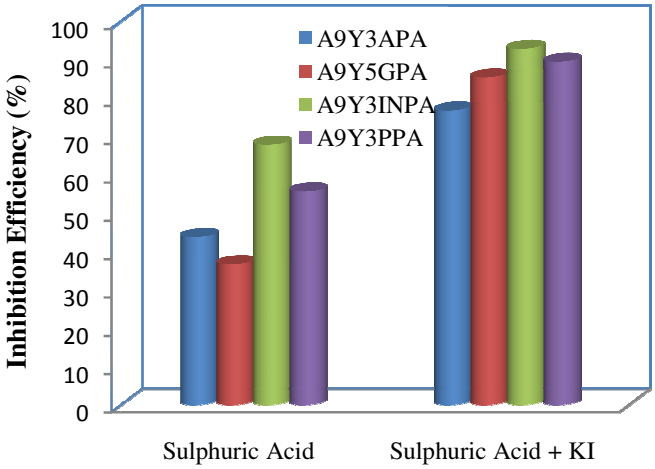

Fig. 2.84: Comparison of inhibition efficiency of Schiff base (1.0mM) in 0.5M H_2SO_4 and 0.5M H_2SO_4+KI

The percentage inhibition of A9Y3APA for 1.0mM concentration in H_2SO_4 medium is 43.75 while it exhibited 76.75% inhibition in the presence of 0.2mM KI which is even higher than the summation of 19.16 + 43.75. This may be attributed to synergism with Cl^-. The inhibition efficiency at 1.0mM concentration of A9Y5GPA along with KI was 85.34 which was higher than the combined η_W% value of KI (19.16%) and η_W% value of inhibitor (36.65%). Similarly the η_W% value of A9Y3INPA and A9Y3PPA with KI are 92.84% and 89.43% respectively which is a clear evidence of synergism. The η_W% value 89.43% for A9Y3PPA with KI is higher than the summation value

of 19.16% and 55.65%. For the other studied concentrations, the η_W % for KI in combination with inhibitor was higher than the summation of η_W % for single KI and single inhibitor, which is synergism in nature.

Synergism parameter

Synergism parameter provides the information about the enhancement of inhibition efficiency through synergism. Aramaki and Hackerman[107] calculated the synergism parameter S_θ using the following equation.

$$S_\theta = \frac{1-\theta_{1+2}}{1-\theta'_{1+2}} \qquad (28)$$

where $\theta_{1+2} = (\theta_1 + \theta_2) - (\theta_1\,\theta_2)$; θ_1 = surface coverage by anion; θ_2 = surface coverage by cation; θ'_{1+2} = measured surface coverage by both anion and cation. The synergism parameters for the various concentrations of Schiff bases obtained by gravimetric analysis are presented in table 2.21. The comparison of synergism parameters for different Schiff bases at various concentrations are depicted in the figure 2.85.

Table. 2.21. Synergism parameter (S_θ) for different concentrations of Schiff bases in combination with 0.2mM KI

C	Synergism Parameter , S_θ			
(mM)	A9Y3APA	A9Y5GPA	A9Y3INPA	A9Y3PPA
0.2	1.34	2.24	2.01	1.83
0.4	1.36	2.48	2.15	2.03
0.6	1.42	3.18	2.9	2.36
0.8	1.73	3.49	3.56	2.64
1.0	1.96	3.71	3.64	3.4

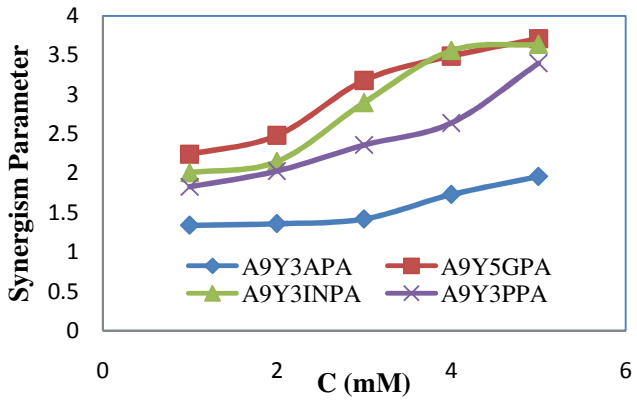

Fig. 2.85: Variation of synergism parameters with concentration of Schiff base

Compared with the inhibition efficiency values of inhibitor (without KI), it was found that the combination of inhibitor and 0.2mM KI has better inhibition efficiency for all studied inhibitor concentrations. S_θ approaches unity when there are no interactions between the inhibitor compounds, while $S_\theta > 1$ points to a synergistic effect; in the case of $S_\theta < 1$, the antagonistic interaction prevails. All values shown in this table are greater than unity. This is an indication that the enhanced inhibition efficiency resulting from the addition of iodide ions to the studied inhibitors are synergistic in nature. From the figure 2.85 it is clear that, the synergism parameter of A9Y5GPA are greater than that of the other inhibitors. It can be concluded that the inhibitors are preferentially adsorbed in a protonated form by coulombic attraction on the metal surface where the anion (iodide) is already chemisorbed and suppresses the corrosion rate by the stabilization of adsorbed anion and by the increase of surface coverage.

Electrochemical impedance spectroscopy studies

The electrochemical impedance measurements were performed at room temperature using the six inhibitors in 0.5M H_2SO_4 medium. The synergistic effect was also studied for the inhibitors A9Y3APA, A9Y5GPA,

A9Y3INPA and A9Y3PPA. Figures.2.86 to 2.105 represent the Nyquist plots and Bode plots of CS specimens in 0.5M H_2SO_4 in the presence of various concentrations of inhibitor and inhibitor + KI. It is evident from the plots that the impedance response of metal specimens has marked difference in the presence and absence of the KI with inhibitors. The EIS parameters such as R_{ct}, R_s and CPE and the calculated values of percentage of inhibition ($\eta_{EIS\ \%}$) of CS specimens are listed in table 2.22 and table 2.23.

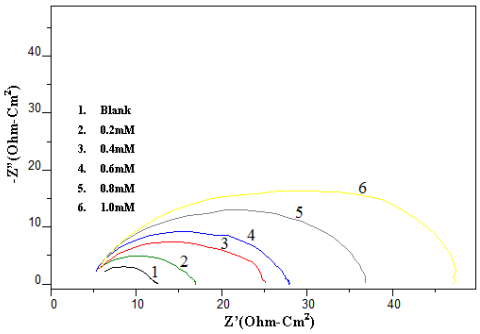

Fig. 2.86: Nyquist plots for A9Y3APA-0.5M H_2SO_4 solutions

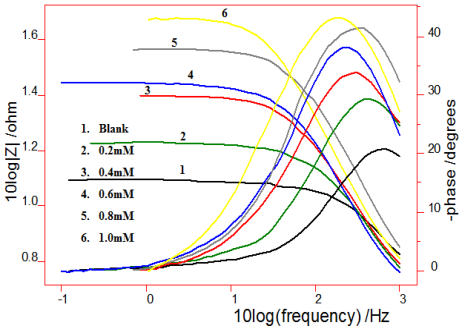

Fig. 2.87: Bode plots for A9Y3APA-0.5M H_2SO_4 solutions

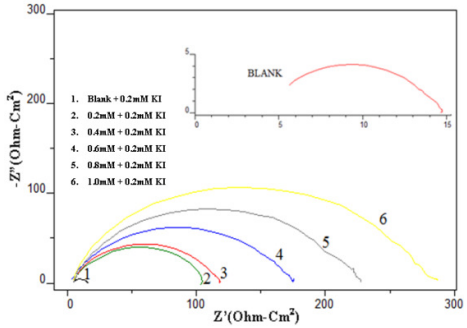

Fig. 2.88: Nyquist plots (Synergistic) for A9Y3APA

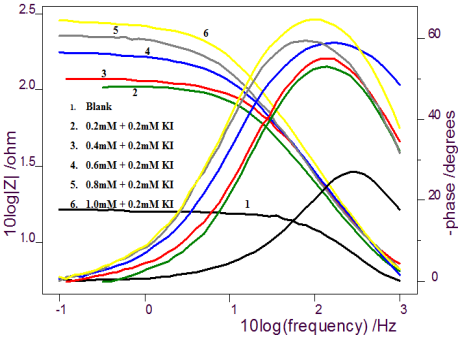

Fig. 2.89: Bode plots (Synergistic) for A9Y3APA

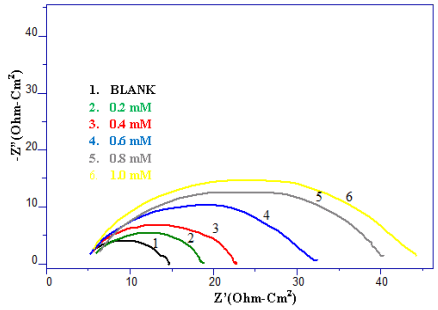

Fig. 2.90: Nyquist plots for A9Y5GPA-0.5M H_2SO_4 solutions

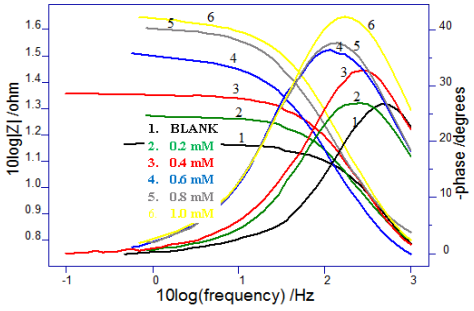

Fig. 2.91: Bode plots for A9Y5GPA-0.5M H_2SO_4 solutions

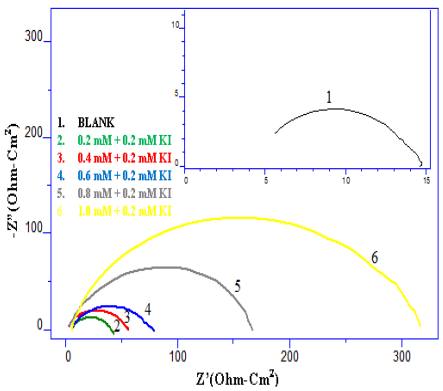

Fig. 2.92: Nyquist plot (synergistic) for A9Y5GPA

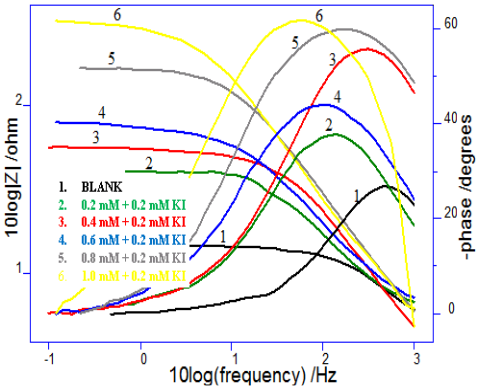

Fig. 2.93: Bode plot (synergistic) for A9Y5GPA

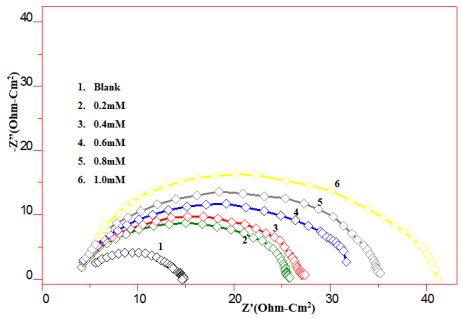

Fig. 2.94: Nyquist plots for A9Y3INPA-0.5M H_2SO_4 solutions

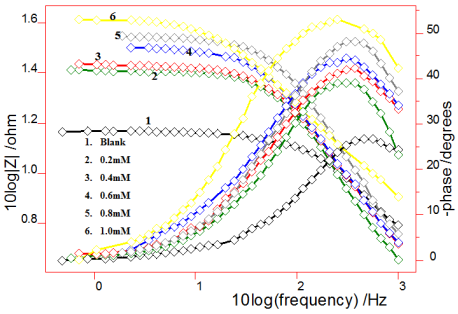

Fig. 2.95: Bode plots for A9Y3INPA-0.5M H_2SO_4 solutions

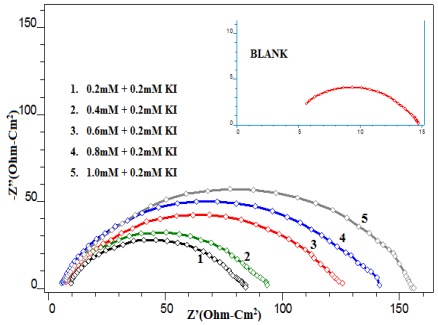

Fig. 2.96: Nyquist plots (synergistic) for A9Y3INPA

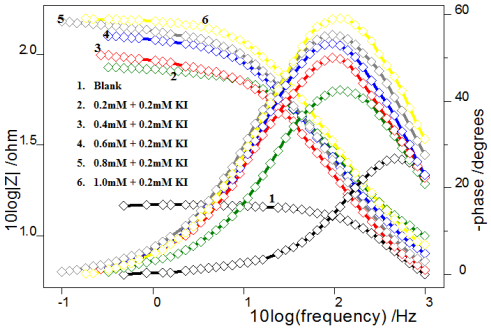

Fig. 2.97: Bode plot (synergistic) for A9Y3INPA

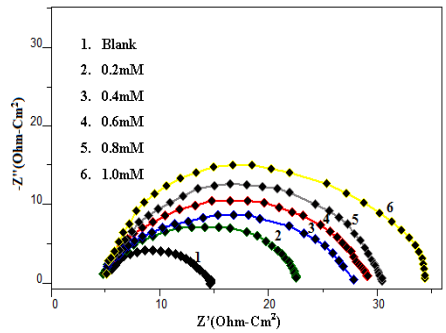

Fig. 2.98: Nyquist plots for A9Y3PPA-0.5M H_2SO_4 solutions

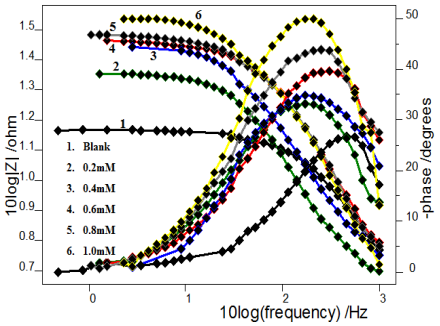

Fig. 2.99: Bode plots for A9Y3PPA-0.5M H_2SO_4 solutions

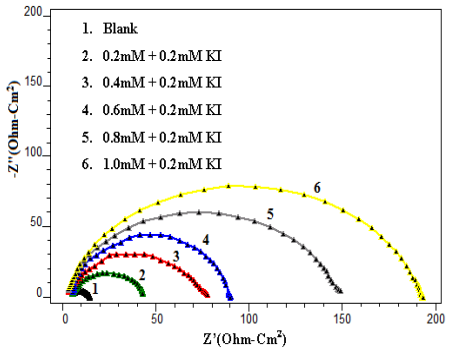

Fig. 2.100: Nyquist plots (synergistic) for A9Y3PPA

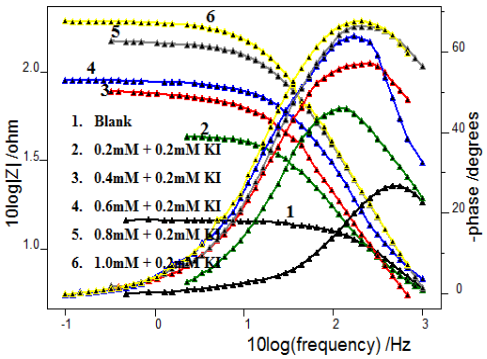

Fig. 2.101: Bode plots (synergistic) for A9Y3PPA

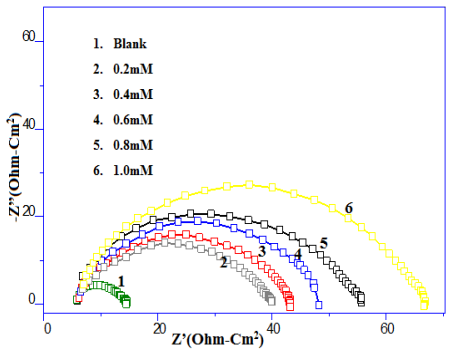

Fig. 2.102: Nyquist plots for A9Y3IMPA-0.5M H_2SO_4 solutions

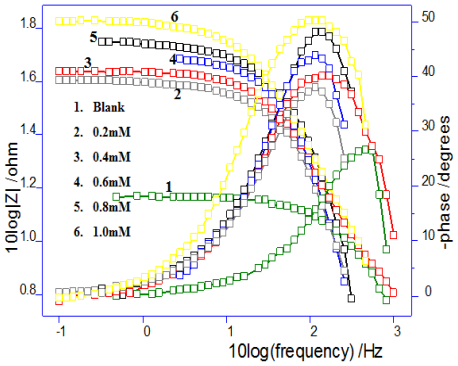

Fig. 2.103: Bode plots for A9Y3IMPA-0.5M H_2SO_4 solutions

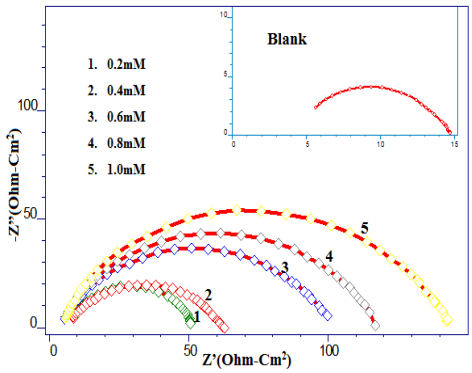

Fig. 2.104: Nyquist plots for A9Y3MPA-0.5M H_2SO_4 solutions

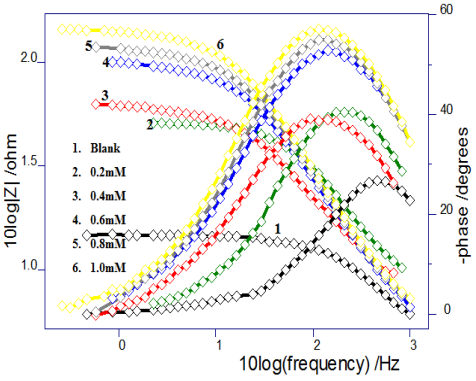

Fig. 2.105: Bode plots for A9Y3MPA-0.5M H_2SO_4 solutions

From the tables 2.22 it is clear that R_{ct} values are increased with increase in concentration of Schiff bases and C_{dl} values are decreased with increase in concentration. In the absence of KI, the inhibition efficiencies of Schiff bases A9Y3APA, A9Y5GPA, A9Y3INPA and A9Y3PPA, calculated from R_{ct} values, were 76.94%, 73.78%, 72.34% and 67.04% respectively for

the concentration of 1.0mM. The η_{EIS} % of Schiff bases A9Y3IMPA and A9Y3MPA were 84.16% and 92.87% at a concentration of 1.0mM.

Table. 2.22. Electrochemical impedance parameters of CS specimens and in 0.5M H_2SO_4 at 30^0C in the absence and presence of inhibitors

Schiff Base	C (mM)	R_{ct} (Ωcm^2)	C_{dl} ($\mu F\ cm^{-2}$)	η_{EIS}%
	Blank	8.9	135	4.18
A9Y3APA	0.2	10.92	103	18.35
	0.4	17.70	95.1	49.72
	0.6	21.09	94.0	57.82
	0.8	28.79	87.1	69.10
	1.0	38.63	75.8	76.94
A9Y5GPA	0.2	11.90	123	25.21
	0.4	15.78	104	43.60
	0.6	23.20	91.4	61.64
	0.8	29.94	83.8	70.27
	1.0	33.94	80.6	73.78
A9Y3IMPA	0.2	33.00	116.0	73.03
	0.4	34.90	109.0	74.50
	0.6	41.30	97.1	78.45
	0.8	47.90	82.9	81.42
	1.0	56.20	78.7	84.16
A9Y3INPA	0.2	20.07	125	55.66
	0.4	21.17	89.8	57.96
	0.6	25.54	85.1	65.15
	0.8	29.02	79.9	69.33
	1.0	32.18	64.7	72.34
A9Y3PPA	0.2	16.54	120	46.06
	0.4	20.69	102	57.00
	0.6	21.92	86.0	59.36
	0.8	22.28	71.2	60.09
	1.0	27.20	66.0	67.04
A9Y3MPA	0.2	39.90	55.6	77.69
	0.4	46.40	115	80.82
	0.6	83.30	81.8	89.32
	0.8	98.70	77.7	90.98
	1.0	124.00	74.5	92.82

Table. 2.23. Electrochemical impedance parameters of CS specimens and in in 0.5M H_2SO_4at 30^0C in the absence and presence of inhibitor + 0.2 mM KI

Schiff Base	C (mM)	R_{ct} (Ωcm^2)	C_{dl} ($\mu F\ cm^{-2}$)	$\eta_{EIS\%}$
	Blank	15.7	104	-
A9Y3APA	0.2	91	99.9	90.22
	0.4	102	93.7	91.27
	0.6	151	91.3	94.11
	0.8	198	79.7	95.51
	1.0	251	65.1	96.45
A9Y5GPA	0.2	30.32	114.3	70.65
	0.4	47.87	100.7	81.41
	0.6	61.01	78.7	85.41
	0.8	147.80	75.7	93.98
	1.0	274.50	73.1	96.76
A9Y3INPA	0.2	65.80	119	86.47
	0.4	76.18	83.7	88.32
	0.6	101.80	77.3	91.26
	0.8	122.60	74.2	92.74
	1.0	133.20	62.8	93.32
A9Y3PPA	0.2	35.6	112	75.00
	0.4	66	94	86.52
	0.6	76.5	79	88.37
	0.8	134	68	93.36
	1.0	177	51	94.97

Table 2.23 clearly indicate that, the R_{ct} values of Schiff bases with KI are higher than that of the corresponding Schiff bases without KI. Also C_{dl} values in the presence of KI are lower than that in the absence of KI for all concentrations. In the presence of KI, the inhibition efficiencies of A9Y3APA, A9Y5GPA, A9Y3INPA and A9Y3PPA, calculated from R_{ct} values, were 96.45%, 96.76%, 93.32% and 94.97 % respectively for the maximum concentration of 1.0mM. The inhibition efficiency values showed that η_{EIS}% of inhibitors increased by the addition of KI.

Impedance behaviour can be well explained by pure electric models and it was similar to that discussed in chapter 4. From tables 2.22 and 2.23, the results suggest that the inhibitor molecules function by adsorption at the metal/solution interface[108] and this adsorption is reinforced by I^- ions. The decrease in C_{dl} may be explained on the basis that the thickness of double layer between the charged metal surface and the solution may be increased on the addition of I^- to the corrosion medium. The η_{EIS}% data revealed that the corrosion inhibition capacities of studied Schiff bases were markedly enhanced by the addition of KI.

Potentiodynamic polarization studies

Potentiodynamic polarization curves of CS in the presence of varying concentration of Schiff bases and Schiff bases + KI in 0.5M H_2SO_4 at 30^0C are shown in figures 2.106 to figure 2.125. Polarization parameters like corrosion current densities (I_{corr}), corrosion potential (E_{corr}), cathodic Tafel slope (b_c), anodic Tafel slope (b_a), inhibition efficiency (η_{pol}%) and linear polarization parameters like polarization resistance (R_p) and inhibition efficiency (η_{Rp}%) for CS specimens in 0.5M H_2SO_4 at 30^0C are listed in table 2.24 and 2.25.

From the analysis of figures and tables it is clear that the inhibition efficiencies are increased with the concentration of inhibitor. The corrosion current density values (I_{corr}) were decreased with increasing concentration. The lowest I_{corr} value of 0.0980 was exhibited by the inhibitor A9Y3MPA and it showed maximum inhibition efficiency of 91.62% at 1.0mM concentration. The R_p values also increased with the concentration and the maximum R_p value of 172.80 ohm was exhibited by the inhibitor A9Y3MPA.

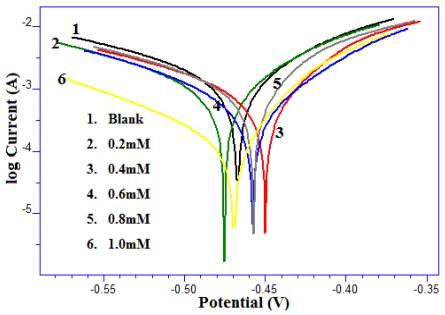

Fig. 2.106: Tafel plots for A9Y3APA-0.5M H_2SO_4 solutions

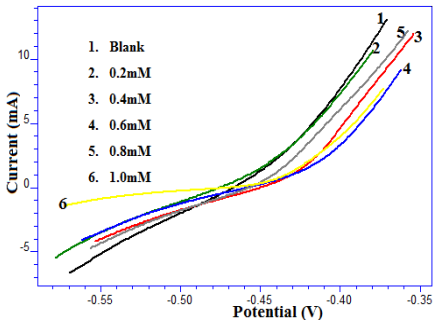

Fig. 2.107: Linear polarization plots for A9Y3APA-0.5M H_2SO_4 solutions

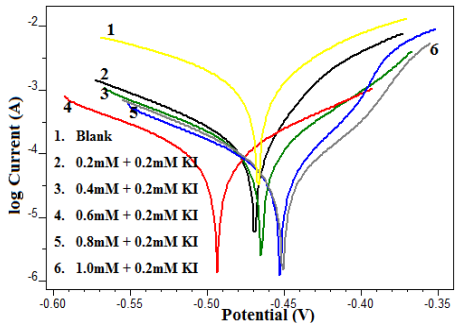

Fig. 2.108: Tafel plots (Synergistic Effect) for A9Y3APA

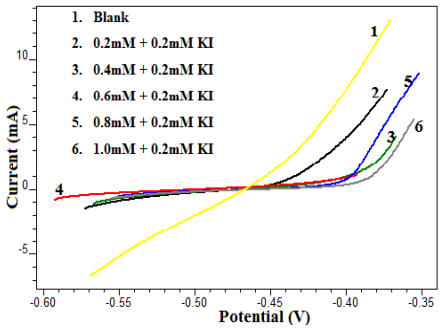

Fig. 2.109: Linear polarization plots (Synergistic Effect) for A9Y3APA

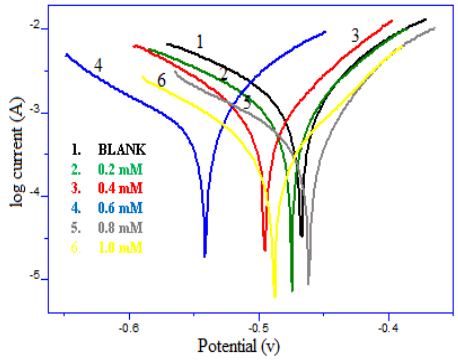

Fig. 2.110: Tafel plots for A9Y5GPA-0.5M H_2SO_4 solutions

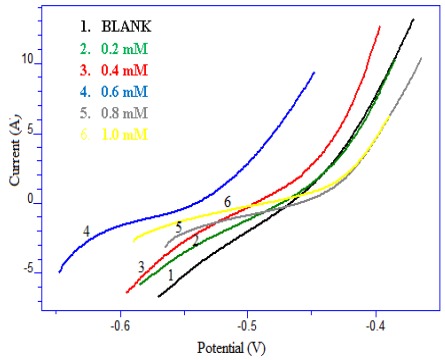

Fig. 2.111: Linear polarization plots for A9Y5GPA-0.5M H_2SO_4 solutions

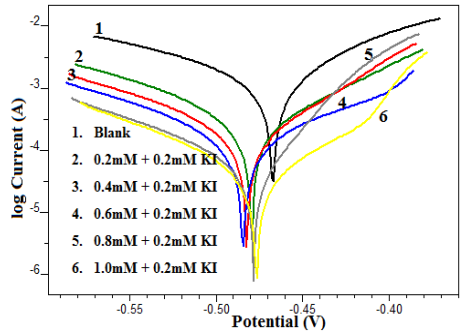

Fig. 2.112: Tafel plots (Synergistic Effect) for A9Y5GPA

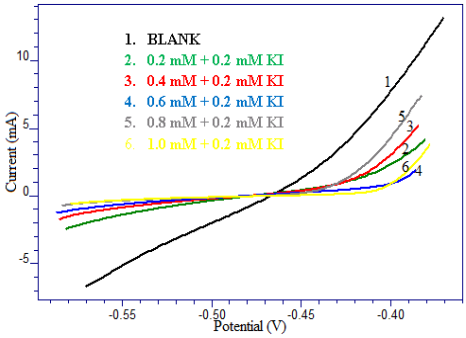

Fig. 2.113: Linear polarization plots (Synergistic Effect) for A9Y5GPA

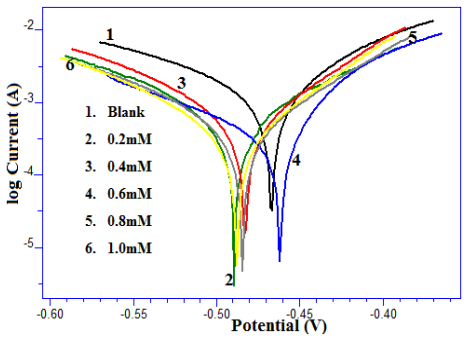

Fig. 2.114: Tafel plots for A9Y3INPA-0.5M H_2SO_4 solutions

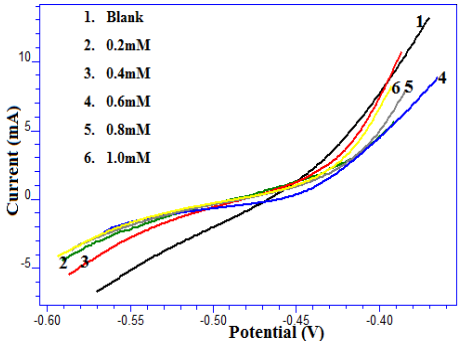

Fig. 2.115: Linear polarization plots for A9Y3INPA-0.5M H_2SO_4 solutions

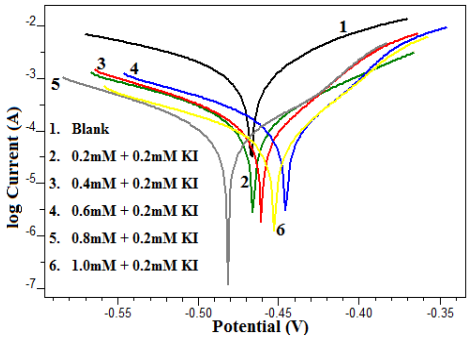

Fig. 2.116: Tafel plots (Synergistic Effect) for A9Y3INPA

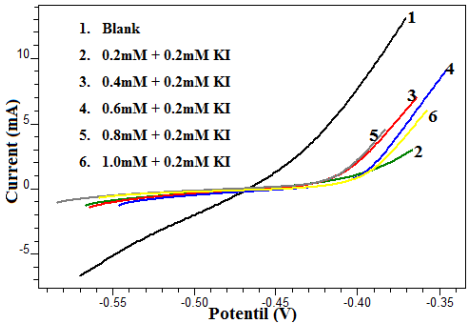

Fig. 2.117: Linear polarization plots (Synergistic Effect) for A9Y3INPA

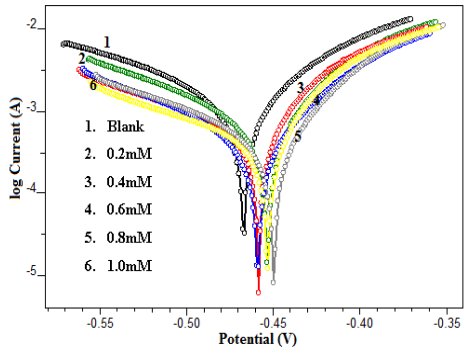

Fig. 2.118: Tafel plots for A9Y3PPA-0.5M H_2SO_4 solutions

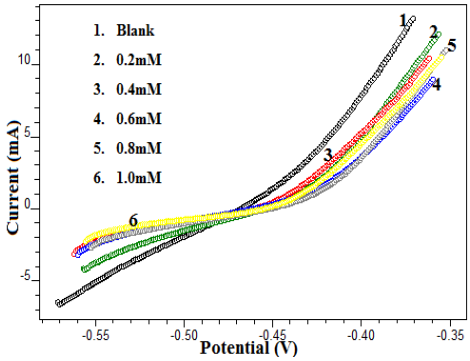

Fig. 2.119: Linear polarization plots for A9Y3PPA-0.5M H_2SO_4 solutions

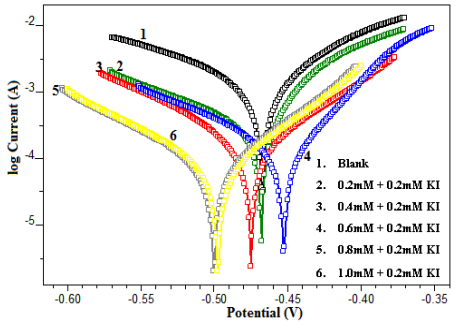

Fig. 2.120: Tafel plots (Synergistic Effect) for A9Y3PPA

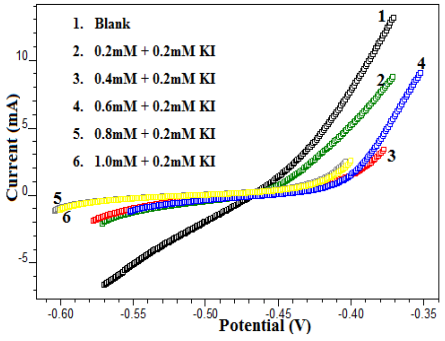

Fig. 2.121: Linear polarization plots (Synergistic Effect) for A9Y3PPA

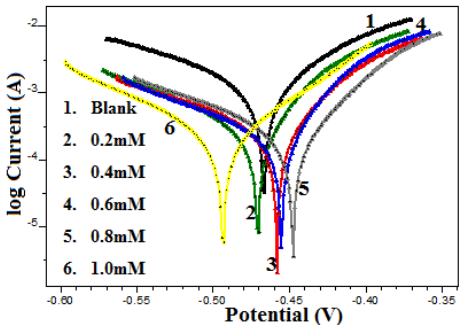

Fig. 2.122: Tafel plots for A9Y3IMPA-0.5M H_2SO_4 solutions

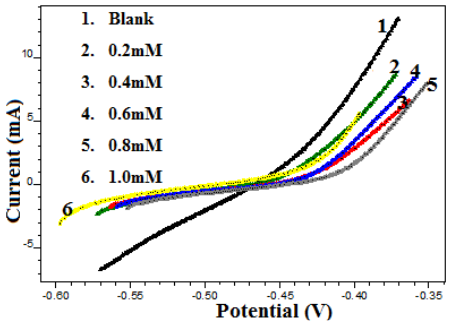

Fig. 2.123: Linear polarization plots for A9Y3IMPA-0.5M H_2SO_4 solutions

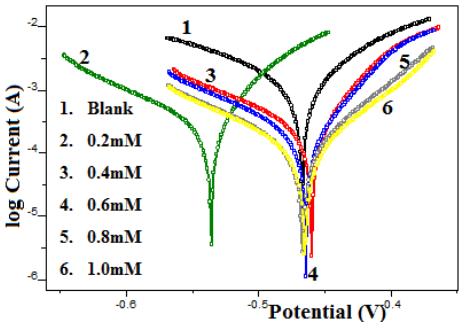

Fig. 2.124: Tafel plots for A9Y3MPA-0.5M H_2SO_4 solutions

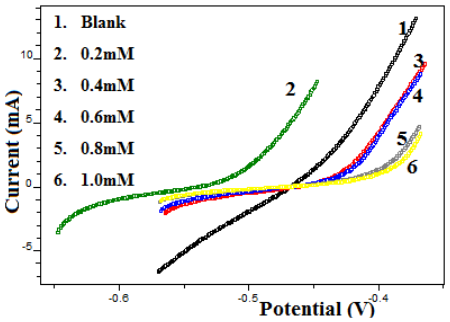

Fig. 2.125: Linear polarization plots for A9Y3MPA-0.5M H_2SO_4 solutions

On the addition of KI to the acidic medium containing A9Y3APA, A9Y5GPA, A9Y3INPA, and A9Y3PPA the I_{corr} values were found to decrease significantly and hence elevated the corrosion inhibition efficiency. The R_p values were also increased by the addition of KI.

In the case of blank solution, the anodic Tafel slope and cathodic Tafel slope were 0.082 V/dec and 0.124 V/dec respectively. Both Tafel slopes were varied by the addition of Schiff bases in the corroding medium. The same trend follows for the system Schiff base + KI. The E_{corr} values were also varied from the E_{corr} of blank. Generally if the shift of E_{corr} is >85 with respect to E_{corr} of uninhibited solution, the inhibitor can be viewed as either cathodic or anodic type. In the present study the maximum shift of E_{corr} was 31mV, suggesting that inhibitor acts as a mixed type inhibitor for CS specimens in 0.5M H_2SO_4.

Table. 2.24. Potentiodynamic and linear polarization parameters of CS specimens in 0.5M H_2SO_4 at 30 ^{0}C in the absence and presence of Schiff bases.

Schiff Base	Tafel Data						Linear Polarisation Data	
	C (mM)	E_{corr} (mV/SCE)	I_{corr} (mA/cm^2)	b_a (V/dec)	$-b_c$ (V/dec)	$\eta_{pol\%}$	R_p (ohm)	$\eta_{Rp\%}$
	Blank	-467	1.1700	0.082	0.124	-	18.32	-
A9Y3APA	0.2	-457	1.0220	0.095	0.114	12.65	22.07	16.99
	0.4	-475	0.8240	0.078	0.116	29.57	24.52	25.29
	0.6	-450	0.7010	0.068	0.117	40.09	26.75	31.51
	0.8	-458	0.4511	0.063	0.103	61.44	37.69	51.39
	1.0	-470	0.1730	0.057	0.097	85.21	90.44	79.74
A9Y5GPA	0.2	-475	0.831	0.072	0.126	28.97	23.90	23.35
	0.4	-494	0.7102	0.071	0.102	39.30	25.61	28.47
	0.6	-541	0.6304	0.080	0.119	46.12	32.83	44.20
	0.8	-461	0.4316	0.063	0.123	63.11	41.83	56.20
	1.0	-488	0.2656	0.065	0.105	77.30	65.69	72.11
A9Y3IMPA	0.2	-483	0.3340	0.069	0.106	71.45	62.25	70.57
	0.4	-462	0.2820	0.062	0.131	75.90	72.78	74.83
	0.6	-468	0.2590	0.062	0.117	77.86	78.90	76.78
	0.8	-445	0.2190	0.052	0.117	81.28	90.93	79.85
	1.0	-493	0.1970	0.068	0.098	83.16	102.65	82.15
A9Y3INPA	0.2	-487.8	0.4920	0.089	0.099	57.95	41.76	56.13
	0.4	-478.2	0.4760	0.065	0.094	59.32	43.05	57.44
	0.6	-477.6	0.4080	0.075	0.117	65.13	51.58	64.48
	0.8	-480.6	0.3530	0.069	0.096	69.83	57.36	68.06
	1.0	-483.2	0.3070	0.062	0.091	73.76	64.04	71.39
A9Y3PPA	0.2	-459	0.6530	0.072	0.116	44.19	31.90	42.57
	0.4	-474	0.5410	0.085	0.141	53.76	38.34	52.22
	0.6	-461	0.5050	0.067	0.113	56.84	43.16	57.55
	0.8	-455	0.4550	0.064	0.126	61.11	45.49	59.73
	1.0	-472	0.4170	0.079	0.145	64.36	50.10	63.43
APY3MPA	0.2	-543	0.2940	0.059	0.107	74.87	68.35	73.20
	0.4	-465	0.2550	0.054	0.114	78.21	82.52	77.80
	0.6	-462	0.1750	0.046	0.106	85.04	112.00	83.64
	0.8	-465	0.1100	0.06	0.102	90.60	155.10	88.19
	1.0	-463	0.0980	0.063	0.102	91.62	172.80	89.40

From the potentiodynamic polarization results, it was clear that the inhibition efficiency of inhibitors was increased in presence of KI. These results also confirm the existence of strong synergism between Schiff base inhibitors and KI in the corrosion inhibition of CS in these solutions. The

values of inhibition efficiency obtained from polarization studies are comparable with impedance studies.

Table. 2.25. Potentiodynamic and linear polarization parameters of CS specimens in 0.5M H_2SO_4 at 30^0C in the absence and presence of Schiff bases with 0.2mM KI

Schiff Base	Tafel Data						Linear Polarisation Data	
	C (mM)	E_{corr} (mV/SCE)	I_{corr} (mA/cm^2)	b_a (V/dec)	$-b_c$ (V/dec)	$\eta_{pol\%}$	R_p (ohm)	$\eta_{Rp\%}$
	Blank	-467	1.1700	0.082	0.124	-	18.32	-
A9Y3APA	0.2	-469	0.173	0.057	0.097	85.21	90.44	79.74
	0.4	-465	0.098	0.063	0.102	91.62	172.8	89.40
	0.6	-470	0.0802	0.088	0.103	93.15	257.2	92.88
	0.8	-453	0.0401	0.03	0.099	96.57	247.2	92.59
	1.0	-451	0.0399	0.04	0.1305	96.59	300.6	93.91
A9Y5GPA	0.2	-472	0.2297	0.072	0.100	80.37	78.91	76.78
	0.4	-475	0.1495	0.058	0.101	87.22	106.80	82.85
	0.6	-482	0.1261	0.099	0.100	89.22	171.20	89.30
	0.8	-475	0.0545	0.037	0.097	95.34	214.10	91.44
	1.0	-466	0.0335	0.053	0.089	97.14	432.10	95.76
A9Y3INPA	0.2	-463	0.1410	0.710	0.107	87.95	131.00	86.02
	0.4	-454	0.1270	0.420	0.097	89.15	162.40	88.72
	0.6	-436	0.1070	0.380	0.104	90.85	112.50	83.72
	0.8	-469	0.0892	0.490	0.096	92.38	223.20	91.79
	1.0	-446	0.0626	0.400	0.112	94.65	255.00	92.82
A9Y3PPA	0.2	-486	0.3930	0.077	0.120	66.41	51.69	64.56
	0.4	-471	0.1370	0.070	0.089	88.29	124.10	85.24
	0.6	-445	0.1229	0.043	0.105	89.50	158.20	88.42
	0.8	-498	0.0669	0.064	0.088	94.28	241.10	92.40
	1.0	-495	0.0614	0.064	0.088	94.75	264.30	93.07

Adsorption isotherm studies in H_2SO_4 medium

The mechanism of adsorption and the surface behaviour of organic molecules can be easily viewed through adsorption isotherms. Different models of adsorption isotherms considered were Langmuir, Temkin, Frumkin and Freundlich isotherms. For the evaluation of thermodynamic parameters it is necessary to determine the best fit isotherm with the aid of correlation coefficient (R^2). Among the isotherms mentioned above, the best description of the adsorption behaviour of Schiff base inhibitors and Schiff base inhibtors

+ KI on CS specimens in 0.5M H_2SO_4 was Freundlich and Langmuir adsorption isotherms .

Figures 2.126 to 2.135 represent the adsorption plots of inhibitors and inhibitors + KI obtained by the weight loss measurements of CS specimens in 0.5M H_2SO_4 at 30^0C for 24 h.

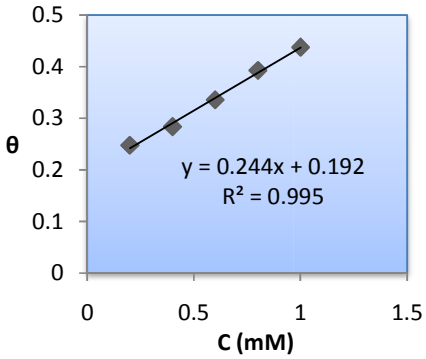

Fig. 2.126: Freundlich adsorption isotherm for A9Y3APA in 0.5M H_2SO_4

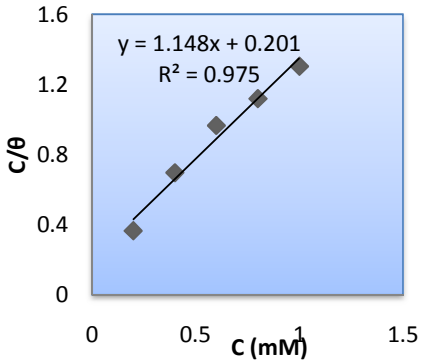

Fig. 2.127: Langmuir adsorption isotherm A9Y3APA + KI

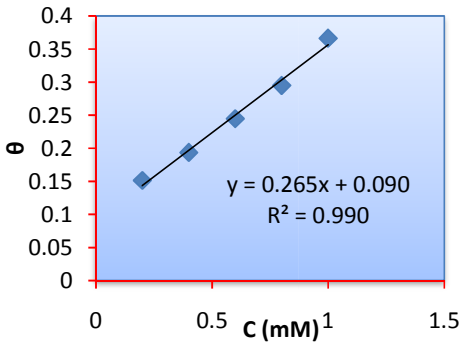

Fig. 2.128: Freundlich adsorption isotherm for A9Y5GPA in 0.5M H_2SO_4

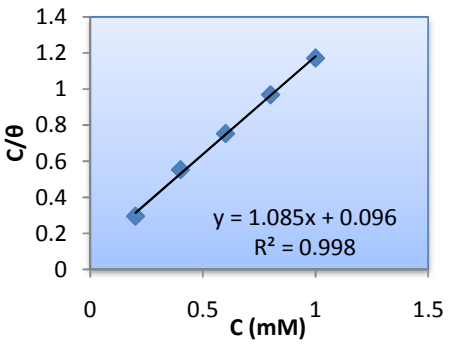

Fig. 2.129: Langmuir adsorption isotherm for A9Y5GPA + KI

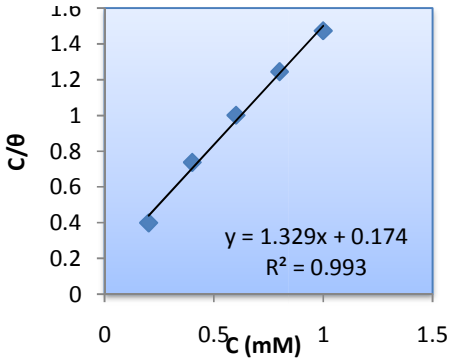

Fig. 2.130: Langmuir adsorption isotherm for A9Y3INPA in 0.5M H_2SO_4

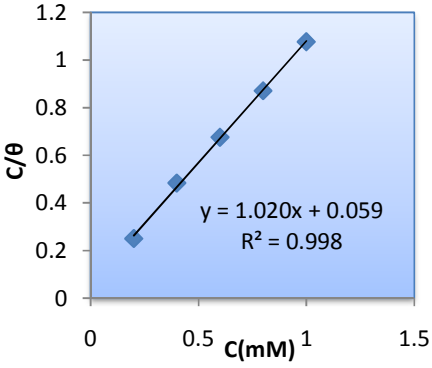

Fig. 2.131: Langmuir adsorption isotherm for A9Y3INPA+KI

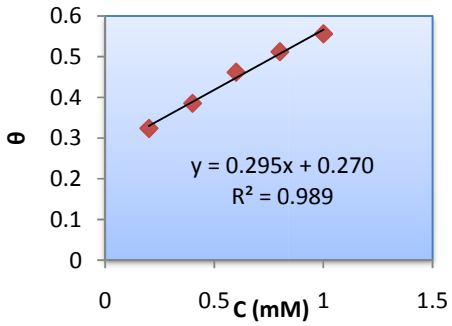

Fig. 2.132: Freundlich adsorption isotherm for A9Y3PPA in 0.5M H_2SO_4

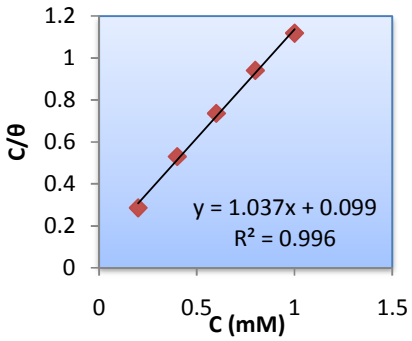

Fig. 2.133: Langmuir adsorption isotherm for A9Y3PPA + KI

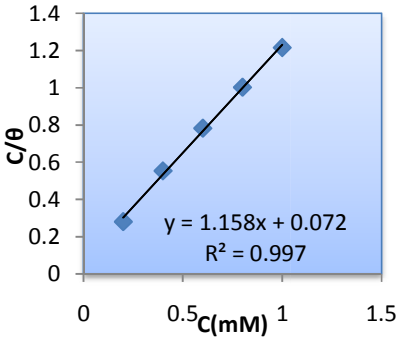

Fig. 2.134: Longmuir adsorption isotherm for A9Y3IMPA in 0.5M H_2SO_4

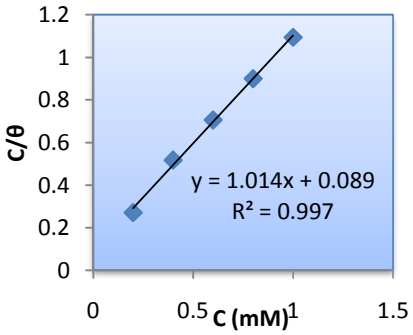

Fig. 2.135: Langmuir adsorption isotherm for A9Y3MPA in 0.5M H_2SO_4

The adsorption equilibrium constant K_{ads} is related to the standard free energy of adsorption ΔG^0_{ads}. Table 2.26 explores thermodynamic parameters obtained from weight loss measurements of CS in 0.5M H_2SO_4 at 30^0C for 24 h.

Table. 2.26. Thermodynamic parameters for the adsorption of Schiff bases on CS in 0.5M H_2SO_4

Schiff base	Isotherm	K_{ads}	ΔG^0_{ads}(kJ/mol)
A9Y3APA	Freundlich	244	-23.9
A9Y3APA+KI	Langmuir	4975	-31.52
A9Y5GPA	Freundlich	266	-24.15
A9Y5GPA+KI	Langmuir	1002	-27.49
A9Y3IMPA	Langmuir	13889	-34.10
A9Y3INPA	Langmuir	5747	-31.88
A9Y3INPA+KI	Langmuir	16949	-34.60
A9Y3PPA	Freundlich	296	-24.42
A9Y3PPA+KI	Langmuir	10101	-33.30
A9Y3MPA	Langmuir	11236	-33.57

The results from the table indicate that the adsorption equilibrium constant values are increased by the addition of KI. In the case of inhibitors A9Y3INPA and A9Y3MPA, the K_{ads} values are 13889 and 11236 respectively which are higher than that of other inhibitors.

The higher values of adsorption equilibrium constant obtained by the addition of KI indicate that the inhibitor molecules strongly adsorbed on the metal surface than inhibitor alone. ΔG^0_{ads} for inhibitor and inhibitor + KI on CS showed negative values indicating the spontaneity of the process. Also increase in the $-\Delta G^0_{ads}$ values for inhibitor + KI systems is a sign of strong interactions that exist between inhibitor and metal surface. In the present investigation, inhibitor and inhibitor + KI molecules showed ΔG^0_{ads} values in between -23.9kJ mol^{-1} and -34.60kJ mol^{-1} suggesting that the adsorption of inhibitor involves both electrostatic and chemical interactions.

Scanning electron microscopy studies

The surface morphology of carbon steel surface was evaluated by scanning electron microscopy (SEM). Figures 2.136 A, B, C and D show the scanning electron micrographs of the bare carbon steel surface, CS specimens without inhibitor, with inhibitor and with inhibitor + KI in 0.5M sulphuric acid medium respectively. The morphology revealed that in the absence of inhibitor, the surface is highly corroded. However in the presence of inhibitor the amount of corrosion is suppressed which was again lowered in the presence of inhibitor + KI. These observations suggest that the inhibitor forms a protective layer on the surface that prevents the attack of acid on the corroding metal surface.

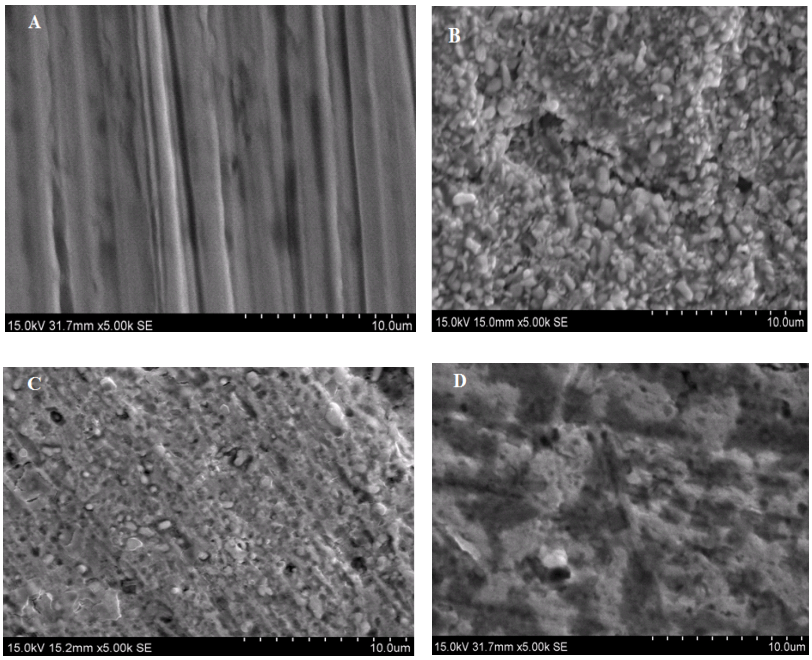

Fig. 2.136: Scanning Electron Micrographs of carbon steel samples: A) polished fresh specimens B) immersed in 0.5M H_2SO_4 solution C) immersed in 0.5M H_2SO_4 solution with 1mM A9Y5GPA D) immersed in 0.5M H_2SO_4 solution with 1mM A9Y5GPA+ 0.2mM KI

Mechanism of inhibition

In uninhibited H_2SO_4 solution, the mechanism of the anodic dissolution reaction of iron follows the reaction pathway from (38) to (40). The protonated inhibitor molecules could adsorb on the metal surface via SO_4^{2-} ions that form interconnecting bridges between the positively charged metal surface and protonated organic cations[109]. Therefore, it can be hypothesized that the reaction pathway in the inhibited solution seems to be through (38) to (41).

$$Fe + SO_4^{2-} \leftrightarrow (Fe\ SO_4^{2-})_{ads} \quad (38)$$

$$(Fe\ SO_4^{2-})_{ads} \leftrightarrow (Fe\ SO_4)_{ads} + 2e^- \quad (39)$$

$$(Fe\ SO_4)_{ads} \leftrightarrow Fe^{2+} + SO_4^{2-} \quad (40)$$

$$(Fe\ SO_4)_{ads} + Inhibitor^+ \leftrightarrow (Fe\ SO_4^{2-}\ Inhibitor^+)_{ads} \quad (41)$$

It is accepted that halide ions facilitate the adsorption of organic inhibitors in acidic media by forming intermediate bridges between metal

surface and positively charged inhibitor molecules. Thus, if the inhibiting effect is due to the protonated species, a synergistic increase in inhibition efficiency should be observed in the presence of the halide additives. The synergistic effect of halide ions was reported to increase in the order of $I^- > Br^- > Cl^-$. The greater influence of the iodide ion is often attributed to its large ionic radius, high hydrophobicity and low electronegativity of iodide, compared to the other ions.

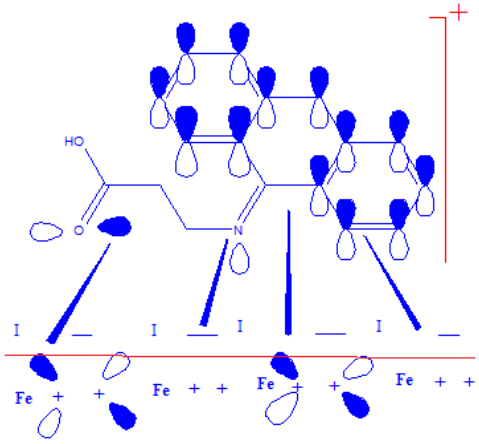

Fig. 2.137: Schematic representation of modes of adsorption of the inhibitor A9Y3APA on CS in 0.5 M H_2SO_4

The halide ions are first adsorbed on the metal surface and the inhibitor is then drawn in to the double layer by the adsorbed halide ion, such that the ion pair formation occurs directly on the metal surface:

$$A_s \rightarrow A_{ads} \quad (42)$$

$$B_s + A_{ads} \rightarrow (BA)_{ads} \quad (43)$$

where B_s and A_s represent inhibitor and halide ion respectively in the bulk solution, while A_{ads} and $(BA)_{ads}$ refers halide ion and ion-pair respectively in the adsorbed state. Figure 2.137 shows the schematic illustration of modes of adsorption of A9Y3APA on carbon steel.

Comparative study on corrosion inhibition efficiency of Schiff bases in HCl and H_2SO_4

The corrosion inhibition efficiency of Schiff bases in 1M HCl and 0.5M H_2SO_4 on CS at a concentration of 1.0mM was compared. For the sake of explanation, this data is represented as bar diagram and shown in the figure 2.138. From the figure it is clear that there are variations in inhibition efficiencies of the Schiff bases in HCl and H_2SO_4 medium. The Schiff base A9Y3APA, A9Y5GPA and A9Y3PPA show low inhibition efficiency in H_2SO_4 than HCl. The inhibition efficiency values of the Schiff bases A9Y3IMPA and A9Y3INPA are comparable in both acids and the inhibitor A9Y3MPA exhibited almost same inhibition efficiency values in both acids.

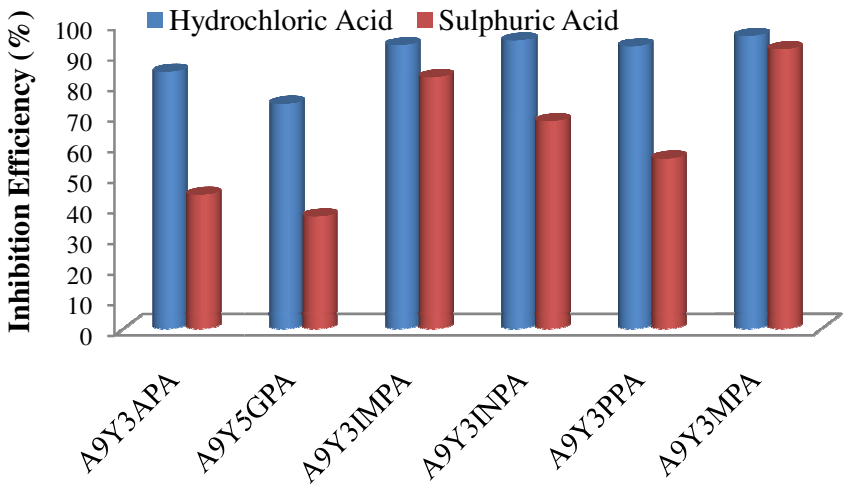

Fig. 2.138: Comparison of inhibition efficiency at 1.0mM concentration of Schiff bases in 1M HCl and 0.5M H_2SO_4 medium at 30^0C for 24 h.

The higher inhibition efficiency exhibited by A9Y3IMPA, A9Y3INPA and A9Y3PPA than A9Y3APA and A9Y5GPA may be due to the presence of aromatic π-electron system. The π-electron cloud interacts with the orbitals of the metal and thus enhances adsorption process. Comparing the inhibition efficiencies of A9Y3IMPA and A9Y3INPA, the lower value exhibited by

A9Y3PPA may be due to the steric hindrance imparted by the phenyl ring which adversely affects the adsorption process. The high inhibition efficiency showed by A9Y3MPA can be attributed to the presence of highly polarisable 'S' atom in the molecule, which can make strong co-ordinate bond with metal atom.

The inhibitive action requires knowledge of the inhibitor at the electrode-solution interface. In acid solution, "the inhibitor compounds may become protonated. The surface charge of steel in both HCl and H_2SO_4 solutions is known to be positive[110]. There is the likelihood of the acid anions of Cl^- and SO_4^{2-} to be specifically adsorbed creating excess negative charge towards the solution. This favours the adsorption by electrostatic interactions of the protonated inhibitor molecules on the negatively charged metal surface. This can be regarded as synergism existing between the acid anions and the protonated inhibitor molecule. All the studied Schiff base inhibitors exhibited better inhibition behaviour in HCl medium than in H_2SO_4 solutions, suggesting that the nature of the ions in the acidic solutions may play a role in the adsorption of the inhibitor. Cl^- ions are known to adsorb strongly than SO_4^{2-} ions. In addition, the reduced contact of SO_4^{2-} with the adsorbed protonated cations may result in a lower" adsorption[111]. The adsorption of the "protonated inhibitor molecules can also occur on the carbon steel surface by direct interaction of the lone pairs of electrons present in the inhibitor molecule with the vacant d-orbital of Fe. These lone pairs of electrons could also form metal inhibitor complexes with Fe^{2+} ions formed from the anodic dissolution of steel. These complexes may adsorb onto the steel surface through vander Waals force, providing more protection against corrosion".

SUMMARY

Weight loss of CS specimens in 1M HCl and 0.5M H_2SO_4 at 30^0C was determined at 24 h in the presence of various concentrations of amino acids [β-alanine (ALA), L-arginine (ARG), L- histidine (HIS), L- phenyl alanine (PHE), L- tryptophan (TRP) and L- cysteine (CYS)] and synthesized six Schiff bases. The inhibition capacity of amino acids in HCl medium increases in the order ARG < PHE ≤ ALA < TRP ≤ HIS < CYS for the maximum concentration of 1.0mM. The inhibition capacity of amino acids in H_2SO_4 medium increases in the order PHE < TRP < HIS ≤ ALA ≤ ARG < CYS for the maximum concentration. Among the isotherm considered, Langmuir isotherm found to provide best description of the adsorption behaviour of the studied amino acids in HCl medium. In the H_2SO_4 medium, ALA and PHE fitted into Freundlich adsorption isotherm and other amino acids fitted into Langmuir adsorption isotherm.

For the concentration of 1.0mM in 1M HCl medium, the inhibition efficiency of Schiff bases increases in the following order A9Y5GPA < A9Y3APA <A9Y3PPA ≤ A9Y3IMPA < A9Y3INPA < A9Y3MPA. It has been found that the inhibition efficiency depends on temperature and decreases with increase in temperature, indicating that at higher temperature, dissolution of carbon steel predominates on the surface. Positive signs of enthalpies with a regular rise reflect the endothermic nature of dissolution and the increasing difficulty of corrosion with the inhibitor. The shift of ΔS to more positive values on increasing the concentration of the inhibitor indicates that the disordering of activated complex rises. In HCl medium, the Schiff

base inhibitor A9Y3APA obeys Freundlich adsorption isotherm and other Schiff base inhibitors obeys Langmuir adsorption isotherms.

In 0.5M H_2SO_4 medium, the corrosion inhibition efficiency of the studied Schiff bases increases in the order A9Y5GPA<A9Y3APA <A9Y3PPA<A9Y3INPA<A9Y3IMPA<A9Y3MPA for all the studied concentrations. The synergistic effect of of inhibitors A9Y3APA, A9Y5GPA, A9Y3INPA, and A9Y3PPA with iodide ion were also performed to enhance the inhibition efficiency. The synergism parameters clearly established that the enhancement in inhibition is due to synergism. The Schiff base A9Y3APA, A9Y5GPA and A9Y3PPA obey Freundlich adsorption isotherm and the remaining Schiff bases obey Langmuir adsorption isotherm. In the synergistic study, all the Schiff bases obey Langmuir adsorption isotherm. In the present investigation, the ΔG_{ads} values of all the inhibitor molecules suggested that the adsorption of inhibitor involves both electrostatic and chemical interactions.

EIS studies reveal that the R_{ct} values were increased with increases in concentration of all the inhibitor molecules in the acid medium. It is evident from the plots that the impedance response of metal specimens has marked difference in the presence and absence of the KI with inhibitors studied. The capacitance values C_{dl} decreases with inhibitor concentration and this decrease in C_{dl} was enhanced upon the addition of I^- ions to the corrosive environment.

The E_{corr} values from polarization studies suggested that the addition of the Schiff base to acid media affected both the cathodic and anodic parts of the curves; it may be assumed that all the studied inhibitors act as a mixed type inhibitor for CS specimens in 1M HCl and 0.5 M H_2SO_4.

Based on the mechanism, the Cl^- and SO_4^{2-} ions could be specifically adsorbed on the metal surface and creates an excess of negative charge on the surface. This will favour the adsorption of protonated Schiff base on the surface, thus interfere the anodic and cathodic reactions and hence reduce the dissolution of Fe to Fe^{2+}. Besides this electrostatic interaction between the protonated Schiff base and the metal surface, other possible interactions are i) interaction of unshared electron pairs in the molecule with the metal ii) interaction of π-electrons with the metal and iii) a combination of types (i–ii). Halide ions facilitate the adsorption of organic inhibitors in acidic media by forming intermediate bridges between metal surface and positively charged inhibitor molecules. Thus, if the inhibiting effect is due to the protonated species, a synergistic increase in inhibition efficiency should be observed in the presence of the halide additives.

All the studied Schiff base exhibit higher inhibition efficiency in HCl medium than H_2SO_4 medium. The effectiveness of inhibitors depends on the chemical composition, their molecular structure and their affinity for the metal surface.

REFERENCES

1. H. H. Uhlig, "*Corrosion and Corrosion Control*", John Wiley and Sons, New York, **1985**
2. O. James, N. C. Oforka, O. K. Abiola, *Int. J. Electrochem. Sci.,* 2, **2007,** 278
3. S. A. Abd El-Maksoud, *Int. J. Electrochem. Sci.,* 3, **2008,** 528
4. O. L. Riggs, Jr., C. C. Nathan (Ed.), *Corrosion Inhibitors*, NACE, Houston, TX, **1973**
5. M. G. Noack, *Mater. Perform*., 21(3), **1982**, 26
6. A. Frignani, G. Trabanelli, F. Zucchi, M. Zucchini, *Proceedings of 5th European Symposium of Corrosion Inhibitors*, Ferrara, Italy, **1980**, 1185
7. V. S. Sastri, *Corrosion Inhibitors: Principles and Applications*, John Wiley, New York, **1998**, 39
8. S. A. Levin, S. A. Gintzbergy, I. S. Dinner, V. N. Kuchinsky, *Proceedings of Second European Symposium on Corrosion Inhibitors,* Ferrara, Italy, **1965**, 765
9. N. Hackerman, *Langmuir*, 3(6), **1987**, 922
10. E. W. Flick, *Corrosion Inhibitors: An Industrial Guide*, William Andrew, 2nd edition, **1993**
11. G. Moretti, F. Guidi, and G. Grion, *Corros. Sci.*, 46 (2), **2004**, 387
12. H. Ashassi-Sorkhabi, M. R. Majidi, and K. Seyyedi, *Appli. Surf. Sci.*, 225 (1-4), **2004**, 176
13. S. Bilgic, A. A. Aksut, *Bri. Corros. J.*, 28 (1), **1993**, 59
14. G. Moretti, F. Guidi, *Corros. Sci.*, 44 (9), **2002**, 1995

15. M. Mobin, M. Parveen, M. Z. A. Rafiquee, *J. Mater. Eng. Perform.,* 22 (2), **2013**, 548
16. H. H. A. Rahman, A. H. E. Moustafa, M. K. Awad, *Int. J. Electrochem. Sci.,* 7, **2012**, 1266
17. K. F. Khaled, N. S. Abdelshafi, A. A. El-Maghraby, A. Aouniti, N. Al-Mobarak, B. Hammouti, *Int. J. Electrochem. Sci.,* 7, **2012,** 1270
18. N. O. Eddy, *J. Advan. Rese.*, 2 (1), **2011**, 35
19. S. Ahn, H. J. Song, J. W. Park, J. H. Lee, I. Y. Lee, K. R Jang, *Korean J. Chem. Eng.*, 27(5), **2010**,1576
20. M. A. Amin, K. F. Khaled, Q. Mohsen, H.A Arida,, *Corros. Sci.*, 52(5), **2010**,1684
21. J. J. Fu, S. N. Li, L. H. Cao, Y. Wang, L. H. Yan, L. D. Lu, *J. Mater. Sci.*, 45(4*)*, **2010,** 979
22. Ranjana, R. Banerjee, M. M. Nandi, *Ind. J. Chem. Tech.*, 7(3), **2010**, 176
23. S. Varvara, M. Popa, G. Rustoiu, R. Bostan, L. Mureşan, *Studia Universitatis Babes-Bolyai Chemia*, *2*, **2009**,73
24. J. J. Fu, S. N. Li, Y. Wang, L. H. Cao, L. D. Lu, *J. Mater. Sci.*, 45(22), **2010,** 6255
25. M. Alagbe, L. E. Umoru, A. A. Afonja, O. E. Olorunniwo, *Anti-Corros. Meth. Mater.*, 56(1*)*, **2009,** 43
26. D. Q. Zhang, Q. R. Cai, X. M. He, L. X. Gao, G. D. Zhou, *Mater. Chem. Phys.*, 112 (2), **2008**, 353
27. K. Barouni, L. Bazzi, R. Salghi, M. Mihit, B. Hammouti, A. Albourine, S. E. Issami, *Mater. Lett.*, 62(19), **2008,** 3325

28. P. Singh, K. Bhrara, G. Singh, *Appl. Surf. Sci.*, 254(18), **2008**, 5927
29. M. M. El-Rabiee, N. H. Helal, Gh.M.A. El-Hafez, W.A. Badawy, *J. Alloy. Compd.*, 459(1-2), **2008**, 466
30. M. A. Kiani, M. F. Mousavi, S. Ghasemi, M. Shamsipur, S. H. Kazemi, *Corros. Sci.*, 50(4), **2008,** 1035
31. W. A. Badawy, K. M. Ismail, A. M. Fathi, *Electrochim. Acta*, 51(20), **2006**, 4182
32. M. Alagbe, L. E. Umoru, A. A. Afonja, O. E. Olorunniwo, *J. Appl. Sci.*, 6(5), **2006**, 1142
33. Z. Ghasemi, A. Tizpar, *Appl. Surf. Sci.*, 252(10), **2006,** 3667
34. O. Olivares, N. V. Likhanova, B. Gómez, J. Navarrete, M. E. Llanos-Serrano, E. Arce, J. M. Hallen, *Appl. Surf. Sci.*, 252(8), **2006**, 2894
35. D. Q. Zhang, L. X. Gao, G. D. Zhou, *J. Appl. Electrochem.*, 35(11), **2005**, 1081
36. M. S. Morad, *J. Appl. Electrochem.*, 35(9), **2005**, 889
37. H. Ashassi-Sorkhabi, Z. Ghasemi, D. Seifzadeh, *Appl. Surf. Sci.*, 249(1-4), **2005**, 408
38. M. Zerfaoui, H. Oudda, B. Hammouti, S. Kertit, M. Benkaddour, *Prog. Org. Coat.*, 51(2), **2004**, 134
39. J. B. Matos, L. P. Pereira, S. M. L. Agostinho, O. E. Barcia, G. G. O. Cordeiro, E. D'Elia, *J. Electroanal. Chem.*, 570(1), **2003**, 91
40. G. K. Gomma, *Bull. Electrochem.*, 14(12), **1998**, 456
41. A. A. El-Shafei, M. N. H Moussa, A. A. El-Far, *J. Appl. Electrochem.*, 27(9), **1997**,1075
42. I. A. Zaafarany, *Int. J. Corros. Scale Inhib*., 3(1), **2014**, 12

43. S. Junaedi, A. A. Al-Amiery, A. Kadihum, A. A. H. Kadhum, A. B. Mohamad, *Int. J. Mol. Sci.,* 14, **2013**, 11915; doi:10.3390/ijms140611915
44. S. Chitra, K. Parameswari, C. Sivakami, A. Selvaraj, *Chemical Engineering Research Bulletin,* 14, **2010**, 1
45. S.D. Toliwal, J. Kalpesh, T. Pavagadhi*, J. Appl. Chem. Res.,* 12, **2010**, 24
46. S. John, B. Joseph, K. K. Aravindakshan, A. Joseph, *Mater. Chem. Phys.* 122, **2010**, 374
47. M. Abdallah, M. Al- Agez, A. S. Fouda, *Int. J. Electrochem. Sci*., 4, **2009**, 336
48. M. Q. Mohammed*, J. Basrah Researches (Sciences),* 37(4A), **2011**, 116
49. H. H. Hassan, E. Abdelghani, M. A. Amin, *Electrochim. Acta,* 52, **2007**, 6359
50. M. Outirite, M. Lagrenee, M. Lebrini, M. Traisnel, C. Jama, H. Vezin, F. Bentiss, *Electrochim. Acta*, 55, **2010**, 1670
51. M.G. Hosseini, M. Ehteshamzadeh, T. Shahrabi, *Electrochim. Acta,* 52, **2007**, 3680
52. S.G. Zhang, W. Lei, M.Z. Xia, F.Y. Wang, *J. Mol. Struct. Theochem.,* 732, **2005**,173
53. N. Saxena, S. kumar, S. P. Mathur, *Chem. Eng. Comm*., 196, **2009**,1451
54. D. Gopi, K. M. Govindaraju, L. Kavitha, *J. Appl. Electrochem*., 40(7), **2010,** 1349

55. M.N. Desai, M.B. Desai, C.B. Shah, S.M. Desai, *Corros. Sci.,* 26 (10), **1986**, 827

56. K. C. Emregül, A. A. Akay, O. Atakol, *Mater. Chem. Phys.,* 93(2–3), **2005**, 325

57. H. Shokry, M. Yuasa, I. Sekine, R. M. Issa, H. Y. El-baradie, G. K. Gomma, *Corros. Sci*., 40 (12), **1998**, 2173

58. M. Scendo, J. Trela , *Int. J. Electrochem. Sci.*, 8, **2013**, 8329

59. S. Thirugnanaselvi, S. Kuttirani, A. R. Emelda, *Trans. Nonferrous Met. Soc. China,* 24(6), **2014**, 1969

60. S. Chitra, K. Parameswari, A. Selvaraj, *Int. J. Electrochem. Sci*., 5, **2010,**1675

61. K.R. Ansari, M.A. Quraishi, Ambrish Singh, *Corros. Sci.,* 79, **2014**, 5

62. S. B. Ade, M. N. Deshpande, D. G. Kolhatkar, *J. Chem. Pharm. Res.,* 4(2), **2012**,1033

63. ASTM G-31-72, "Standard Recommended Practice for the Laboratory Immersion Corrosion Testing of Metals", American Society for Testing and Materials (ASTM) Philaldelphia, P. A, **1990**, 401

64. G. S. Haynes, R. Baboian, "Laboratory Corrosion Tests and Standards", ASTM Special technical publication, 866, American Society for Testing and Materials, (ASTM) Philadelphia, P. A, **1990**

65. M. M. El-Naggar, *Corros. Sci.,* 42, **2000**, 773

66. S. Deng, X. Li, H. Fu, *Corros. Sci.,* 53, **2011**, 3596

67. M. Hosseini, S. F. L. Mertens, M. Ghorbani, R. M. Arshadi, *Mater. Chem. Phys*., 78, **2003**, 800

68. E. Cano, J. L. Polo, A. La Iglesia, J. M. Bastidas, *Adsorption*, 10, **2004**, 219
69. M. Bouklah, N. Benchat, B. Hammouti, A. Aouniti, S. Kertit, *Mater. Lett.,* 60, **2006**, 1901
70. E. Barsoukov, J. R. Macdonald, eds., *Impedance Spectroscopy; Theory, Experiment and Applications, 2nd ed.,* Wiley Interscience Publications, **2005**
71. C. Gabrielle, "Identification of Electrochemical Processes by Frequency Response Analysis" Solartron Instrumentation Group, **1980**.
72. M. Kendig, J. Scully, *Corros.*, 46, **1990**, 22
73. S. Fletcher, *J. Electrochem. Soc.*, 141, **1994**, 1823
74. P. M. Gomadam, J. W. Weidner, *Int. J. Energy Res.,* 29, **2005**, 1133 doi: 10.1002/er.1144
75. A. J. Bard, L. R. Faulkner, "*Electrochemical Methods, Fundamentals and Applications*", Wiley Inter Science Publications, New York, **2000**
76. S. W. Dean, R. A. Woodroof, J. S Nicholas, ASTM STP 866, *American Society for Testing and Materials*, Philadelphia,**1985**, 228
77. J. R. Scully, *"The polarization resistance method for the determination of Instantaneous Corrosion rate: A new"*, NACE corrosion/98, Houston, **1998**, 304
78. D. P. Schweinsberg "*Dynamic Electrochemistry and metallic corrosion*" QUT press, 1992
79. G. E. badea, A. Caraban, M. Sebesan, S. Dzitac, P. Cret, A. Setel, *J. Sustain Energy,* 1, **2010,** 1

80. J. O. M. Bockris, A. K. N. Reddy, "*Modern Electrochemistry",* 2, Plenum Press, New York, **1977**

81. H. Ashassi-Sorkhabi, B. Shaabani, D. Seifzadeh , *Electrochim. Acta*, 50, **2005,** 3446

82. M. Stern, E. D. Weisert, *Proc. ASTM*, 59 , **1959**, 1280

83. L. Elkadi, B. Mernari, M. Traisnel, F. Bentiss, M. Lagrenée, *Corros. Sci.,* 42, **2000**, 703

84. O. E. Barcia, O. R. Mattos, N. Pebere, B. Tribollet, *J. Electrochem. Soc.*, 140, **1993**, 2825

85. S. Martinez, M. Metikos-Hukovic, *J. Appl. Electrochem.*, 33, **2003**, 1137

86. H. Cang, W. Y. Shi, J. L. Shao and Q. Xu, *Int. J. Electrochem. Sci.*, 7, **2012**, 3726

87. P. R. Roberge, *Handbook of Corrosion Engineering*, Mc-Graw-Hill companies, **1999**

88. K. M. Ismail, *Electrochim. Acta*, *52*, **2007**, 7811

89. O. Olivares–Xometl, N.V. Likhanova, R. Martinez-Palou, M.A. Dominguez-Aguilar, *Mater. Corros.,* 60, **2009**, 14

90. M.R. Singh, K. Bhrara and G. Singh, *Port. Electrochim. Acta,* 26, **2008**, 479

91. N. I. Kairi, J. Kassim, *Int. J. Electrochem. Sci.,* 8, **2013,** 7138

92. A. R. S. Priya, V. S. Muralidharam, A. Subramannia, *Corros*., 64, **2008**, 541

93. M. E. Azhar, B. Mernari, M. Traisnel, F. Bentiss, M. Lagrenée, *Corros. Sci.,* 43, **2001**, 2229

94. A. Yurt, A. Balaban, K. S. Ustün, G. Bereket, B. Erk, *Mater. Chem. Phys.,* 85, **2004**, 420

95. J. R. Macdonald, W. B. Johnson, J. R. Macdonald (eds), Theory in impedance Spectroscopy, John Wiley & Sons New York NY USA, **1987**

96. A. K. Singh, S. K. Shukla, M. Singh, M. A. Quraishi. *Mater. Chem. Phy.,* 129, **2011**, 68

97. M. A. Quraishi and J. Rawat, *Mater. Chem. Phys.*, 70, **2001**, 95

98. X. Li, S. Deng, H. Fu, *Corros. Sci.,* 51, **2009**, 1344

99. E. S. Ferreira, C. Giacomelli, F. C. Giacomelli, A. Spinelli, *Mater. Chem. Phys.,* 83, **2004**, 129

100. F. Bentiss, M. Lebrini, M. Lagrenée, *Corros. Sci.,* 47**, 2005,** 2915

101. W. Li, Q. He, S. Zhang, C. Pei, B. Hou, *J. Appl. Electrochem*., 38, **2008**, 289

102. E. A. Noor, A. H. Al-Moubaraki*, Int. J. Electrochem. Sci.,* 3, **2008**, 806

103. F. Bentiss, M. Traisnel, M. Lagrenée. *Corros. Sci*., 42, **2000**,127

104. D. P Schweinsberg, G. A. George, A. K. Nanayakkara, D. A. Steinert, *Corros. Sci.,* 28, **1998**, 33

105. K. R Ansari, D. K. Yadav, E. E. Ebenso, M. A. Quraishi, *Int. J. Electrochem. Sci.*, 7, **2012**, 4780

106. A. K. Singh, M. A. Quraishi, *J. Appl. Electrochem*., 40, **2010**, 1293

107. K. Aramaki, M. Hackerman, *J. Electrochem. Soc*., 116**, 1969,** 568

108. M. MaCafferty, N. Hackerman, *J. Electrochem. Soc.,* 119, **1972,** 146

109. R. Solmaz, M. E. Mert, G. Karda, B. Yazici, M. Erbil, *Acta Phys. Chim. Sin.,* 24(7), **2008**, 1185

110. S. Deng, X. Li, *Corros. Sci.,* 5, **2012**, 407

111. M. E. Ikpi, I. I. Udoh, P. C. Okafor, U. J. Ekpe, E. E. Ebenso, *Int. J. Electrochem. Sci.,* 7, **2012,** 12193